Three-Dimensional Modelling of Coral Reefs for Structural Complexity Analysis

Grace C. Young

Somerville College
University of Oxford

A thesis submitted for the degree of
Doctor of Philosophy

Michaelmas 2017
OSS Student No. 764886

Abstract

Coral reefs are some of Earth's most biodiverse and economically valuable ecosystems. Simultaneously they are among the most threatened by anthropogenic factors including global climate change. Their unique three-dimensional (3D) structural complexity is part of what enables them to provide their ecosystem services. It strongly affects species richness, abundance, and other indicators of ecosystem health.

This thesis explores the relationship between coral reef 3D structural complexity and ecosystem features. It has developed a new, low-cost method for creating and analysing photogrammetric 3D models of shallow reefs from diver-held camera footage. 3D models are analysed at scales 1-175 cm in terms of point-to-point distances, linear rugosity (R), fractal dimension (D), and vector dispersion ($1/k$). The 3D models' accuracy and precision were determined by comparisons with ground truths. The 3D models have root mean square errors of 1.35-1.48 cm in the X, Y and Z dimensions. Values of R from the 3D models were 86.8% accurate compared to *in-situ* chain-and-tape measurements. Values of D and $1/k$ were 86.9-99.6% accurate compared with ground truths from 3D printed objects modelled underwater. Data collected around Utila, Bay Islands, Honduras in the Caribbean showed that 3D metrics automatically calculated from the 3D models had the same predictive power for fish abundance and diversity as the more traditional Habitat Assessment Score (HAS). Like HAS, the 3D metrics explained 12-34% of variation in the fish data. A controlled experiment furthermore tested how $1/k$ affected sessile epibenthic organism settlement around Utila after one year. Results from approximately 200 3D printed recruitment tiles showed that $1/k$ significantly affected algae settlement, but not coral spat, polychaete, sponge, or bryozoan settlement. The results suggested that the surfaces of artificial reefs can be designed to minimise algal recruitment and that the availability of sheltered, reef-facing area influences epibenthic settlement more strongly than $1/k$ at the 1 cm scale. Finally, a convolutional neural network (CNN) learned patterns between the 3D models and fish data with just 85 data points. The CNN is a promising approach for analysing larger data sets without 3D metrics.

We suggest 3D models become a standard approach for measuring reef structural complexity. Not only can they explain as much variation in fish abundance and diversity as traditional measurements, but also they can non-destructively produce a variety of 3D metrics at numerous spatial scales and keep a permanent record of reef structure over time.

Three-Dimensional Modelling of Coral Reefs for Structural Complexity Analysis

Grace C. Young

Somerville College

University of Oxford

A thesis submitted for the degree of

Doctor of Philosophy

Michaelmas 2017

OSS Student No. 764886

This thesis is dedicated to Captain Bonnie Jean Waggoner,
my grandmother.

Contents

Acknowledgements **v**

Thesis Abstract **vii**

Declaration of Authorship **ix**

Formatting Notes **x**

1 Introduction **1**
1.1 The Economic and Ecological Value of Coral Reefs 1
1.2 The Importance of Coral Reef Structural Complexity 2
1.3 Metrics for Structural Complexity 7
1.4 Methods for Quantifying Coral Reef Topography 13
1.5 Thesis Aims 17

2 Cost and Time-Effective Method for Multi-Scale Measures of Rugosity, Fractal dimension, and Vector Dispersion from Coral Reef 3D Models **20**
2.1 Context 20
2.2 Author Contributions 22
2.3 Publication: Young, G. C., *et al.* "Cost and time-effective method for multi-scale measures of rugosity, fractal dimension, and vector dispersion from coral reef 3D models." *PLOS ONE* 12.4 (2017): e0175341. 22
2.4 Supplementary Material: Teaching Guides 41
2.5 Supplementary Material: Interactive 3D Models 42

3 Three-Dimensional Models of Coral Reefs Predict Caribbean Fish Abundance and Diversity **43**
3.1 Context 43
3.2 Author Contributions 45
3.3 Publication: Young, G. C., *et al.* "Three-Dimensional Models of Coral Reefs Predict Caribbean Fish Abundance and Diversity." *In Prep.* . 47

4 How Centimetre-Scale Structural Complexity Affects Sessile Epibenthic Organism Settlement on a Caribbean Reef 89
4.1 Context . . . 89
4.2 Author Contributions . . . 91
4.3 Publication: Young, G. C., *et al.* "How centimetre-scale structural complexity affects sessile epibenthic organism settlement on a Caribbean reef." *In Prep.* . . . 93

5 Convolutional Neural Networks Predict Fish Abundance from Underlying Coral Reef Texture 129
5.1 Context . . . 129
5.2 Author Contributions . . . 130
5.3 Publication: Young, G. C., *et al.* "Convolutional Neural Networks Predict Fish Abundance from Underlying Coral Reef Texture." *In prep.* 131

6 General Discussion 151
6.1 Key Findings & Implications . . . 151
6.2 Broad Applications . . . 155
6.3 Limitations and Future Directions . . . 161
6.4 Concluding Remarks . . . 169

References 171

Appendices

A Description of Data: 3D Models and Fish Data from Bonaire, Summer 2017 (Summer Following Chapter 3) 182

B Description of Data: 3D Models and Fish Data from Honduras, Summer 2017 (Summer Following Chapter 3) 183

C 3D Reconstruction as a Monitoring Strategy for Restoration of *Acropora palmata* on Coral Reefs in Bonaire 184

Acknowledgements

Thank you to my outstanding supervisors, Professor Alex Rogers, Dr. Dan Exton, and Dr. Victor Adrian Prisacariu. I am incredibly thankful for my peers in the Ocean Research and Conservation Group, especially Dr. Vanessa Lovenburg, Dr. Jesse van der Grient, Dr. Oliver Ashford, Dr. Michelle Taylor, Dr. Anni Djurhuus, Jack Laverick, Dr. Tom Hart, Hila Levy, Dr. Catherine Head, Dr. Caitlin Black, and Max Bodmer. Special shout out to Dr. Dominic Andradi-Brown for giving me direction in my foray into ecology, for organising our first field courses in rebreather diving, and for connecting me with the team at Operation Wallacea, which provided funding and permits for fieldwork. Equal thanks to my peers in the Active Vision Group, especially Dr. Duncan Frost, Dr. Piotr Bilinski, Oscar Rahnama, and Ruth Fong. Professor David Murray, I am grateful that you encouraged me and brought me into the Group. Dr. Daniel Lunn, I have ten words for you: zero-inflated negative binomial generalized linear mixed models with random effects.

The data in this thesis would not have been possible to collect if not for the dive operations staff at Operation Wallacea and Coral View, Utila. Particularly thank you to Grace Williams, Faye-Marie Crooke, Rich Astley, Sarah Laverty, and those divers listed in each chapter's acknowledgements. You made me not regret my decision to run an experiment with half a metric tonnes worth of coral settlement tiles that we carried across the island. Shagun Gupta, I still cannot believe that you stayed up until sunrise to help me demold the settlement tile casts.

Hundreds of hours of labour can turn into just one sentence in an academic paper. Chapter 4: "Tiles were retrieved from the reef between late-July and early-August..." Shout out to Shorvin Mcfield and Calvin Woods who helped jerry-rig milk crates so that they could safely hold many tiles while attached to lift bags that transported tiles to the surface. Faye, Grace, and Caitlin thank you for helping train the divers on how to use lift bags. Thanks to those divers who worked overtime to retrieve tiles: Jonathon Burroughs, Faye-Marie Crooke, Mary Ellen Fluharty, Tobias Hodnett, Anna Kelly, Jack Laverick, Shorvin Mcfield, Kirsty Porter, Naomi Slator, Prasanna Stephan Wijesinghe, Grace Williams, and Gina Wright.

Thanks to my fellow graduate students at Somerville College, especially Jeffery Martin. Also thanks to my team at the NASA Frontier Development Lab for helping bring me to speed on the machine learning methods that informed Chapter 5: Dr. Chedy Raissi, Dr. Yarin Gal, Adam Cobb, Agata Rozek, and Sean Marshall.

Finally, I would not have been able to pursue this degree without the Marshall Scholarship. Thank you to the Marshall Commission and to the people who helped me apply, especially Kim Benard, Professor John Osendorf, Bizzy Walton, and my parents. I am thankful for my Grandma Bonnie, to whom this thesis is dedicated, for cheering me along the way to Oxford. Thanks also to the scholarship from the Society of Naval Architects and Marine Engineers that financially enabled me to peruse my first expedition with the Ocean Research and Conservation Group. Also thank you to the teams and individuals who have fuelled my passion for ocean engineering, including families at Mission 31, SailFuture, National Geographic, and the Pisces VI submarine.

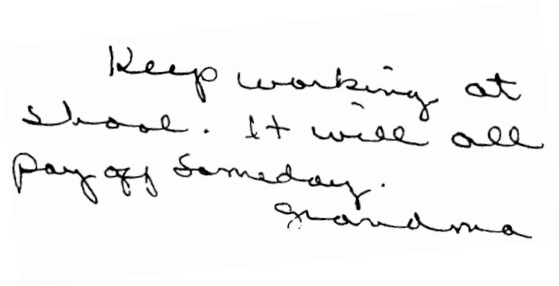

— Capt. Bonnie Jean Waggoner, 2015

Thesis Abstract

Coral reefs are some of Earth's most biodiverse and economically valuable ecosystems. Simultaneously they are among the most threatened by anthropogenic factors including global climate change. Their unique three-dimensional (3D) structural complexity is part of what enables them to provide their ecosystem services. It strongly affects species richness, abundance, and other indicators of ecosystem health.

This thesis explores the relationship between coral reef 3D structural complexity and ecosystem features. It has developed a new, low-cost method for creating and analysing photogrammetric 3D models of shallow reefs from diver-held camera footage. 3D models are analysed at scales 1-175 cm in terms of point-to-point distances, linear rugosity (R), fractal dimension (D), and vector dispersion ($1/k$). The 3D models' accuracy and precision were determined by comparisons with ground truths. The 3D models have root mean square errors of 1.35-1.48 cm in the X, Y and Z dimensions. Values of R from the 3D models were 86.8% accurate compared to *in-situ* chain-and-tape measurements. Values of D and $1/k$ were 86.9-99.6% accurate compared with ground truths from 3D printed objects modelled underwater. Data collected around Utila, Bay Islands, Honduras in the Caribbean showed that 3D metrics automatically calculated from the 3D models had the same predictive power for fish abundance and diversity as the more traditional Habitat Assessment Score (HAS). Like HAS, the 3D metrics explained 12-34% of variation in the fish data. A controlled experiment furthermore tested how $1/k$ affected sessile epibenthic organism settlement around Utila after one year. Results from approximately 200 3D printed recruitment tiles showed that $1/k$ significantly affected algae settlement, but not coral spat, polychaete, sponge, or bryozoan settlement. The results suggested that the surfaces of artificial reefs can be designed to minimise algal recruitment and that the availability of sheltered, reef-facing area influences epibenthic settlement more strongly than $1/k$ at the 1 cm scale. Finally, a convolutional neural network (CNN) learned patterns between the 3D models and fish data with just 85 data points. The CNN is a promising approach for analysing larger data sets without 3D metrics.

We suggest 3D models become a standard approach for measuring reef structural complexity. Not only can they explain as much variation in fish abundance and

diversity as traditional measurements, but also they can non-destructively produce a variety of 3D metrics at numerous spatial scales and keep a permanent record of reef structure over time.

Declaration of Authorship

I hereby declare that the work presented within this thesis is my own, conducted under the supervision of Professor Alex D. Rogers (University of Oxford, Department of Zoology), Dr Dan Exton (Operation Wallacea), and Dr Victor Adrian Prisacariu (University of Oxford, Department of Engineering Sciences); except those instances where others' contributions are specifically acknowledged. Any material and information quoted, paraphrased, or referenced from other sources, including figures, tables, or graphs, has been clearly indicated and their origins properly cited.

All data chapters (*i.e.,* chapters 2–5) are original scientific research papers that I have lead authored. The Director of Graduate Studies (Professor Adrian Thomas) granted me the permission to submit my thesis as a collection of papers prepared as for publication, but not necessarily yet published. I have written the manuscripts, and the majority of the work is directly attributable to me. Specific author contributions for each chapter are listed in CRediT Taxonomy (Contributor Roles Taxonomy), a nomenclature developed especially to identify scientific researchers' contributions in modern, collaborative projects (Allen et al., 2014; Brand et al., 2015). CRediT defines fourteen classifications for author contributions. I have contributed via all, or nearly all, of them for each chapter, as specified in chapters' author contributions sections.

This thesis is submitted in fulfilment of the requirements for the degree of Doctor of Philosophy at University of Oxford. It has not been submitted for any other qualification at any institution.

Formatting Notes

The main body of chapter 2 has been published (*PLoS One*), and appears as it was typeset in the journal to preserve formatting and readability. This stylistic choice is in accordance with the University's Examination Regulations for Research Degrees in Biological Sciences (Plant Sciences and Zoology), which permits that papers be incorporated as offprints bound in the body of the thesis (Section 1.10, Examination Regulations 2017-2018). The main bodies of chapters 3–5 constitute separate publications, each under revision for journals as indicated. They are presented as typescript pages, a stylistic choice also in accordance with Examination Regulations.

I realized I knew this woman. She's 3.5 billion years old. Her name is Mother Nature, and she's lived through more climate changes than anybody. So I called her up and she agreed to an interview ...

— Thomas Friedman, Journalist and Author, Oxford Sheldonian Theatre, January 2017

1 Introduction

Contents

1.1 The Economic and Ecological Value of Coral Reefs . . 1
1.2 The Importance of Coral Reef Structural Complexity 2
1.3 Metrics for Structural Complexity 7
1.4 Methods for Quantifying Coral Reef Topography . . . 13
1.5 Thesis Aims 17

1.1 The Economic and Ecological Value of Coral Reefs

Far more than a pretty facade, coral reefs not only have aesthetic and cultural value, but also are hugely important to human welfare. They support fisheries and tourism, protect shorelines, and perform carbon sequestration (Burke et al., 2011). In purely monetary terms, reef ecosystem services are valued at well over USD$1 trillion globally (Costanza et al., 2014; Hoegh-Guldberg et al., 2015; Heron et al., 2017). Other indicators reveal an even greater value for humans. For example, half a billion people depend directly on reefs for their livelihoods, and some 30 million reside in coastal and island communities that would cease to exist without reefs (TEEB, 2010).

Reefs cover just 0.1–0.5% of the ocean floor (Moberg and Folke, 1999), and yet they host an astounding one-quarter to one-third of all marine species (Plaisance et al., 2011; Fisher et al., 2014). Just 6.3 m^2 of coral can host over 525 species of crustaceans alone (Plaisance et al., 2011). *How is this possible?* Unfortunately we do not know. Reefs are one of the most productive, diverse, and complex systems on Earth, and they remain a mystery. Current methods for assessing marine ecosystems are inadequate (Plaisance et al., 2011), and estimates for undescribed marine species range from two-thirds to 91% (Mora et al., 2011; Appeltans et al., 2012; Fisher et al., 2014).

The tragedy here is that reefs, along with other marine ecosystems, are disappearing. The present generation may be the last with the opportunity to study living reefs, as trends predict sharp declines in reef structural complexity and diversity over the next few decades (Newman et al., 2015), bringing 90% of reefs in danger of total collapse by 2050 (Burke et al., 2011; Heron et al., 2017). Most of the world's coral reefs are already destroyed or severely degraded as a result of the combined effects of overfishing, pollution, disease, acidification and climate change (Carpenter et al., 2008; McClanahan et al., 2014; Heron et al., 2017).

Understanding current reef ecosystem dependencies is essential to restoring and conserving marine habitats. Towards that end, this thesis studies a particular feature of reefs: their structural complexity. The thesis investigates how reef structural complexity can be quantified; how it correlates with fish abundance and diversity; how it influences the settlement of coral larvae and other epibenthic creatures; and how it can integrate into learning algorithms that yield ecological insights. But first—*what is structural complexity and why do we care about it?*

1.2 The Importance of Coral Reef Structural Complexity

Structural complexity, the term I shall hereinafter use, is also called surface roughness (*e.g.,* Hobson (1972)), surface texture (*e.g.,* Hills and Thomason (1998)), topographic complexity (*e.g.,* Walker et al. (2009)), spatial heterogeneity (*e.g.,*

Luckhurst and Luckhurst (1978); Pittman et al. (2009)) or, more verbosely, "the spatial arrangement and diversity of surface types" (McCormick, 1994). The descriptor has implications across fields, particularly in engineering, geology and, more recently, ecology.

In studies spanning decades, ecologists have found multiple measures of structural complexity to be primary drivers of biodiversity (Hiatt et al., 1960; McCormick, 1994; Knudby and LeDrew, 2007; Dustan et al., 2013; Richardson et al., 2017). It is a key feature of a healthy ecosystem, not simply because living things create structure, but also because structure must exist for living things to thrive. An analogy is in urban development: The availability of housing, shopping centres, places of work, *etc.* brings people to certain areas, and *vice-versa*; the people in those areas create those structures. In this context, Scleractinian corals (*i.e.,* stony or hard corals), sponges, and other reef-building organisms are examples of ecosystem engineers because they control other organisms' access to resources (Jones et al., 1997; Ritson-Williams et al., 2009). They are also examples of ecological facilitators because they enable positive species interactions (Bruno et al., 2003; Idjadi and Edmunds, 2006).

Underwater, a complex structure has a relatively large surface area with many refuges (hiding places) for creatures of various sizes (Beukers and Jones, 1997); it scatters light, allowing organisms to find areas of shade as they need (Obura, 2005); and it rescales turbulence, creating niches (Johansen et al., 2008) and pockets of nutrient flow (Hearn et al., 2001). Figure 1.1 illustrates the concept of structural complexity in marine habitats.

A marine ecosystems' structural complexity therefore influences several reef processes that are integral to a healthy reef, including fish recruitment, which affects grazing intensity, which affects algae cover, which affects coral recruitment, which in turn affects structural complexity and so on (Mumby and Steneck, 2008). Figure 1.2 depicts how these intertwined causes and effects integrate conceptually.

Several studies show that structural complexity correlates with key features of a healthy marine ecosystem. From a meta-analysis of 158 publications examining the

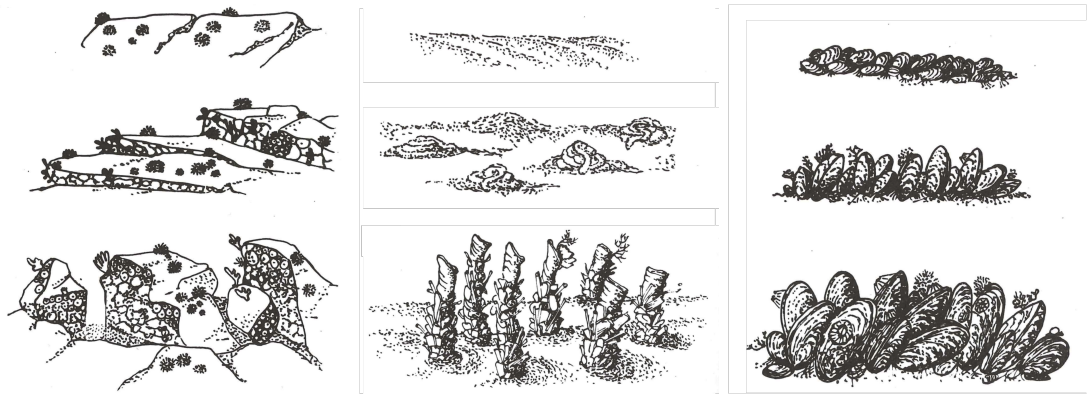

Figure 1.1: Depictions of structural complexity in three contrasting marine habitats (from left to right: rocks, flora, and mussel bed) Structural complexity increases from low to high from top to bottom. More complex habitats are associated with greater diversity because they provide ecosystem services to creatures living there, such as refuges and variable light and hydrodynamic conditions. Credit: Sebens (1991) with permission.

role of structural complexity[1] across 150 reef locations worldwide, Graham and Nash (2013) noted several recurring correlations. Fish density and biomass, algal cover, live coral cover, and urchin density all correlated with structural complexity, as summarized in Table 1.1. Their meta-analysis additionally suggested that structural complexity positively correlated with tourism and shoreline protection, although it could corroborate this claim only with qualitative data.

Publications since Graham and Nash (2013) have either bolstered or not refuted the study's conclusions. Perhaps the only other study on the same relatively large scale, Darling et al. (2017) surveyed 157 sites across Seychelles, Maldives, the Chagos Archipelago, and Australia's Great Barrier Reef. The study found that structural complexity[2] and reef zone (crest, flat, or slope) most strongly predicted reef fish abundance, biomass, species richness, and trophic structure. The other predictors they measured were: coral traits, diversity, and life histories. These other predictors drove structural complexity and provided additional predictive power, but were not as strong predictors as structural complexity and reef zone. Recent studies have also been able to attribute region-wide flattening of Caribbean coral

[1]Graham and Nash (2013) assessed papers that measured structural complexity by rugosity via the chain-and-tape method, as discussed in Section 1.3: *Metrics for Structural Complexity.*

[2]Darling et al. (2017) quantified structural complexity by having a diver rate a reef on a six-point visual scale, from 0 (flat) to 5 (highly complex); this and other metrics are discussed in Section 1.3: *Metrics for Structural Complexity.*

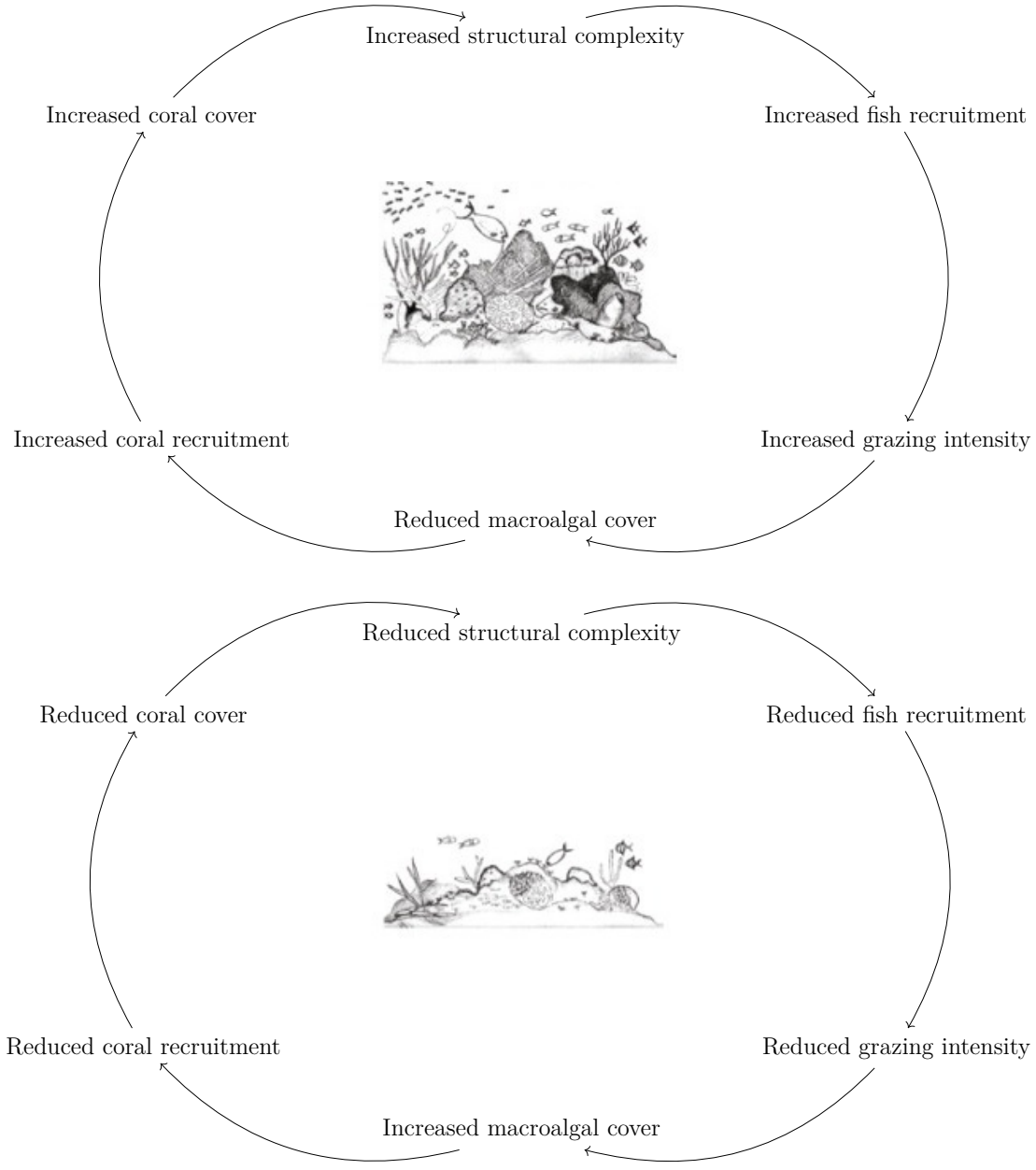

Figure 1.2: Cascading feedback mechanisms on a marine ecosystem. Top diagram shows dependencies within an ecosystem with high structural complexity. Lower diagram shows the same dependencies within a low-complexity ecosystem. Inset drawings (credit Mumby and Steneck (2008) with permission) depict example ecosystems. Diagram by author (G. Young); concepts from Mumby and Steneck (2008) with permission.

Table 1.1: General trends between structural complexity (as measured by chain-and-tape rugosity) and reef ecosystem features that were highlighted in the meta-analysis by Graham and Nash (2013). Strong correlations had a Spearman's rank correlation coefficient (ρ) of $0.60 \leq \rho \leq 0.79$, while weak correlations had $0.20 \leq \rho \leq 0.39$. Rather than reporting precise values of ρ, general trends are summarized for clarity and simplicity. The precise values of ρ depend upon factors such as the fish family, reference source, and fish-counting method. All correlations were signifigant ($P \leq 0.05$). Ecological notes are quoted from Graham and Nash (2013).

Variable	Correlation with Structural Complexity	Ecological Notes
Fish Density and Biomass	+, strong	"[this correlation is] likely mediated through density-dependent competition and refuge from predation."
Algal Cover	−, strong	"[this correlation] may reflect the important role complexity plays in enhancing herbivory by reef fishes."
Live Coral Cover	+, weak	"[coral] may be creating much of the structure, resulting in a collinear relationship; however, there is also evidence of enhanced coral recovery from disturbances where structural complexity is high."
Urchin Density	−, strong	"[this correlation] may be driven by urchins eroding reef structure or by their gregarious behaviour when in open space."

reefs (Alvarez-Filip et al., 2009) to declines in coral and fish species (Newman et al., 2015), with the loss of physical habitat structure leading potentially to a three-fold reduction in Caribbean fisheries productivity (Graham, 2014; Rogers et al., 2014).

As an indicator of overall ecosystem health, structural complexity could inform reef management decisions. For example, a manager might identify areas with low structural complexity and choose to enhance those areas through protection, or by transplanting organisms or artificial structures. Alternatively, a manager may choose to prioritize the protection of a region with high structural complexity because with a minimal birds-eye-view surface area it will likely contain maximal organism density. Structural complexity is also relatively easy to measure as a quantitative variable, so managers can record and compare it over time to reveal statistically how decisions impact the reef. For these reasons, several papers suggest that structural complexity

measurements should be incorporated into reef monitoring programs (Wedding et al., 2008; Hinderstein et al., 2010; Mumby et al., 2014; Darling et al., 2017).

This section has introduced the concept of structural complexity and why it is important on coral reefs. The following section describes means of quantifying structural complexity, and in doing so it further, and more precisely (mathematically), defines what structural complexity is. Crucially, these metrics provide unbiased means of repeatedly assessing structural complexity across locations, and thereby are the ways in which structural complexity can be incorporated into experiments or monitoring programs.

1.3 Metrics for Structural Complexity

Measuring complexity is itself a complex task. While structural complexity is in some ways intuitive, quantifying it is not. For example, a human would instinctively rate the surfaces in Fig. 1.3 as having low, medium, and high structural complex relative to each other. *But how might a computer come to the same conclusion?* Viewed at different scales, the surfaces could appear to have vastly different structural complexities. From far away, the medium complex surface may appear as a flat plane. Likewise, extremely close-up, part of the highly complex surface is a flat plane. Moreover, if a computer only sampled points on the tops of the pyramids on the medium complexity surface (Fig. 1.3(b)), then it would see a flat plane, the same as the low complexity surface. Quantitative, replicable measurements of structural complexity are necessary for humans or computers to reliably predict structural complexity and its dependent features, such as how creatures of different sizes perceive the structure and their ambit, how particulate matter will lodge itself on the structure, how sediment will either settle on or roll off the structure, or how light will scatter on the structure.

Engineers were some of the first to devise ways of measuring structural complexity. They did so for practical reasons, out of necessity. For example, *how do you communicate what type of sandpaper is best for a job?* You can describe its grit, a standard classification of roughness. *A part only works when its roughness is "right;"*

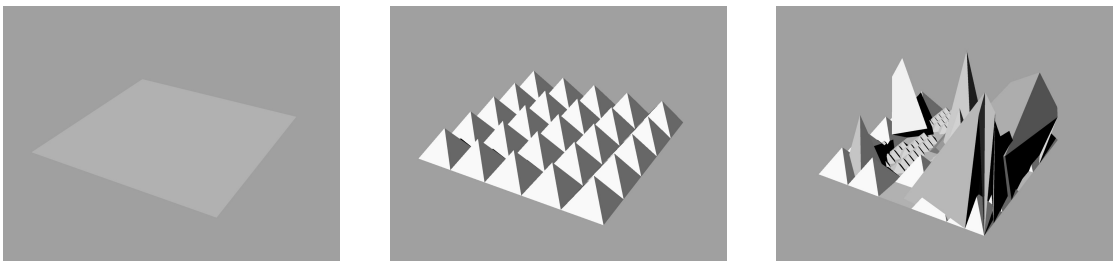

(a) (b) (c)

Figure 1.3: Abstract surfaces (drawn as examples) with low, medium, and high structural complexity, relative to each other, from left to right.

what does "right" mean in this case? "Right" might mean that the part's average roughness falls within a certain range, where roughness is quantified as the absolute deviation of the surface from a mean line over a sampling length as in Thomas (1981). *How can you determine the degree of wear a surface has undergone?* You might calculate the root mean square of the surface profile as in Myers (1962).

Thomas (1981) overviews 36 of the "proliferation" of "redundant parameters for characterizing surface roughness" in the field of engineering. The parameters range from fairly straightforward, such as average peak-to-valley height, mean separation between the highest peaks and lowest valleys over a unit distance, and root mean square deviation of the profile, to reasonably involved, such as distance over which an exponential autocorrelation function decays to 10% of its initial value, "skewness" measured by the third central moment of the profile amplitude probability density function, and others. The author gets close to a concise way of characterizing surface roughness; he suggests a classification incorporating average roughness, skewness, high-spot count, and extrema density. However, there is danger in oversimplifying. *Where do you set the unit distance? Which parameters are most meaningful for a given application and easiest to acquire with the available measurement tools?* For this reason, Thomas (1981) concludes that the parameters are non-superfluous:

> *If he [the user] finds that in his experience the most effective parameter for his purpose is the difference between say the fifth highest peak and the seventh lowest valley within a millimetre, then this is the parameter which he should use, and he should harass the instrument manufacturer [or reef researcher, in our case] until it is provided.*

In other words, each measurement has its merits. Geologist Hobson (1972) likewise avoids defining structural complexity in an all-encompassing way. His chapter in *Spatial Analysis in Geomorphology* reads much like the conclusion of Thomas (1981):

> *A single concise definition of surface roughness is probably impossible. The only usable definitions are incomplete because they describe only a few of the physical or mathematical properties of a surface. There may be as many of these definitions as there are roughness studies themselves.*

Ecologists first considered structural complexity in the context of forests. They had to (and have to) consider it as an ecosystem feature interdependent with other features, such as species function and composition. To quote an example from a forest-centred paper:

> *[A] structural attribute such as dead wood can also be a good indicator of functional attributes such as decomposition and nutrient cycling processes [Franklin et al., 1981]*. Similarly, compositional attributes, such as species composition and abundance can be indicators of structural attributes such as canopy layering [Franklin et al., 2002]*, or of functional attributes such as flowering and bark shedding [Kavanagh, 1987]*.*
> *full reference in McElhinny et al. (2005)

McElhinny et al. (2005) rise to the challenge of devising a metric, or rather a suite of metrics, to help better understand the interdependent factors that contribute to structural complexity in a forest ecosystem. They list 36 revealing attributes upon which a measure of structural complexity that is "an efficient and effective biodiversity surrogate" can be based. Attributes they list are as specific as canopy cover, standard deviation of tree height, and volume of coarse woody debris, among others. Like their predecessors in engineering and geology, they note the broad nature of the work: "Structural complexity is a relative, rather than absolute concept" (McElhinny et al., 2005).

In the same style as McElhinny et al. (2005) did for forests, Table 1.2 summarizes the existing metrics for quantifying coral reef structural complexity, presented in alphabetical order. In other publications these metrics are also referred to as "morphometrics" (*e.g.,* Pittman et al. (2009)), "terrain descriptors" (*e.g.,* Robert et al. (2017)), or more verbosely "quantitative descriptor variables of relevance to benthic habitat" (Wilson et al., 2007a). Even a cursory scan of Table 1.2 shows that

the statement by McCoy and Bell (1991) still holds true: "The study of habitat structure has spawned a bewildering complexity of narrowly defined terms, the same term often possessing several meanings."

Table 1.2: Mathematically distinct metrics for quantifying coral reef 3D structural complexity. Where metrics have been referred to with several names, SD is an abbreviation for standard deviation. All variables are described after their first usage.

Metric	Mathematical Description	References
Coefficient of variation in substratum heights	$\frac{1}{\bar{z}}\sqrt{\frac{\sum_{i=0}^{n_pts}(z_i-\bar{z})^2}{n_{pts}}}$, where z_i is the height of the surface at point i, $\bar{z}$ is the average z height, and n_{pts} is the total number of points on the surface or needles on the profile gauge (Fig. 1.4).	Included in overview by McCormick (1994), it was the only metric they reviewed that could not differentiate between surface types commonly found on coral reefs.
Fractal dimension	There are several methods for estimating fractal dimension. The simplest is that for a line, where it equals: $\frac{log(N(x_1)/N(x_2))}{log(x_2/x_1)}$, See explanation in Fig. 1.5 — x_1 is a length of a straight line and $N(x_1)$ is the number of times that straight line fits head-to-tale along the irregular line. x_2 and $N(x_2)$ follow likewise, but x_2 is a different length.	Originally developed by Mandelbrot (1982), and then applied to corals by Mark (1984); Martin-Garin et al. (2007); Wilson et al. (2007a); Reichert et al. (2017), among others.
Rugosity via chain-and-tape method	$\frac{\text{length undraped chain}}{\text{length draped chain}}$, as illustrated in Fig. 1.6.	Developed by Luckhurst and Luckhurst (1978); Risk (1972).
Rugosity via non-traditional methods	$\frac{\text{surface area}}{\text{planar area}}$, as illustrated in Fig. 1.6.	Also called "the ratio of 3D/2D surface area" (Burns et al., 2015), "tortuosity" (Leon et al., 2015), "surface rugosity" (Pittman et al., 2009), or "area-based rugosity" (Friedman et al., 2012).
SD of the angle θ_1 in Fig. 1.4	$\sqrt{\frac{\sum_{i=0}^{n_pts}\left(\theta_{1_i}-\bar{\theta_1}\right)^2}{n_{pts}}}$, where θ_1 is the angle in Fig. 1.4 and $\bar{\theta_1}$ is the average of θ_1.	Developed by McCormick (1994), who called this "vector SD" and noted that is essentially a 2D version of vector dispersion.

continued on next page ...

Table 1.2 continued: Mathematically distinct metrics for quantifying coral reef 3D structural complexity. Where metrics have been referred to with several names, the synonymous names are listed in the References column. SD is an abbreviation for standard deviation. All variables are described after their first usage.

Metric	Mathematical Description	References
SD of the angle θ_2 in Fig. 1.4.	$\sqrt{\frac{\sum_{i=0}^{n_pts}\left(\theta_{2_i}-\bar{\theta_2}\right)^2}{n_{pts}}}$, where θ_2 is the angle in Fig. 1.4.	Included in overview by (McCormick, 1994), who called this "substratum angle SD."
SD of substratum heights	$\sqrt{\frac{\sum_{i=0}^{n_pts}\left(z_i-\bar{z}\right)^2}{n_{pts}}}$	Included in overview by McCormick (1994). Dustan et al. (2013) used this metric as well, but called it "Digital Reef Rugosity."
Slope	$\frac{z_{i+1}-z_i}{\Delta x}$, where Δx is the spacing between the pins on the profile gauge (Fig. 1.4) or points in a 3D point cloud.	Applied to coral reef 3D models by Burns et al. (2015); Friedman et al. (2012), among others.
Slope-of-the-slope	$\frac{z_{i+2}-2z_{i+1}+z_i}{(\Delta x)^2}$	Also referred to as curvature, Burns et al. (2015) applied this metric to coral reef 3D models.
Sum of consecutive height differences	$\sqrt{\sum_{i=0}^{n_{pts}}(z_{(i+1)}-z_i)^2}$, where $z_{(i+1)}$ is adjacent to the point with height z_i.	Developed by McCormick (1994).
Vector dispersion	$\frac{n_{srf}-R}{n_{srf}-1}$, where $R^2=\left(\sum_0^i cos_{x_i}\right)^2+\left(\sum_0^i cos_{y_i}\right)^2+\left(\sum_0^i cos_{z_i}\right)^2$ and cos_{x_i} is the directional cosine of vector normal to the ith surface with respect to the X-axis; cos_{y_i} the same, but with respect to the Y-axis; and so on; n_{srf} is the number of non-overlapping triangles formed by contiguous equally-spaced points.	Developed by Carleton and Sammarco (1987).

continued on next page ...

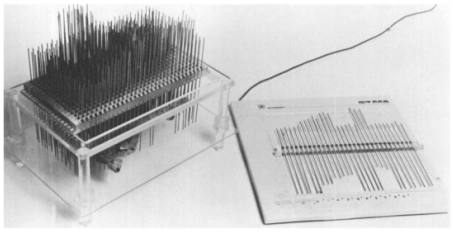

(a) Profile gauge (Carleton and Sammarco, 1987)

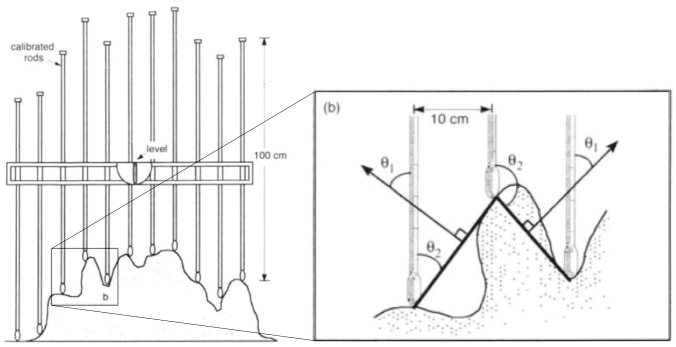

(b) Profile gauge (McCormick, 1994)

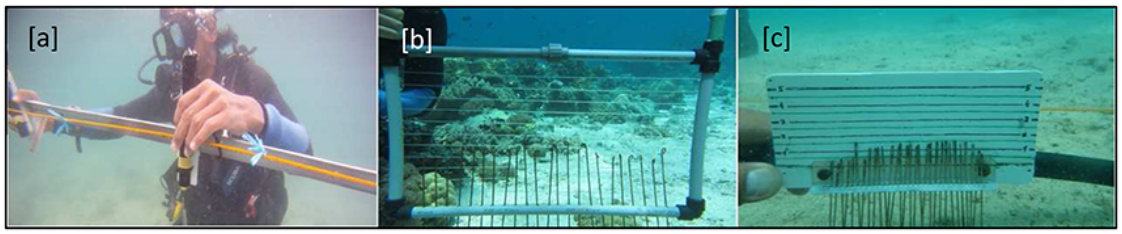

(c) Profile gauge variant (Yanovski et al., 2017)

Figure 1.4: Examples of profile gauges used to capture topographic information for several of the structural complexity calculations listed in Table 1.2. (a) "Three-dimensional profile gauge for measuring surface irregularity and other physical characteristics of benthic substrata, and digitizing board used for entering data into computer." Credit: Carleton and Sammarco (1987) with permission. (b) "Profile gauge used to measure surface topography. Inset shows the angular measures used in the calculation of vector SD (θ_1) and substratum angle SD (θ_2)." Credit: McCormick (1994) with permission ©Inter-Research 1994. (c) Devices by for taking "Point-Intercept Contour" measurements (Yanovski et al., 2017). Avalible through Creative Commons Attribution License (CC BY).

Table 1.2 continued: Mathematically distinct metrics for quantifying coral reef 3D structural complexity. Where metrics have been referred to with several names, the synonymous names are listed in the References column. SD is an abbreviation for standard deviation. All variables are described after their first usage.

Metric	Mathematical Description	References
Visual scores	Rugosity, height, and refuge size categories	Developed by Gratwicke and Speight (2005b) for the habitat assessment score (HAS). Reviewed by Wilson et al. (2007b).

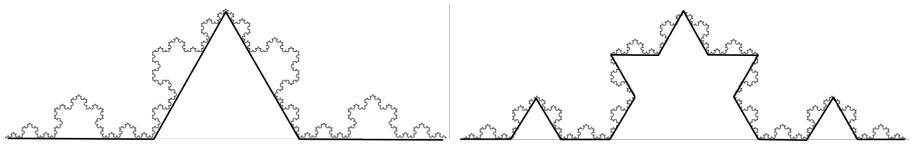

(a) $x_1 = 1$ unit of length; $N(x_1) = 4$ **(b)** $x_2 = \frac{1}{3}$ unit of length; $N(x_2) = 16$

Figure 1.5: Illustration of the fractal dimension calculation. $N(x)$ is the number of line segments of length x it takes to cover the complex curve. On this example, fractal dimension equals $log(N(x_1)/N(x_2))/log(x_2/x_1) = log(4/16)/log(\frac{1}{3}/1) \approx 1.26$. Original images of Koch snowflake available through a Creative Commons license (CC BY-SA 3.0) and modified by author (G. Young).

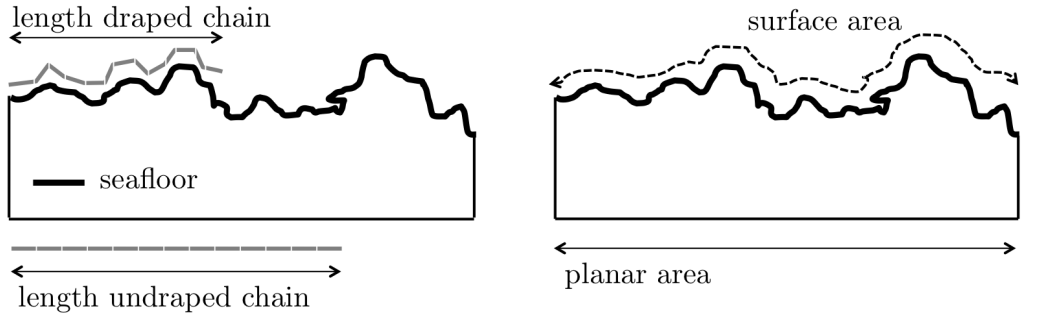

(a) $R_1 = \frac{\text{length undraped chain}}{\text{length draped chain}}$ **(b)** $R_2 = \frac{\text{surface area}}{\text{planar area}}$

Figure 1.6: Illustration of rugosity calculations. (a) Rugosity via chain-and-tape method (R_1), where R_1 = length undraped chain/length draped chain. (b) Rugosity via non-traditional methodology (R_2), where R_2 = surface area/planar area. Illustrations by author (G. Young).

1.4 Methods for Quantifying Coral Reef Topography

Table 1.2 reviewed metrics that have been used to quantify coral reef structural complexity. With the exception of visual scores, each metric requires a mathematical surface that represents the reef. Metrics can therefore only be as precise and accurate as the surface representation used to calculate them.

Technological advances in the last decade have enabled several methods that can create such surface representations. By far, the chain-and-tape method is most widely employed by marine researchers. It is so ubiquitous that the most recent (as of Sunday 27$^{\text{th}}$ May, 2018) meta-analysis of structural complexity on coral reefs was only able to compare studies that used either the chain-and-tape

method or the value derived from such a measurement because of the "limited scale and replication" of studies employing alternative methods (Graham and Nash, 2013). The meta-analysis admits, in the first sentence of its abstract, that relying on this metric alone has "restricted our understanding of the role of complexity in the ecosystem." Others have made similar warnings, stressing the need for alternate methods (Friedlander and Parrish, 1998; Merks et al., 2003; Goatley and Bellwood, 2011; Plaisance et al., 2011).

The following describes methods for quantifying coral reef topography. Methods are listed in roughly chronological order, based on the publications of them being applied on reefs. Note that several studies focus on classification of seabed imagery; *e.g.,* Dartnell and Gardner (2004) used sonar to classify seafloor as either rock, gravelly-muddy sand, muddy sand, or mud. While classifications can be tied to concepts of structural complexity, they do not yield point cloud representations of reef structure and are therefore not included in this list.

Chain-and-Tape Developed by Risk (1972), for this measurement a diver drapes a chain over the seabed (Fig. 1.6(a)). He then calculates the ratio between the length that the draped chain reaches and the total length of the chain. Surfaces where the chain lies flat have a ratio close to 1, whereas surfaces where the chain dips greatly have higher ratios, indicating complexity. Commonly chains are 3–10 m in length with link lengths less than 1.5 cm (Graham and Nash, 2013). While it is a quick and inexpensive means of estimating rugosity, it can cause damage to the benthos and yield potentially misleading results (Goatley and Bellwood, 2011).

Profile Gauge A profile gauge contains pins that drop onto a surface (example in Fig. 1.4 of Section 1.3, page 12). The pins' positions reveal the contour of a surface. It does not record surface underhangs (it is as if you draped a blanket over the surface) and the contour resolution is limited to the spacing of the pins. It was a popular method in studies >20 years old, including Carleton and Sammarco (1987) and McCormick (1994). It was also used by

the more recent study by Yanovski et al. (2017) (Fig. 1.4), who call it the "Point-Intercept Contour" method. Like the chain-and-tape method, it can damage the benthos and yield potentially misleading results (Goatley and Bellwood, 2011).

Sonar (SOund, NAvigation and Ranging) Sonar has been widely used to capture bathymetric data since the technology's conception in 1912. The invention was spurred by the *Titanic* disaster, which forefronted ships' need to detect and avoid icebergs and other submerged structures. Pratson and Edwards (1996) summarize its early history, with hundreds of studies showing its modern applications (*e.g.,* Huvenne et al. (2002); Wilson et al. (2007a); Zawada et al. (2010)). The spatial resolution of 3D reconstructions from sonar depends upon several variables, principally the sonar's frequency, viewing angle, and its distance or depth from the structure. Generally sonar's resolution is lower than that obtained by optical cameras (Campos et al., 2011). Low frequency systems such as GLORIA (6.5 kHz) can map spatial resolution on the order of tens of meters (*e.g.,* Moore and Normark (1994)). High frequency systems such as the 200 kHz system used by Purkis et al. (2005) can map spatial resolutions on the order of centimetres. The main drawbacks of sonar in this context (of creating 3D seafloor maps for scientific study) are (a) cost, which can be tens of thousands of dollars, depending on equipment and support vessel or vehicle, (b) minimum depth requirement of about 15 m, although the exact depth depends on a range of factors as discussed by Costa et al. (2009), and (c) negative effects upon marine life (Williams et al., 2015).

Structure-From-Motion (SfM) Photogrammetry For this method, a computer vision algorithm determines 3D structure from overlapping 2D images of a scene. The images must capture the scene from different angles. The algorithm's mathematical foundations date back to the 1830s, the same decade as the invention of the camera (Kraus, 2007). The first instances of photogrammetry being applied underwater date back to the Cold War

(Pollio, 1968; Leatherdale and Turner, 1983). Bythell et al. (2001) are one of the first to apply the method to coral reefs for ecological studies, and its power has increased substantially with computing power (Beall et al., 2010; Hu et al., 2012; Campos et al., 2015; Burns et al., 2015; Leon et al., 2015). Structure-from-Motion (SfM) is a type of photogrammetry; the term implies that the camera is moving through the environment. A downside of this method is that it cannot model structural elements that the camera cannot see, such as the underneath of under-hangs or other occluded features. This method is used in this thesis and is further discussed in Chapters 2–3.

Raster Satellite Imagery Purkis et al. (2008) successfully combined information from satellite imagery, vessel-based acoustic bathymetry, acoustic current profiles, and underwater visual census (derived from 2D photo mosaics and point-observations from divers) to calculate rugosity and other measures of structural complexity (or "seabed character and architecture"). In general, however, satellite imagery cannot provide fine details of underwater structure because of its limited spatial resolution (Hu et al., 2012).

Stereo Imagery with Underwater Position Estimation Pizarro et al. (2009) and Johnson-Roberson et al. (2010) developed this method with data from underwater vehicles. Mahon et al. (2011) showed how the same method could be used with data from a snorkeller or diver swimming with a stereo camera rig. In both cases, underwater positions are estimated by simultaneous localization and mapping (SLAM) algorithms. Previous studies did not state spatial accuracy of their 3D reconstructions, but Friedman et al. (2012) applied a similar method and suggest the spatial resolution is on the order of centimetres.

Laser Scanning (including LiDAR) Lasers measure distance by illuminating a target with a laser and analysing the reflected light. Pittman and Brown (2011) among others have used this method to map reefs up to 50 m deep at a resolution of ≈4 m; they explain: "Water depth was calculated by comparing the return times from a green laser reflected off the substratum

and an infrared laser reflected off the sea surface to form a height datum, together with information on aircraft altitude and heading and GPS surface height data." LiDAR can be an alternative to sonar in shallow water coral reef ecosystems (<50 m depth); the two methods are compared by Costa et al. (2009).

Digital Reef Rugosity (DRR) Developed by (Dustan et al., 2013), DRR is collected with a digital level gauge, an instrument that uses readings from a ceramic pressure transducer to estimate depth 0–30 m with a resolution of 0.41 ± 1.5 cm (plus uncertainty from wave height variation). As used by (Dustan et al., 2013), the DRR recorded depth every second while a diver (or vehicle, in theory) moved the DRR at about 10 cm/sec; the device could thereby estimate a point on the reef contour approximately every 10 cm.

Methods have also been combined. For example, Kunz and Singh (2013) combined footage from single camera with range data from a multibeam sonar from an underwater vehicle to create 3D models with spatial resolution on the order of several centimetres. Robert et al. (2017) combined SfM photogrammetry with multibeam echosounder data from underwater vehicles to create 3D models with spatial resolution on the order of several millimetres.

All the methods presented above, except chain-and-tape, can return a point cloud representing the contour of the reef, and those points can be used to calculate any of the metrics of structural complexity listed in Table 1.2. Researchers will choose the best method for quantifying reef topography in their given context based on the resources available to them and the required spatial scale of their model.

1.5 Thesis Aims

Alice: Would you tell me, please, which way I ought to go from here?
The Cheshire Cat: That depends a good deal on where you want to get to.
— Lewis Carroll, *Alice in Wonderland*

Considering the existential crisis facing coral reefs, it is natural to wonder whether academics' time is better spent on active conservation rather than pursuit of pure knowledge. While this thesis research will add to our body of knowledge, it also has a very practical conservation objective. Understanding how and what structural complexity correlates to the health of dependent marine life will help determine how best to replicate the most effective structures, either when restoring degraded reefs or constructing artificial reefs. While such restoration efforts do not address the root causes of coral reef destruction (*e.g.,* pollution, climate change, acidification) they do offer a means to preserve reef-dependent marine life until we can resolve the root problems.

The following chapters (2–5) address previously unanswered questions related to the role of structural complexity in the marine environment. The research employs a method, 3D modelling from structure-from-motion photogrammetry, that is currently used only by a handful of marine researchers. Each chapter includes a stand-alone publication as the main text, in addition to a context section highlighting its relationship to other parts of the thesis and an author contributions section acknowledging the input of others.

Chapter 2 describes a new method for rendering and interpreting 3D models of small ($\approx$ 2 x 2 m) patches of coral reef using consumer grade electronics. It also outlines a protocol for routinely determining models' precision and accuracy, and establishes the precision and accuracy of the 3D models that are used in subsequent chapters. Three of the metrics for quantifying reef structural complexity from Table 1.2 are honed in upon: rugosity, fractal dimension, and vector dispersion. The rationale for choosing those metrics and the methods for calculating them are detailed in the chapter. To our knowledge, the method has already been used by a variety of researchers worldwide (detailed in 2.1). There is therefore potential for the method to have far-reaching impact, beyond the research described in subsequent chapters of this thesis.

For Chapter 3, 85 patches of coral reef (2x2 m) in the Caribbean were 3D modelled by applying the method described in the previous chapter. Data from

the 3D models is paired with fish survey data that was collected above each section of 3D modelled reef. The study assesses correlations between the metrics of structural complexity and the fish survey data. It compares how well the 3D metrics predict fish survey date compared to the more traditional metrics of rugosity and Habitat Assessment Scores (HAS). We show why 3D modelling is complementary or preferable to other methods of quantifying reef topography.

Whereas the preceding chapter describes a correlation study, chapter 4 describes a controlled experiment. We actively manipulate the structural complexity of recruitment tiles in terms of one of the metrics, vector dispersion, described in Table 1.2. The experiment attempts to better understand the reasons behind correlations with structural complexity metrics and the settlement of epibenthic organisms, including corals, sponges, algae, polychaetes, and bryozoans.

The preceding chapters make several allusions to how increased computing capacity and/or additional data could yield further ecological insights. Chapter 5 describes one pipeline for processing vastly more 3D models. The pipeline uses computer vision techniques, so that the whole 3D model feeds into a learning algorithm that regresses residential fish abundance. It therefore does away with metrics of structural complexity, replacing them with the whole 3D model. It uses the data from Chapter 3 to demonstrate the data analysis paradigm. While the results are inconclusive, it discusses how further data and pipeline refinement could yield ecological insights.

Finally, the general discussion in chapter 6 highlights overarching trends from the previous four data chapters and unexpected features and limitations of the methods. It also presents thoughts for future studies of coral reef structural complexity, particularly in regards to technologies that may be, or are being, developed for such assessments. As a whole, the thesis aims to add to the body of scientific knowledge regarding coral reef structural complexity, particularly on the technologies and mathematical models for quantifying structure and its associated features.

The engineer's first problem in any design situation is to discover what the problem really is.

— Sir Henry Royce OBE

Engineers like to solve problems. If there are no problems handily available, they will create their own problems.

— Scott Adams, Cartoonist

2

Cost and Time-Effective Method for Multi-Scale Measures of Rugosity, Fractal dimension, and Vector Dispersion from Coral Reef 3D Models

Contents

2.1 Context 20
2.2 Author Contributions 22
2.3 Publication: Young, G. C., *et al.* "Cost and time-effective method for multi-scale measures of rugosity, fractal dimension, and vector dispersion from coral reef 3D models." *PLOS ONE* 12.4 (2017): e0175341. . 22
2.4 Supplementary Material: Teaching Guides 41
2.5 Supplementary Material: Interactive 3D Models . . . 42

2.1 Context

This chapter, 'the methods chapter,' describes a method for rendering and interpreting 3D models of small (≈2 x 2 m) patches of coral reef using consumer grade electronics. It also outlines a protocol for routinely determining model precision and accuracy. The method was developed especially to meet the functional

requirements of expeditions led by Operation Wallacea, the organisation that facilitated fieldwork for Chapters 2–4 of this thesis. Ultimately Operation Wallacea became just one example of an organisation that has made excellent use of the method. A variety of researchers and enthusiasts can and have also employed the method. It has several features that distinguish it from the few other published methods for cost-effectively creating 3D models of reefs, as summarised below.

(a) The method can render 3D models from footage filmed on an uncalibrated consumer-grade camera. The footage may be shaky, shot in non-ideal (underwater) lighting conditions, and/or have particulate matter tainting frames. The paper includes example renderings, but 2D depictions of 3D scenes are not ideal, so Section 2.5 (Supplementary Material: Interactive 3D Models) contains instructions for viewing the models in 3D.

(b) The precision and accuracy of the 3D models is suitable for ecological studies. The method achieved coefficents of variation <2% for all 3D metrics of structural complexity and root mean square errors <1.5 cm in all dimensions, as detailed in the paper.

(c) The total computing load required for the method (including filming, rendering, and analysing) can be divided between students' laptops (*i.e.,* laptops up to 5 years old with standard capability or ≥8 GB RAM, 600MB free disk space). This enables students to 'own' their data from collection to analysis and be responsible for backing it up, as it is stored locally on their machines.

(d) All processing can take place offline; this was necessary because Internet is at best unreliable on many remote research sites, such as where Operation Wallacea operates.

(e) All steps of the method, including computation of structural complexity metrics, can be completed with free or low-cost software that students can download onto their own computers and learn after a 6-hour workshop; this was accomplished by providing open-source Python scripts that preformed

the desired computations at the click of a button. The teaching materials for these workshops are available via Section 2.4 (Supplementary Material: Teaching Guides) and all Python scripts are available open-source.

(f) Researchers can obtain several data points for a site, and data points can be spaced apart by arbitrary distances. Each data point is a 3D model of reef at the quadrat-scale (0.25–4 m^2).

(g) The method is fast and automated enough for researchers to fully process their data on same day that they collected it; in other words, data analysis is not a bottleneck or time sink.

To our knowledge, researchers in the following locations have already employed the method: Indonesia, Madagascar, Honduras, and Cuba by Operation Wallacea, Bonaire by two Oxford Masters students and the Coral Restoration Foundation, Tobago by Cardiff University researcher Kathryn Ellen Whittey, Chagos by two Oxford doctoral students, and the Maldives by the Four Seasons Resort coral restoration team.

2.2 Author Contributions

Author contributions are listed at the end of the manuscript in CRediT Taxonomy (Contributor Roles Taxonomy) nomenclature (Allen et al., 2014).

2.3 Publication: Young, G. C., *et al.* "Cost and time-effective method for multi-scale measures of rugosity, fractal dimension, and vector dispersion from coral reef 3D models." *PLOS ONE* 12.4 (2017): e0175341.

Pages 23–40 of this thesis include an offprint of the publication. This formatting choice is consistent with the University's Examination Regulations for Research Degrees in Biological Sciences (Plant Sciences and Zoology).

PLOS ONE

RESEARCH ARTICLE

Cost and time-effective method for multi-scale measures of rugosity, fractal dimension, and vector dispersion from coral reef 3D models

G. C. Young[1,2]*, S. Dey[3], A. D. Rogers[1☯], D. Exton[2☯]

1 Department of Zoology, University of Oxford, Oxford, United Kingdom, **2** Operation Wallacea, Wallace House, Lincolnshire, United Kingdom, **3** ThinkSee3D Ltd., Eynsham, United Kingdom

☯ These authors contributed equally to this work.
* grace@robots.ox.ac.uk

Citation: Young GC, Dey S, Rogers AD, Exton D (2017) Cost and time-effective method for multi-scale measures of rugosity, fractal dimension, and vector dispersion from coral reef 3D models. PLoS ONE 12(4): e0175341. https://doi.org/10.1371/journal.pone.0175341

Editor: Konradin Metze, University of Campinas, BRAZIL

Received: February 2, 2017

Accepted: March 24, 2017

Published: April 13, 2017

Data Availability Statement: Rhino-Python scripts for computing linear rugosity, fractal dimension, and vector dispersion in Rhino are hosted on GitHub https://github.com/gracecalvertyoung/Rhino-Python-3D-Coral-Reefs and maintained by the corresponding author.

Funding: Operation Wallacea (www.opwall.com) provided support in the form of salaries for authors GCY and DE. The Marshall Scholarship (www.marshallscholarship.org) also provided support in the form of salary for author GCY. ThinkSee3D Ltd.

Abstract

We present a method to construct and analyse 3D models of underwater scenes using a single cost-effective camera on a standard laptop with (a) free or low-cost software, (b) no computer programming ability, and (c) minimal man hours for both filming and analysis. This study focuses on four key structural complexity metrics: point-to-point distances, linear rugosity (*R*), fractal dimension (*D*), and vector dispersion (*1/k*). We present the first assessment of accuracy and precision of structure-from-motion (SfM) 3D models from an uncalibrated GoPro™ camera at a small scale (4 m^2) and show that they can provide meaningful, ecologically relevant results. Models had root mean square errors of 1.48 cm in X-Y and 1.35 in Z, and accuracies of 86.8% (*R*), 99.6% (*D* at scales 30–60 cm), 93.6% (*D* at scales 1–5 cm), and 86.9 (*1/k*). Values of *R* were compared to *in-situ* chain-and-tape measurements, while values of *D* and *1/k* were compared with ground truths from 3D printed objects modelled underwater. All metrics varied less than 3% between independently rendered models. We thereby improve and rigorously validate a tool for ecologists to non-invasively quantify coral reef structural complexity with a variety of multi-scale metrics.

Introduction

Using an array of metrics in studies spanning decades, ecologists have shown that structural complexity drives biodiversity [1–4]. This is especially true on tropical coral reefs, one of the planet's most biodiverse and productive ecosystems [5], where metrics of structural complexity correlate strongly with indicators of reef health such as fish abundance, coral, and macroalgal cover [6–8]. Causes and effects are intertwined in these cases: living things create structure, and structure must pre-exist for those living things to find shelter from predators, scavenge, avoid turbulence, or perform other actions necessary for them to thrive [9–12]. To more precisely understand the nature of the correlations between structural complexity and ecological parameters, for example in a way that could inform the design of artificial reefs, marine

(www.thinksee3d.com) provided support in the form of salary for author SD. Funders had no additional roles in the study design, data collection and analysis, decision to publish, or preparation of the manuscript.

Competing interests: Our commercial affiliations do not alter our adherence to PLOS ONE policies on sharing data and materials.

ecologists require precise tools for assessing 3D structure of underwater habitats. It is important and timely to develop and employ such tools because our window-of-opportunity is closing for studying healthy reef ecosystems: reef complexity has been shown to be in significant decline, leading to ecosystem collapse [13–16].

Popular methods of assessing underwater structural complexity include chain-and-tape rugosity and Habitat Assessment Scores (HAS) [17]. The most common of these is chain-and-tape rugosity, whereby a chain of known length is laid along the contours of the seabed, and the ratio of its draped to undraped length gives a rugosity value [18, 19]. Alternatively, divers can visually score a range of structural variables using HAS [17]. Although both methods have revealed correlations, they result in a cursory understanding of complexity that is inadequate for addressing fine-scale ecological questions [20] or informing artificial reef designs [21] and, moreover, may be fundamentally misleading because of factors such as observer bias and dimensionality reduction [2, 22, 23]. Marine researchers have long called for a modern method of assessing structural complexity to address these concerns [6, 8, 24]. Such a method could be incorporated into monitoring programs to improve time and cost efficiency, accuracy, and detail [25, 26].

Three-dimensional (3D) computer models are a solution for assessing reef structural complexity. 3D models generated from images via structure-from-motion (SfM) algorithms have successfully been implemented to assess terrestrial complexity (*e.g.,* [27, 28]). A few papers have presented methodologies for creating coral reef 3D models from cost-effective photogrammetry [16, 29–33]. The approach is not novel, but here we take the method further by (1) increasing its accessibility to a wider audience by reducing hardware and software costs, and (2) expanding the metrics that can be used by non-programmers to assess structural complexity and the quality of their 3D models. Expanding metrics gives researchers additional tools to answer ecological questions about 3D surfaces–*e.g., At what scales does the structure provide refuge spots for prey to hide? How does a surface trap particulate matter?* We also show how footage from a single uncalibrated GoPro camera can produce 4 m^2 3D models with fine resolution and precision (to 1.5 cm with variations less than 3%).

We chose the SfM-software PhotoScan Standard (Agisoft LLC; $179 commercial, $59 educational—Mac, Windows, Linux; 30 day free trial) to render models for its ease-of-use and efficiency compared to its competitors and open-source alternatives; see discussion in [34]. We chose 3D modelling software Rhinoceros 3D ("Rhino"; Robert McNeel & Associates; $695–995 commercial, $195 educational—Mac, Windows; 90 day free trial) to analyse models for its easy-of-use, robustness, customizability, and library of built-in functions. Other software options were less favourable for a variety of reasons, including cost, platform limitations, and availability of a software development kit allowing us to write analysis scripts suited to our ecological applications.

Several papers emphasize the importance of calibration prior to photogrammetry, especially for highly distorted lenses such as that on a GoPro camera [35–37]. To date other studies using underwater photogrammetry have calibrated their cameras either from image meta-data that PhotoScan reads automatically or manual processing [30, 38, 39]. We show, however, that PhotoScan's built-in proprietary algorithm (which uses Brown's distortion model and no meta-data from our images), plus setting the camera to a narrow field-of-view, is capable of rendering accurate models at scales 1.5 cm—2 m. Because it does not assume camera calibration, this method could be used on historical footage, where camera model or calibration may be unknown.

We present the method alongside robust quantification of four structural variables: point-to-point distances, linear rugosity (R), fractal dimension (D), and vector dispersion ($1/k$). Per 4 m^2 of modelled reef area, our method requires three minutes of in water filming time (with a

single GoPro camera; ≈ $300) and approximately two hours of processing time on a standard laptop (≥8 GB RAM, 600 MB free disk space). Model rendering is largely automated, with each model requiring only 10 minutes human-computer time. We provide assessments of accuracy and repeatability using ground truths from known objects, as well as a comparison with chain-and-tape *in-situ* measurements of *R*. Our framework is ready-to-go to for use by non-programmers, and could be extended to gather any other conceivable structural complexity metric by a user with intermediate Python programming ability.

Materials and methods

Underwater filming

All filming occurred on reefs 5 ± 2 m deep off the Caribbean island of Utila, Honduras (16.0950° N, 86.9274° W) under a research permit from the Instituto de Conservación Forestal (#ICF-DE-MP-080-2016). We used GoPro cameras (Hero 3, 3+ or 4) in GoPro flat port underwater housings because they were readily available and widely used within contemporary reef monitoring efforts and recreational dive communities, although any similar camera should produce similar results. Cameras were in video mode, with all default settings except: resolution 1080p (for consistency across cameras), field-of-view narrow (to minimize distortion caused by the fish eye lens), sharpness medium (to minimize prominence of particulate matter), capture rate 24-30 frames per second, and white balance 6500K (for consistency and to suppress blue hues). Only ambient light illuminated scenes.

A SCUBA diver filmed over a 2 x 2 m quadrat following a lawnmower pattern (Fig 1). The camera remained a constant height 0.5–1.0 m above the scene's highest point. It was aimed straight down at the substratum, the lens moving in one plane rather than following the contours of the scene. Underwater visibility needed only to be clear in the 0.5–1.0 m vertical distance between the camera and the reef, so even sites with relatively low visibility could be rendered. The orientation of the camera did not change between adjacent swim passes (Fig 1), meaning the diver either back-finned on an adjacent pass or held the camera still as he rotated his body.

3D model generation

We rendered models in PhotoScan following the standard process well described in the PhotoScan user manual and by other papers in the field (*e.g.,* [37]). Raw video footage was converted into sequences of still images using the free software FFmpeg (www.ffmpeg.org). Sequential images should contain 60–80% overlap, which in practice meant extracting at 3 frames per second. Approximately 300-600 images captured one 2 x 2 m quadrat.

Images loaded into PhotoScan were rendered into a 3D model following the standard process of (1) aligning photos, (2) building dense point cloud, (3) building mesh, and (4) building texture. All processes were set to medium quality with default settings, except meshes' maximum face counts were set to 3,000,000 (to increase models' fine-scale resolution). PhotoScan performs camera calibration automatically using Brown's distortion model with assumed focal information. Photo alignment was successful even though we did not supply calibration information nor did the photos have EXIF data. Clarity of the model was then visually assessed. Any models in which the quadrat was not clear enough to be used as a scale bar would be rejected. However, no models rendered as part of this study needed to be rejected.

A rendered model was then exported as a wavefront (.OBJ) file and imported into Rhino for further analysis. Firstly, a model was scaled by setting a quadrat's corner-to-corner length to 2 m using the Rhino "Scale" command. Secondly, the model was oriented using the "Rotate" command. For simplicity, we placed all quadrats flat underwater (*i.e.,*parallel to the ocean

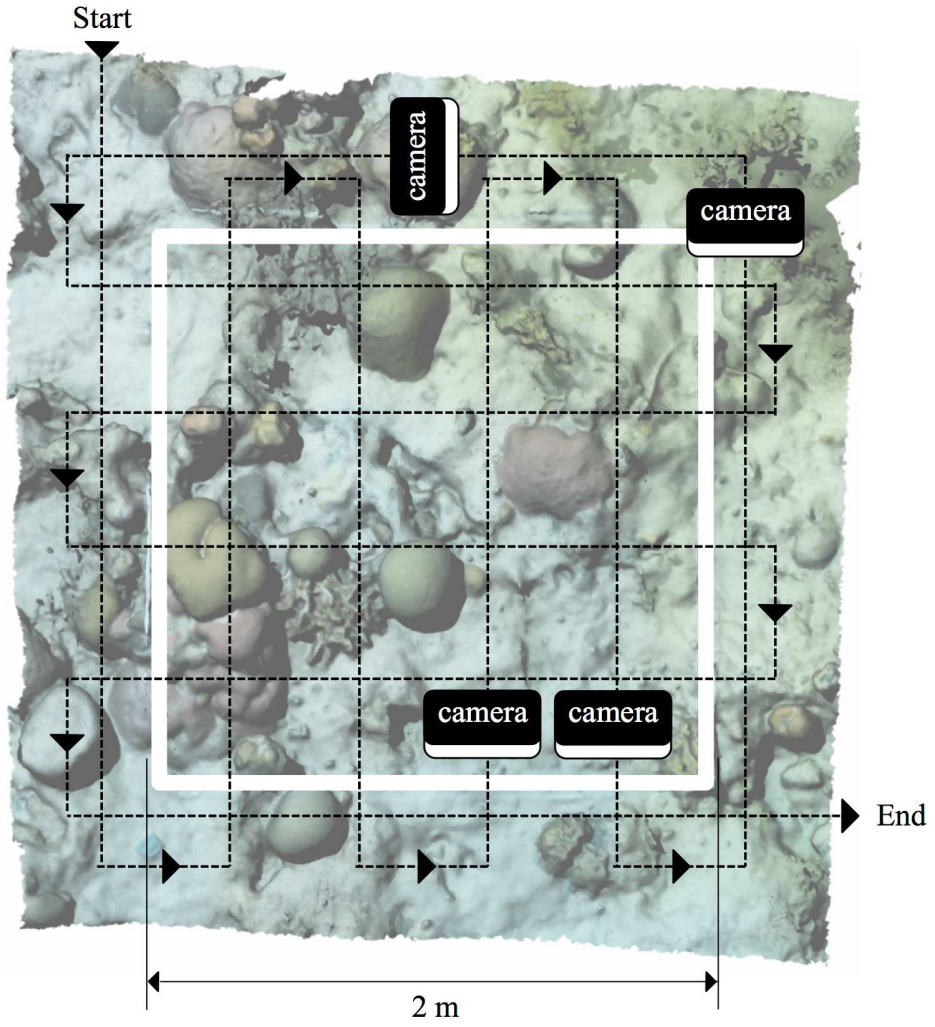

Fig 1. Method for filming 2 x 2 m underwater quadrat. A diver followed a lawnmower pattern (dotted line) over the quadrat, making 5–6 passes over each 2 m span of the quadrat and keeping the camera's height and orientation consistent.

https://doi.org/10.1371/journal.pone.0175341.g001

surface) and therefore rotated all models such that a quadrat corner rested squarely on the positive X and Y-axes. If a quadrat was placed at an angle underwater, however, divers could record the slope of the quadrat (*e.g.,* by tying a float indicating vertical or by recording the depths of the highest and lowest corners) and then rotate their 3D model accordingly.

Assessment metrics

We analysed our 3D models in Rhino using four metrics: point-to-point distances, rugosity (R), fractal dimension (D), and vector dispersion ($1/k$). In addition, we assessed the precision of the models by repeatedly filming several scenes and quantifying variance between independent renderings. Students previously unfamiliar with the software involved learned to independently render and analyse models after a three-hour tutorial, so this method is suitable for rapid uptake.

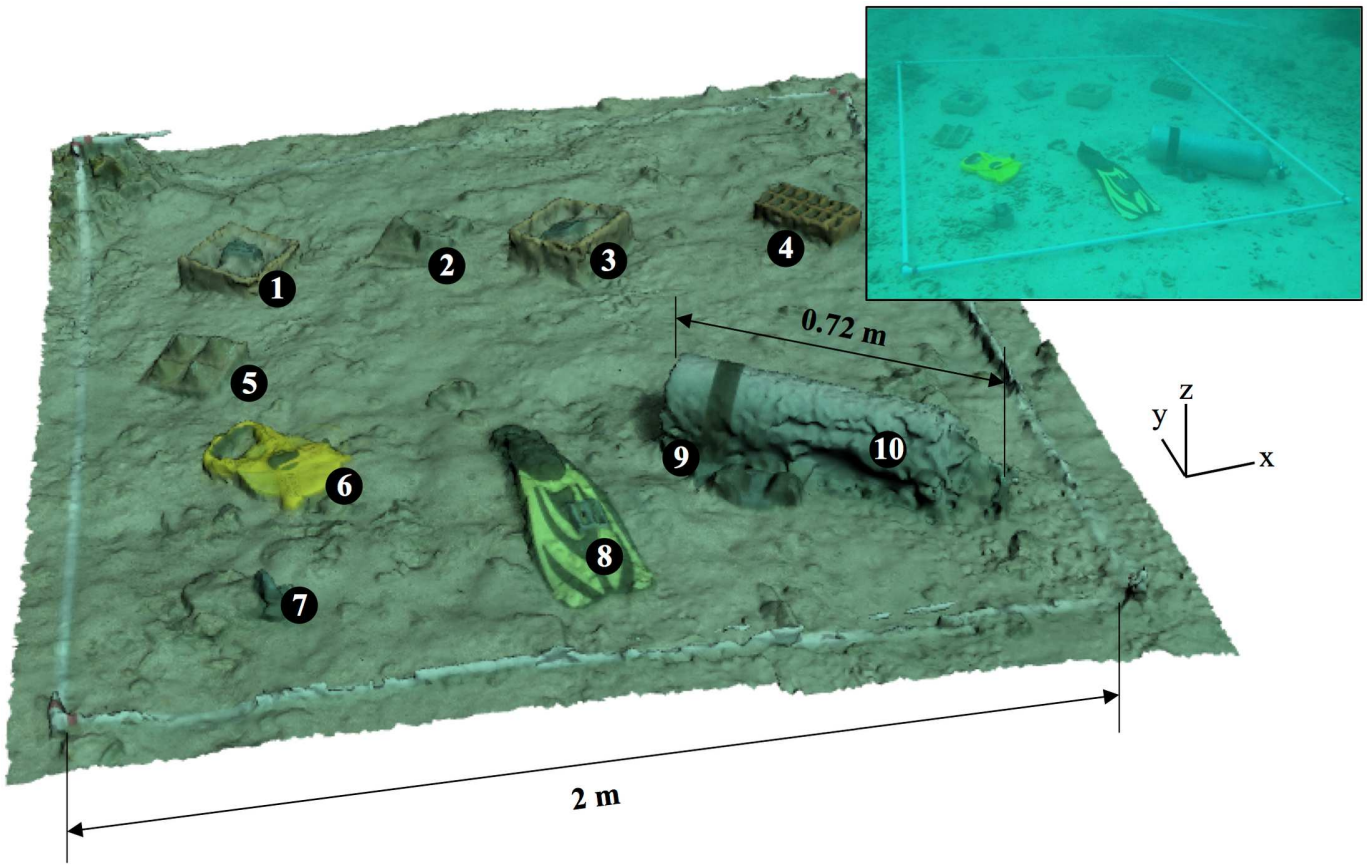

Fig 2. Objects of known dimensions 3D modelled inside 2 x 2 m quadrat. Two example dimensions, the quadrat length and the length of a standard SCUBA cylinder, are shown. Inset is a photo of the in-water scene. Objects of muted colors roughly matching the tones of the surrounding reef were chosen, representing a range of sizes and shapes. The 10 objects were: (1) pyramid-shaped mould, (2) pyramid-shaped tile, (3) natural-shaped mould, (4) brick, (5) pyramid-shaped tile, (6) transect tape, (7) dive weight (8) dive fin, (9) weight belt, and (10) SCUBA cylinder.

https://doi.org/10.1371/journal.pone.0175341.g002

Point-to-Point distances. To demonstrate the proportional accuracy of our 3D models, we rendered an underwater scene containing ten man-made objects and compared objects' known dimensions (ground truths) to their dimensions in the model. Objects of muted colors roughly matching the tones of the surrounding reef were chosen, representing a range of sizes and shapes (Fig 2). Known dimensions ranged from 0.8–65.0 cm in the X-Y plane and 2.0–18.0 cm in Z. No key dimensions were taken under an overhang, as an overhang will not render well using our filming method because we only move the camera in the X-Y plane, an issue further discussed below.

The accuracy of a measurement was computed with Eq 1:

$$Accuracy = 1 - \frac{|UW\ 3DM - Ground\ Truth|}{Ground\ Truth}\%, \quad (1)$$

where *UW 3DM* is the dimension measured on the underwater 3D model, and *Ground Truth* is the known dimension.

Rugosity. We chose rugosity as a complexity metric because it is standard in traditional coral reef research—so standard that the most recent (as of March 2017) meta-analysis of structural complexity on reefs was only able to compare rugosities because of the "limited scale

and replication" of studies employing alternative methods [8]. Rugosity is typically measured using the chain-and-tape method and quantified as the length the chain reaches as it falls over topography divided by the total length of the chain [18, 19]. It is not to be confused with "surface rugosity," a term describing the ratio of 3D surface area to projected planar area, or with "roughness," a term describing qualitative features or referencing the Hausdorff dimension.

To measure linear rugosity on a 3D model in Rhino, we first created a curve that followed the topography of the model. The curve was created with the Rhino built-in command "MeshIntersect," which provides a cross-sectioning tool that allows the user to select a slice of user-determined linear length of the model by intersecting a mesh plane with the 3D reef mesh. In practice this can be performed between any two coordinates on the model. Here, in order to compare our 3D model-derived results with *in-situ* chain-and-tape measurements, curves were selectively positioned to match their in-water counterparts. We then ran a custom Rhino Python script (github.com/gracecalvertyoung/Rhino-Python-3D-Coral-Reefs/tree/master/Rugosity) using the "RunPythonScript" command. The script asked the user to select surface contours, and then it laid virtual chains along each contour and returned rugosities. Rugosity (R) equalled the distance that a virtual chain fell along the curve (R_N) divided by the total length of the chain (R_D). The virtual chain comprised of linear segments each the length of a chain link (2 cm was used), which the script created from the input contour with the build-in Rhino function "rs.DivideCurveEquidistant."

The virtual chain was laid via either (1) the extendible-chain method (Fig 3A) or (2) the fixed-length chain method (Fig 3B). The extendible chain method determined how long a chain would need to be to cover the input curve, while the fixed-length chain method determined how far a chain of a set length (1 m was used) would fall along the input curve. This second method more closely resembled traditional chain-and-tape measurements, although it is a less accurate estimate of the overall reef complexity because of the chain's limited length.

Results from both methods were compared against *in-situ* chain-and-tape measurements. For the purposes of this comparison, 3D model-derived rugosity was the average of three adjacent virtual chains spaced 4 cm apart to account for an *in-situ* chain not laying perfectly straight.

Fractal dimension. We choose fractal dimension (D) as a complexity metric because it is a sophisticated and accurate means of assessing surface complexity that has been shown to be well suited to describing coral reefs [40–43]. Developed by [44], D is between 2 and 3 for a surface, with a greater number indicating greater complexity. It allows structural complexity to be explored within set size categories; *e.g.,* researchers can define a size category based on a particular species of interest and its unique habitat requirements, or calculate complexity for multiple categories in a particular reef area [45, 46].

Contemporary studies in the field of pattern recognition (machine learning and/or computer vision) have presented alternatives to, or improvements on, traditional fractal dimension (*e.g.,* [47–49]), as further discussed under Future Study. However, these approaches are better suited to image analysis programs (*e.g.* MATLAB, as [50] uses) than within Rhino. Going from Rhino to an image analysis program for our use-case would introduce additional steps and software into the method. Therefore, in order to maintain a simplified and streamlined method while still providing useful ecological metrics, we choose to calculate D at multiple scales in Rhino.

There are several methods for calculating D, and different methods will yield different results [45, 50, 51]. While no method is definitively superior to all, [52, 53] suggest an area-based method is appropriate for calculating D of surfaces. We therefore implemented an area-based method, following [52], who estimated D of rock surfaces (an application similar to ours).

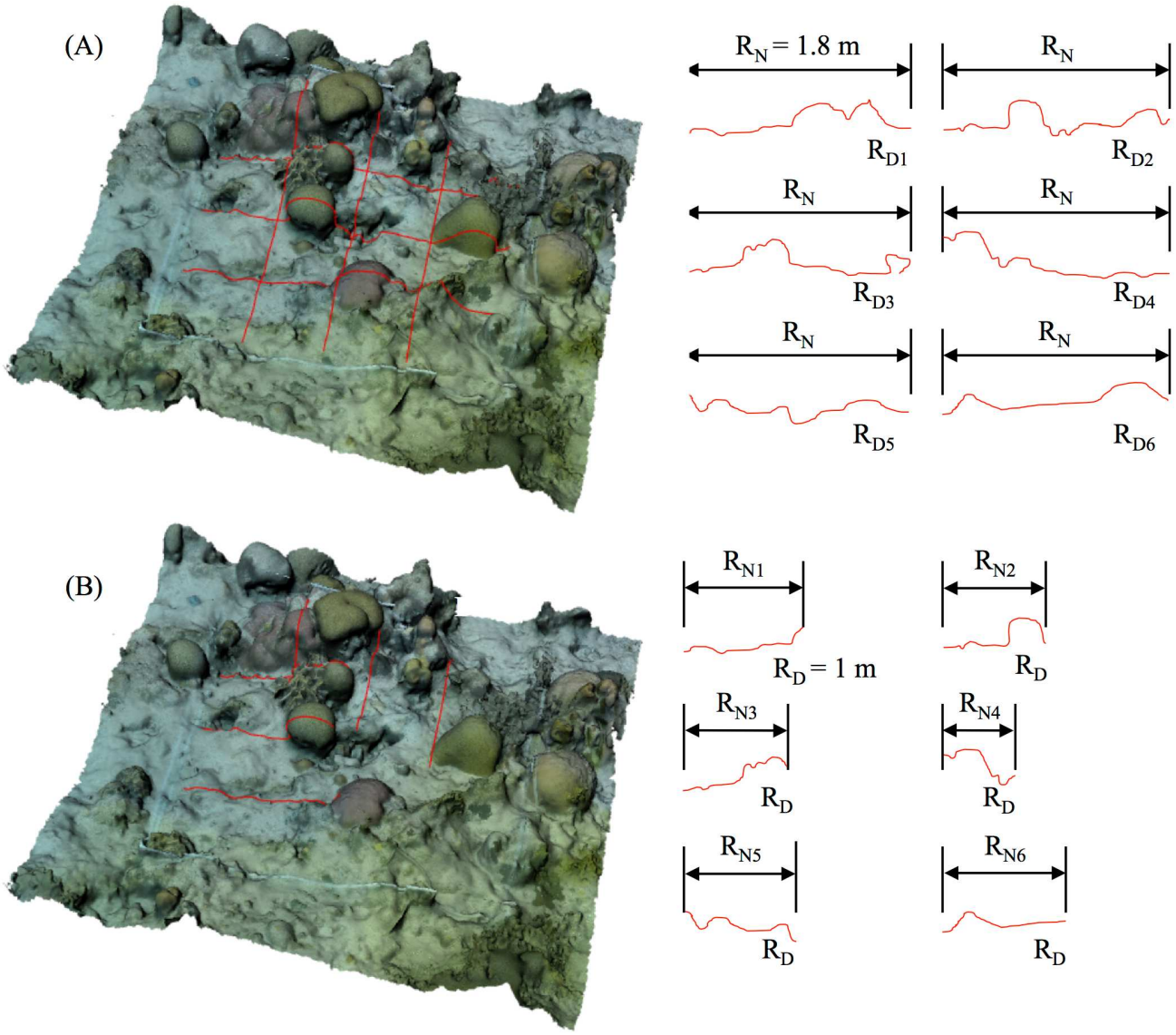

Fig 3. Methods for quantifying linar rugosity on 3D model. Six virtual chains with link length 2 cm were laid in a grid pattern over 3D modelled quadrats. A: The extendible-chain method determines how long a chain would need to be to cover the input curve. R_N is the draped length of the chain. R_{D_n} is the undraped length of chain *n*. B: The fixed-length chain method determines how far a chain of a set length (1 m was used) would reach over the curve; this method more closely resembles traditional chain-and-tape measurements, although it can miss details because of the chain's limited length. R_{N_n} is the draped length of chain *n*. R_{D_n} is the undraped length of the chain.

https://doi.org/10.1371/journal.pone.0175341.g003

Following [52], *D* indicates how surface area changes with resolutions. It is the slope of a model's resolution (δ) versus surface area (S(δ)) on logarithmic scales (Fig 4). We chose our resolutions, δ = 0.01, 0.05, 0.15, 0.3, 0.6, and 1.2 m, based on the refuge size categories of [17], who found holes of those size categories to be key factors influencing fish species abundance on coral reefs.

To measure *D* on a 3D model in Rhino, we ran a custom Rhino Python script (https://github.com/gracecalvertyoung/Rhino-Python-3D-Coral-Reefs/tree/master/Fractal_Dimension) using the "RunPythonScript" command. The script first re-rendered the model at

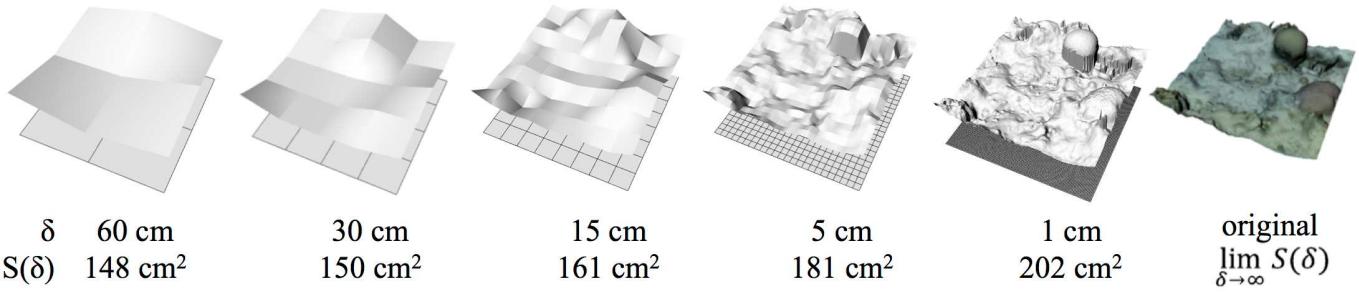

Fig 4. Fractal Dimension (*D*). *D* describes the relationship between a model's resolution, or minimum pixel size, (δ) and its surface area S(δ). Above, the same patch of coral reef is rendered at five resolutions. The grid below each rendering is composed of squares, each of width δ, that are projected onto the original surface. Surface area always increases with finer resolution. *D* is 2—the slope logS(δ)/log(δ).

https://doi.org/10.1371/journal.pone.0175341.g004

resolution δ by projecting a grid of points spaced at δ onto the model, akin to dropping a blanket of points onto the model. The script then connected adjacent points to form a new, virtual quilt-like surface. The area of that surface was then plotted against δ on logarithmic scales and the slopes between points, or *D*, determined. For resolutions 0.05-0.01 m, $D_{0.05-0.01}$ is (log(S(δ = 0.01)) − log(S(δ = 0.05)) / (log(0.01) − log(0.05)), and so on.

We compared 3D model-derived measurements of *D* to ground truths to gauge the accuracy and resolution of our 3D models in terms of *D*. The ground truths were three different theoretical structures that were 3D printed. The shapes placed underwater, hereafter refered to as the printed structures, matched the shapes of the 3D prints but were concrete, cast in moulds created from the 3D printed shapes. The accuracy of a measurement was calculated as a percentage (Eq 2).

$$Accuracy_D = 1 - \frac{|UW\ 3DM - Ground\ Truth|}{Ground\ Truth - 1}\%, \quad (2)$$

where *UW 3DM* is the value of *D* derived from the underwater 3D model and *Ground Truth* the value of *D* derived from the ground truth. Unlike Eq 1, one is subtracted from *Ground Truth* in the denominator because fractal dimension can only vary between 2 and 3 for a surface.

Vector dispersion. Vector dispersion (*1/k*) was determined as an appropriate metric for measuring benthic structural complexity by [54]. It measures the uniformity in angles of a surface. Mathematically, it estimates vector variance for all normal vectors of individual planar surfaces. It is a value between 0 and 1, where 0 indicates a flat plane and a number closer to 1 indicates a more complex surface. Like *R* and *D*, *1/k* must be calculated for a specified resolution; we choose 1 cm following [54]. In basic terms, a surface with a high value of *1/k* at 1 cm resolution would trap particulate matter more easily, be less easy to roll a ball of diameter 1 cm over (or clumps of sediment), and reflect light more variedly than a surface with a lower value of *1/k*.

To measure *1/k* in Rhino, we ran a custom Rhino Python script using the "RunPythonScript" command (https://github.com/gracecalvertyoung/Rhino-Python-3D-Coral-Reefs/tree/master/Vector_Dispersion). Whereas [54] created the grid of points with a profile gauge over the physical surface, our script projected a grid of points, spaced 1 cm apart, onto the highest Z-points of the 3D modelled reef. The script then created triangles between adjacent points and computed the directional cosines of triangles' normal vectors (Fig 5). It then computed

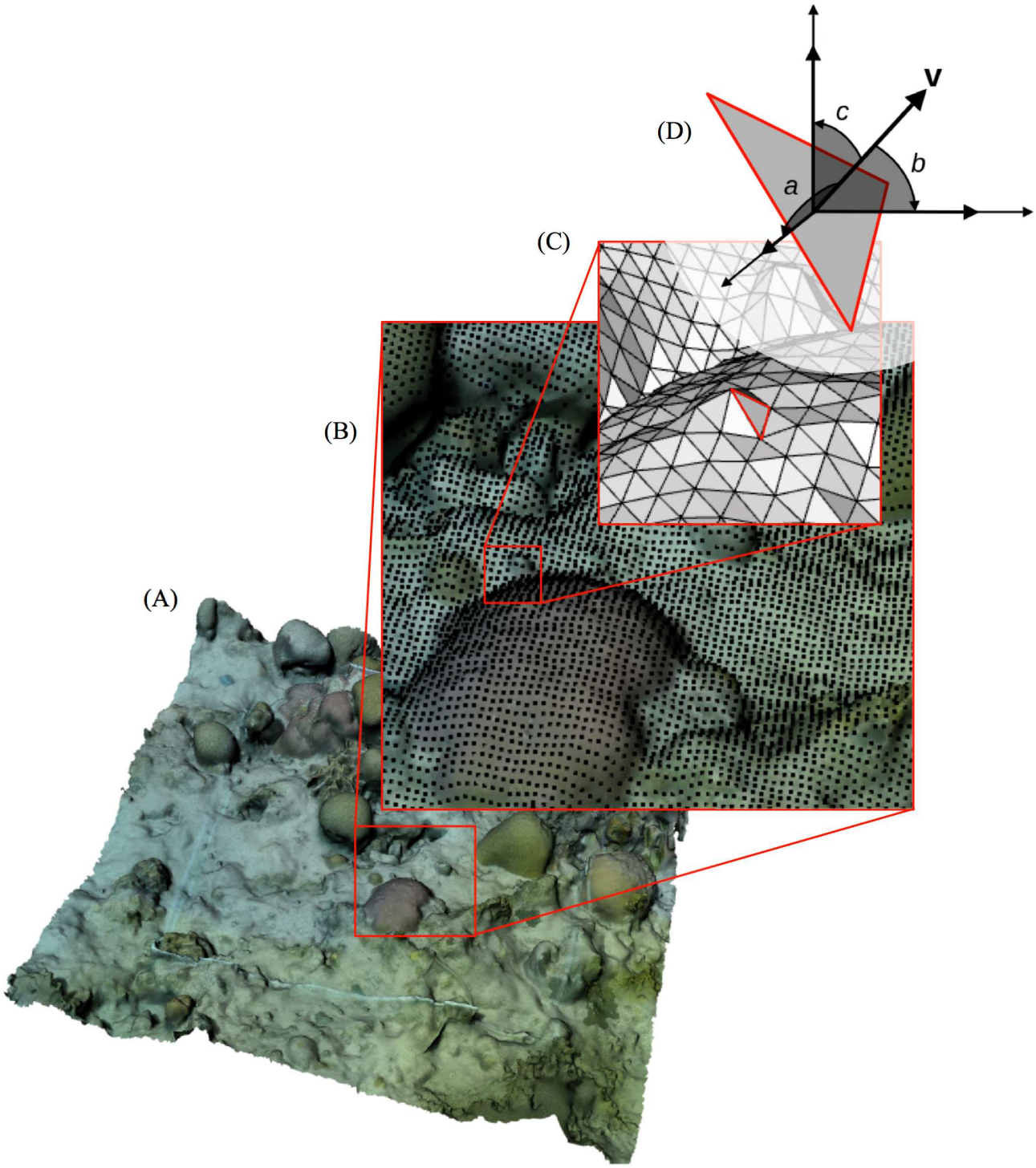

Fig 5. Process for computing vector dispersion (*1/k*). A: The user positions the scaled 3D model such that the quadrat lays flat along the X-Y plane or, if the quadrat was tilted underwater, tilted at the appropriate angle. The script then performs steps B-D. B: Project grid of points spaced 1 cm apart (as in [54]) onto the model such that each point falls on the highest point of the model. C: Connect adjacent points with triangles, creating *i* triangles. D: Compute the directional cosines of each triangle's normal vector (cos_x, cos_y, and cos_z labelled a, b, and c in the inset), and combine them as in Eq 3 for *1/k*. Diagram D modified from material available through Creative Commons License.

https://doi.org/10.1371/journal.pone.0175341.g005

1/k using Eqs 3 and 4.

$$R1 = \sqrt{\left(\sum_{1}^{i} cos_x\right)^2 + \left(\sum_{1}^{i} cos_y\right)^2 + \left(\sum_{1}^{i} cos_z\right)^2} \quad (3)$$

$$1/k = \frac{i - R1}{i - 1}, \quad (4)$$

where i is the number of triangles created between surface points and cos_x is the directional cosine of a triangle's normal vector in the X direction, cos_y in the Y direction, and so on.

We compared *1/k* measurements from an underwater 3D model to ground truths (the same three printed structures used to validate measurements of *D*) in order to gauge the accuracy and resolution of our 3D models in terms of *1/k*.

Precision. We independently modelled eight 2 x 2 m quadrants three times each to evaluate the repeatability and consistency of our method in terms of the above metrics. *R* was computed using the extendible-chain method as the average of six virtual chains laid over the quadrat (as in Fig 3). *D* was computed for the resolutions δ = 0.01, 0.05, 0.15, 0.3, 0.6, and 1.2 m. *1/k* was computed as the average over 1.6 m^2) of the quadrat.

Results and discussion

The method took 3 minutes in-water filming per 2 x 2 m quadrant, significantly less time than did placing quadrats, laying out transect tape, or other activities of the dives. It was important that the diver keep the camera orientation consistent on adjacent swim passes (Fig 1) because if the diver instead rotated the camera with his body, the footage was too blurry or disparate for the SfM algorithm to render the model. We found that filming the perpendicular set of swim-overs (Fig 1) was necessary for consistently successful photo alignment, even though this step was not required by other studies that use SfM with diver-held monocular footage (*e.g.,* [37]). Our added step could be necessary because of our absence of calibration data, the small-scale of the quadrat, or non-manual intervention during photo alignment compared to other studies. The minimal time committed to this step (≈ 1.5 min dive time) made it worthwhile in ensuring model quality.

Assessment metrics

Point-to-Point distances. Dimensions on the underwater 3D model matched strongly with their true dimensions in both the X–Y (n = 48, R2 = 0.99; $p < 0.001$; Wilcoxon matched pairs test) and Z planes (n = 25, R2 = 0.83; $p < 0.01$; Wilcoxon matched pairs test). The root mean square errors (RMSE) of our models were 1.48 cm in X-Y and 1.35 cm in Z. The slopes of the regression plots (Fig 6) indicate that models underestimated dimensions in both X-Y and Z.

Measurements had accuracies of 89 ± 12% (mean ± SD) and 78 ± 13% in X-Y and Z respectively. These results are on-par with those of [30], who found their centimetre-scale underwater models to underestimate surface area and volume by 18% and 8% respectively. The improved accuracies of [30] were to be expected because they modelled smooth, bright, multicoloured objects in a tank of water, which should render better than natural scenes in the ocean.

Our accuracies are lower than what is possible from *in-situ* underwater SfM 3D models: [31] report RMSE errors of 0.605 mm from close-range photogrammetry from calibrated consumer-grade stereo-cameras. Our lower accuracy was to be expected, as we did not calibrate cameras and used a considerably less time-consuming rendering process compared to other

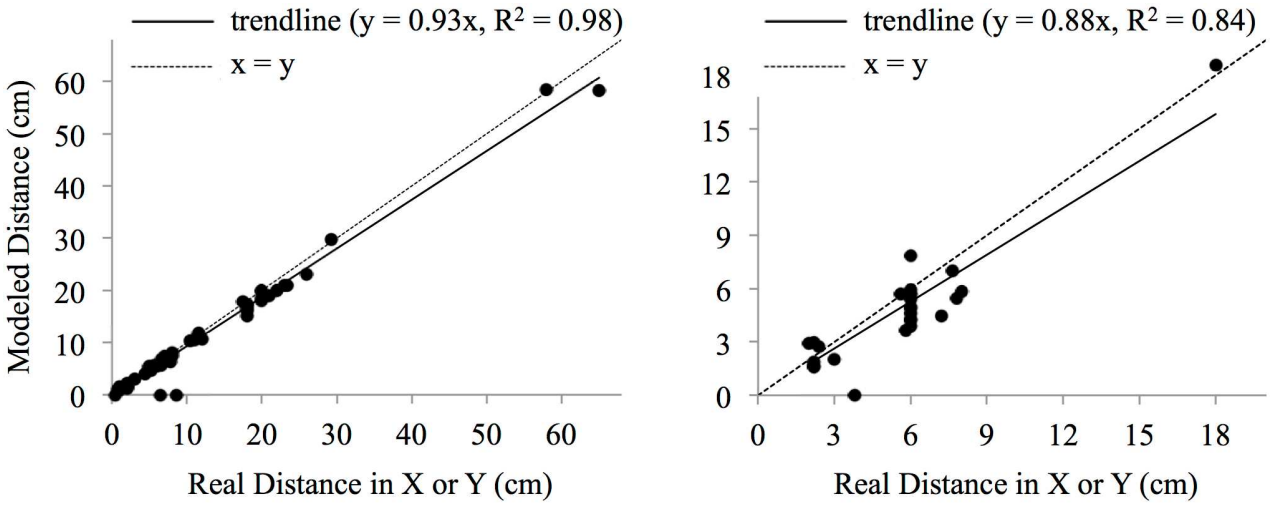

Fig 6. Accuracy of 3D model in terms of point-to-point distances. The root mean square errors (RMSE) of our models were 1.48 cm in X-Y and 1.35 cm in Z, with models underestimating dimensions in both X-Y and Z.

https://doi.org/10.1371/journal.pone.0175341.g006

methods: *e.g.*, methods that include manually removing outlier points on 3D models, manually identifying ground control objects, and/or using PhotoScan's high or ultra-high quality settings. [55] showed that models from calibrated GoPro footage can achieve RMSE errors of 0.40 mm; users requiring models accurate at scales finer than 1.5 cm should consider a method requiring higher hardware/software effort and cost or at minimum calibrate their cameras.

Our reduced accuracy in Z compared to X-Y was expected because the camera travelled only in the X-Y plane. Having divers film around objects to capture more Z-plane features may improve Z-plane accuracies as well as capture structures precluded by overhangs. We performed a few trials filming perpendicular to the surface terrain, or *around* objects, but it led to unwanted noise in the models or yielded unsuccessful photo alignment—complications likely caused by the extended background water column introducing moving particulates and not containing features for the SfM algorithm to align. A solution could be PhotoScan's "mask" feature, but trade-offs with dive time and ease-of-use would need to be considered.

Overall the results indicate that measurements taken from 3D modelled reef in any direction can be treated with a high degree of confidence. This is further supported by the consistently accurate results obtained from the varying selection of shaped and sized objects, which gives reassurances when working with the highly variable structure of the natural world. It is worth noting that some objects rendered better than others. For example, looking closely at Fig 2, the surface of the SCUBA tank appears to have a texture less smooth than the real life object; this could be because it is somewhat shiny and therefore not ideal for photogrammetry. These texture discrepancies are better estimated by the metrics of rugosity, fractal dimension and vector dispersion rather than point-to-point distances, however, and so are discussed in more detail later. Importantly at this stage, it had no impact on the accuracy of point-to-point distance measurements, meaning our models are well suited to the collection of size data.

Rugosity. Models' rugosities matched strongly with traditional *in-situ* chain-and-tape measurements (Fig 7), both via the extendible-chain method ($n = 34$, $R^2 = 0.86$; $p < 0.001$; one-sample t-test) and the fixed-length chain method ($n = 18$, $R^2 = 0.83$; $p < 0.001$; one-sample t-test).

Reported as accuracies using Eq 1, the extendible chain method had an accuracy of 85.7 ± 22.8% and the fixed length chain method had an accuracy of 86.8 ± 7.8%. These

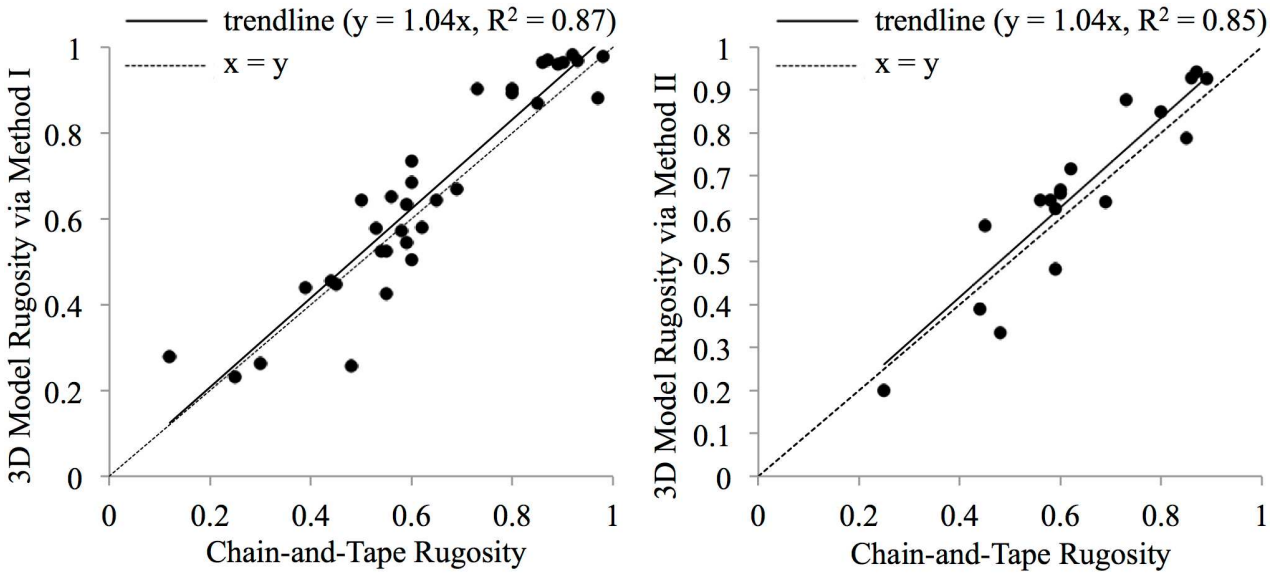

Fig 7. *In-situ* chain-and-tape measurements compared to those taken with a virtual chain on a 3D model. Method I is the extendible-chain method and Method II is the fixed-length chain method. The extendible chain method had an accuracy of 85.7 ± 22.8% and the fixed length chain method had an accuracy of 86.8 ± 7.8%.

https://doi.org/10.1371/journal.pone.0175341.g007

accuracies are on par with the accuracies of 85.3 ± 0.6% [33] and 89% [56], the only other studies to compare linear rugosity from a SfM 3D model (albeit using different methods) to chain-and-tape measurements.

Fractal dimension. *D* values from underwater 3D models matched well with ground truths. The highest accuracy occurred for measurements at the largest measured resolution, 30–60 cm (99.67 ± 0.11%) and accuracy decreased only to 93.57 ± 2.13% at the finest resolution, 1–5 cm (Fig 8; Table 1). Reduced accuracy at the finer scale was understandable, as smaller details are logically more difficult to capture because of complications such as particulate matter in the water interfering with image resolution. *D* values were marginally underestimated at the 1–30 cm resolutions, which is visibly demonstrated by the excessively smooth appearance of modelled objects (Fig 8).

The higher accuracy of *D* compared to point-to-point distances, rugosity, and *1/k* indicates that models are well-suited to convey overall complexity, even though some features may not perfectly match their ground truths.

Vector dispersion. *1/k* matched well with ground truths, with an overall accuracy of 86.94 ± 4.55% (Table 1). There was no consistency in whether the models over- or underestimated *1/k*. This level of accuracy can be considered above satisfactory, and further validates that the underwater 3D models used here accurately represent the structural complexity of their study areas. While no other study to our knowledge has computed accuracies in terms of *D* or *1/k*, our accuracies are on the high-end of the wide range reported by other studies computing surface area and volume from photographic models, accuracies which range 1–17% and 2–9% for surface area and volume, respectively [38].

Precision

The rendering of multiple models of the same reef area demonstrated the high repeatability of the method. Table 2 shows that coefficient of variation (CV) in measurements were all below

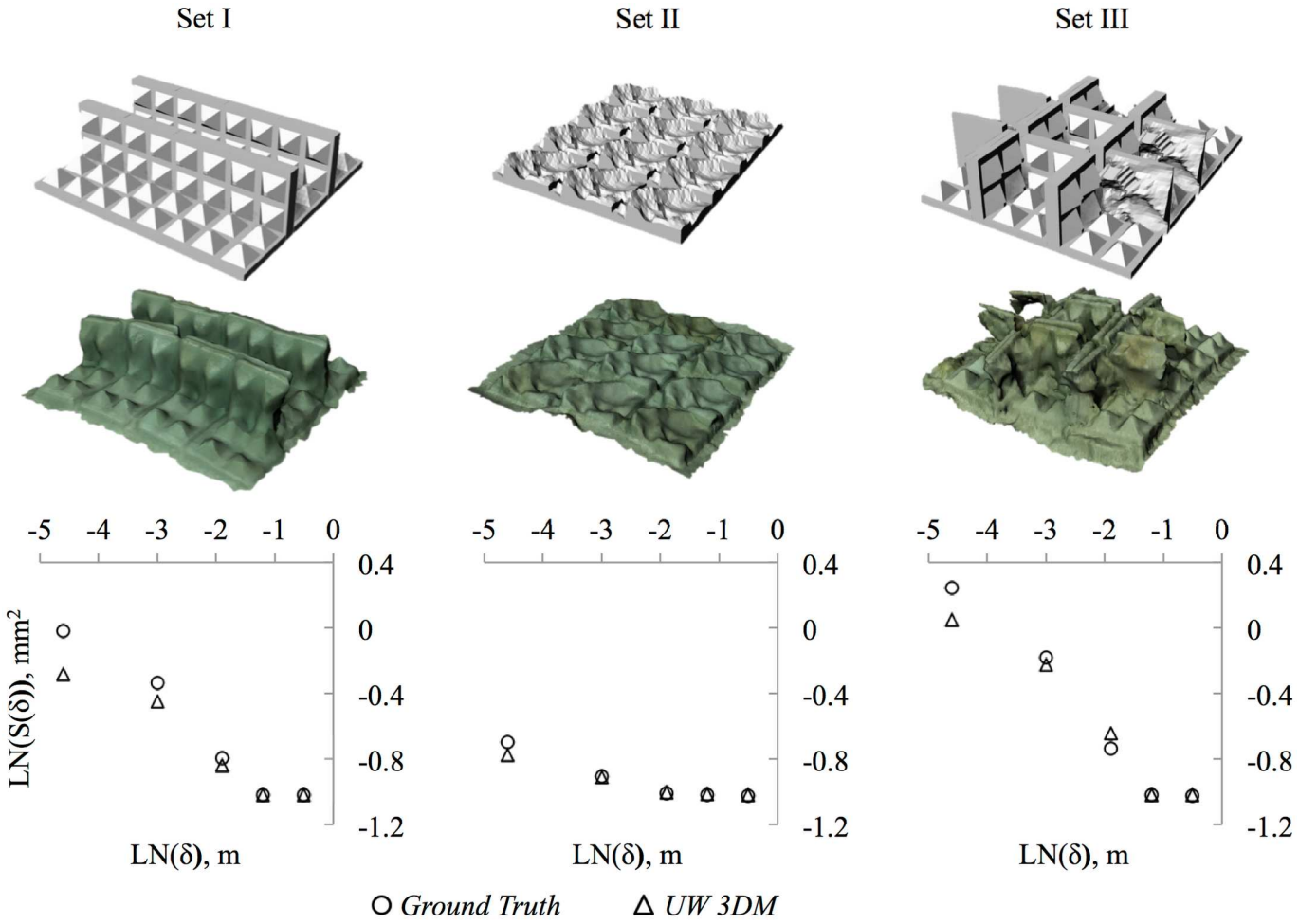

Fig 8. Fractal Dimension (*D*) of underwater 3D-printed objects at five spacial scales compared to ground truths. 3D printed structures were placed underwater and 3D modelled. Their surface areas were computed at five spatial scales (60, 30, 15, 5, and 1 cm) to compute *D*, which is the slope of model's resolution versus model's surface area on logarithmic scales. Surface areas at the 60 and 30 cm resolutions matched nearly perfectly between the ground-truth structures (top row) and the underwater 3D models (*UW 3DM*), while the 3D models slightly underestimated surface area at finer resolutions.

https://doi.org/10.1371/journal.pone.0175341.g008

2.8% (for rugosity) and as low as 0.6% (for D between 1–5 cm). The slight variations could result from human influences such as inconsistency in filming technique, scaling along the quadrat, and placement of rugosity lines or point clouds over the model. While no other study to our knowledge has computed precision in terms of *D* or *1/k*, our results are on the low-end of the range of 1–10% reported by [38] for surface rugosity from photogrammetric models. Similar to our method, [38] modelled six scenes 7–10 times to derive their CVs.

Future study

To further refine the filming technique and model rendering process, it would be helpful to assess the accuracy of measurements along the Z plane for larger objects, as this study only measured up to 18 cm in Z. It would also be useful to explore how model quality is affected by water conditions, available lighting (quality/quantity), depth, and other environmental factors (*e.g.*, [57] look at sun and wind patterns to find the optimum daytime for filming).

Table 1. Accuracies of Underwater 3D Models (*UW 3DM*) in terms of fractal Dimension (*D*) and vector dispersion (*1/k*). Accuracies computed using Eq 2 for *D* and Eq 1 for *1/k*. Sets I, II, and III are pictured in Fig 8.

Measurement	Accuracy (%)	Set	*Ground Truth*	*UW 3DM*
$D_{0.60-0.30}$	99.67 ± 0.11	I	2.0032	2.0056
		II	2.0026	2.0071
		III	2.0003	2.0033
$D_{0.30-0.15}$	95.26 ± 4.59	I	2.3257	2.2606
		II	2.0131	2.0138
		III	2.4096	2.54
$D_{0.15-0.05}$	93.26 ± 2.01	I	2.4148	2.3516
		II	2.0952	2.0138
		III	2.5085	2.383
$D_{0.05-0.01}$	93.57 ± 2.13	I	2.1975	2.1044
		II	2.131	2.086
		III	2.264	2.1687
1/k	86.94 ± 4.55	I	0.249	0.226
		II	0.194	0.171
		III	0.304	0.359

https://doi.org/10.1371/journal.pone.0175341.t001

Computing additional metrics of structural complexity could also assist with long-term reef monitoring strategies and benthic community assessments. Metrics such as surface area, volume, slope, and average height could be of interest, as could any of those reviewed by [2] or [58]. Slope in particular is not addressed in our study, as all our quadrats were placed flat (parallel to the ocean surface) for simplicity and consistency. To incorporate slope into 3D models, the models should be rotated to the appropriate angle prior to obtaining metrics, or rugosity could be decoupled from slope [56]. We attempted to tie a small fishing float to the corner of a quadrat to indicate its angle with respect to the surface, but, unsurprisingly, the float moved too much to render in the 3D model. On future studies, divers might record a quadrat's angle by noting the depths of two corners of the quadrat and positioning the 3D model accordingly. Advanced users may also wish to implement other numerical approaches for estimating fractal dimension and/or metrics from the field of pattern recognition (machine learning and/or computer vision) such as lacunarity [47], color texture analysis based on fractal geometry [48], and/or local fractal dimension [49]. These state-of-the-art methods are presented for image analysis, but it would be possible to apply them on a coral reef 3D model by converting the 3D model into a "heat map" or 2D array of the quadrat. Once the heat map is generated, existing toolboxes in MATLAB (*e.g.,* as [50] uses) would likely be more suited to the calculations than Rhino-Python scripts. That said, a user would still need to initially process the model in Rhino to scale, rotate, and identify the quadrat area.

Conclusion

While 3D modelling from underwater photogrammetry is a reasonably established method for representing and assessing coral reef structures, it remains largely reliant on sophisticated or

Table 2. Precision of 3D models. Models showed low variation in terms of rugosity (*R*), vector dispersion (*1/k*) and fractal Dimension (*D*). Eight quadrats were each modelled three times. The coefficient of variation (CV) was the average standard deviation of measurements divided by the average measurement.

	R	$D_{1.20-0.60}$	$D_{0.60-0.30}$	$D_{0.30-0.15}$	$D_{0.15-0.05}$	$D_{0.05-0.01}$	*1/k*
CV	2.8%	0.7%	1.3%	1.0%	2.8%	0.6%	1.9%

https://doi.org/10.1371/journal.pone.0175341.t002

costly hardware and/or software that can restrict accessibility to the wider research and conservation community. We present a cost-effective and automated technique that demonstrates how a single uncalibrated GoPro camera can produce accurate and precise models at small spatial scales (1.5 cm to 2 m), with variations in structural complexity between models below 3% and a high level of accuracy when compared to ground-truth measurements. We also provide useful tools for non-programmers to quantify reef 3D structures via a suite of ecologically-relevant metrics. By expanding beyond simple rugosity measurements to include fractal dimension (D) and vector dispersion ($1/k$), we provide researchers with a more thorough approach to exploring the quantity and quality of 3D complexity, including the ability to focus on complexity ranges that are ecologically relevant to target organisms.

Acknowledgments

Thanks to Operation Wallacea for facilitating fieldwork and to the Marshall Commission for supporting author GCY. Also thanks to Ellenah Page, Shamus Birch, Ellen Purdue, Katherine Shepherd, Iain Mackie, and Faye-Marie Crooke for their assistance collecting data.

Author Contributions

Conceptualization: GCY SD ADR DE.

Data curation: GCY.

Formal analysis: GCY.

Funding acquisition: GCY SD DE ADR.

Investigation: GCY.

Methodology: GCY SD.

Project administration: GCY.

Resources: GCY DE.

Software: GCY.

Supervision: ADR DE.

Validation: GCY.

Visualization: GCY.

Writing – original draft: GCY.

Writing – review & editing: ADR DE.

References

1. Hiatt RW, Strasburg DW, Monographs SE, Jan N. Ecological Relationships of the Fish Fauna on Coral Reefs of the Marshall Islands. Ecological Monographs. 1960; 30(1):65–127. https://doi.org/10.2307/1942181
2. Mccormick MI. Comparison of Field Methods for Measuring Surface Topography and their Associations with a Tropical Reef Fish Assemblage. Marine Ecology Progress Series. 1994; 112:87–96. https://doi.org/10.3354/meps112087
3. Knudby A, LeDrew E. Measuring Structural Complexity on Coral Reefs. Proceedings of the American Acadamy of Underwater Sciences 26th Symposium. 2007; p. 181–188.
4. Dustan P, Doherty O, Pardede S. Digital Reef Rugosity Estimates Coral Reef Habitat Complexity. PLoS ONE. 2013; 8(2). https://doi.org/10.1371/journal.pone.0057386 PMID: 23437380

5. Alvarez-Filip L, Dulvy NK, Côteé IM, Watkinson AR, Gill Ja. Coral Identity Underpins Architectural Complexity on Caribbean Reefs. Ecological Applications. 2011; 21(6):2223–2231. https://doi.org/10.1890/10-1563.1 PMID: 21939056
6. Friedlander AM, Parrish JD. Habitat Characteristics Affecting Fish Assemblages on a Hawaiian Coral Reef. Journal of Experimental Marine Biology and Ecology. 1998; 224(1):1–30. https://doi.org/10.1016/S0022-0981(97)00164-0
7. Wilson MFJ, O'Connell B, Brown C, Guinan JC, Grehan AJ. Multiscale Terrain Analysis of Multibeam Bathymetry Data for Habitat Mapping on the Continental Slope. Marine Geodesy. 2007; 30(1–2):3–35. https://doi.org/10.1080/01490410701295962
8. Graham NAJ, Nash KL. The Importance of Structural Complexity in Coral Reef Ecosystems. Coral Reefs. 2013; 32:315–326. https://doi.org/10.1007/s00338-012-0984-y
9. Hixon MA, Beets JP. Predation, Prey Refuges, and the Structure of Coral-Reef Fish Assemblages. Ecological Monographs. 1993; 63(1):77–101. https://doi.org/10.2307/2937124
10. Carr MH, Hixon MA. Artificial Reefs: The Importance of Comparisons with Natural Reefs. Fisheries. 1997; 22(4):28–33. https://doi.org/10.1577/1548-8446(1997)022%3C0028:ARTIOC%3E2.0.CO;2
11. Hearn C, Atkinson M, Falter J. A physical derivation of nutrient-uptake rates in coral reefs: Effects of roughness and waves. Coral Reefs. 2001; 20(4):347–356. https://doi.org/10.1007/s00338-001-0185-6
12. Johansen JL, Bellwood DR, Fulton CJ. Coral reef fishes exploit flow refuges in high-flow habitats. Marine Ecology Progress Series. 2008; 360:219–226. https://doi.org/10.3354/meps07482
13. Alvarez-Filip L, Dulvy NK, Gill Ja, Cote IM, Watkinson aR. Flattening of Caribbean Coral Reefs: Region-Wide Declines in Architectural Complexity. Proceedings of the Royal Society B: Biological Sciences. 2009; 276(1669):3019–3025. https://doi.org/10.1098/rspb.2009.0339 PMID: 19515663
14. Ledlie MH, Graham NAJ, Bythell JC, Wilson SK, Jennings S, Polunin NVC, et al. Phase shifts and the role of herbivory in the resilience of coral reefs. Coral Reefs. 2007; p. 641–653. https://doi.org/10.1007/s00338-007-0230-1
15. Newman SP, Meesters EH, Dryden CS, Williams SM, Sanchez C, Mumby PJ, et al. Reef Flattening Effects on Total Richness and Species Responses in the Caribbean. Journal of Animal Ecology. 2015; 84(6):1678–1689. https://doi.org/10.1111/1365-2656.12429 PMID: 26344713
16. Burns JHR, Delparte D, Kapono L, Belt M. Assessing the impact of acute disturbances on the structure and composition of a coral community using innovative 3D reconstruction techniques. Methods in Oceanography. 2016; p. 1–11.
17. Gratwicke B, Speight MR. The Relationship Between Fish Species Richness, Abundance and Habitat Complexity in a Range of Shallow Tropical Marine Habitats. Journal of Fish Biology. 2005; 66(3):650–667. https://doi.org/10.1111/j.0022-1112.2005.00629.x
18. Risk MJ. Fish Diversity on a Coral Reef in The Virgin Islands. Atoll Research Bulletin. 1972; 153:1–6. https://doi.org/10.5479/si.00775630.153.1
19. Luckhurst E, Luckhurst K. Analysis of the Influence of Substrate Variables on Coral Reef Fish Communities. Marine Biology. 1978; 323(49):317–323. https://doi.org/10.1007/BF00455026
20. Harborne AR, Mumby PJ, Ferrari R. The effectiveness of different meso-scale rugosity metrics for predicting intra-habitat variation in coral-reef fish assemblages. Environmental Biology of Fishes. 2012; 94(2):431–442. https://doi.org/10.1007/s10641-011-9956-2
21. Perkol-Finkel S, Shashar N, Benayahu Y. Can artificial reefs mimic natural reef communities? The roles of structural features and age. Marine Environmental Research. 2006; 61(2):121–135. https://doi.org/10.1016/j.marenvres.2005.08.001 PMID: 16198411
22. Goatley CHR, Bellwood DR. The Roles of Dimensionality, Canopies and Complexity in Ecosystem Monitoring. PLoS ONE. 2011; 6(11). https://doi.org/10.1371/journal.pone.0027307
23. Kerry JT, Bellwood DR. The effect of coral morphology on shelter selection by coral reef fishes. Coral Reefs. 2012; 31(2):415–424. https://doi.org/10.1007/s00338-011-0859-7
24. Merks R, Hoekstra A, Kaandorp J, Sloot P. A Problem Solving Environment for Modelling Stony Coral Morphogenesis. Computational Science—ICCS 2003. 2003; 2657:639–648. https://doi.org/10.1007/3-540-44860-8_66
25. Wedding LM, Friedlander AM, McGranaghan M, Yost RS, Monaco ME. Using Bathymetric Lidar to Define Nearshore Benthic Habitat Complexity: Implications for Management of Reef Fish Assemblages in Hawaii. Remote Sensing of Environment. 2008; 112(11):4159–4165. https://doi.org/10.1016/j.rse.2008.01.025
26. Mumby P, Flower J, Chollett I, Box S, Bozec Y. Towards reef resilience and sustainable livelihoods: A handbook for Caribbean Coral Reef Managers. Exeter, Devon, UK: University of Exeter; 2014.

27. Westoby MJ, Brasington J, Glasser NF, Hambrey MJ, Reynolds JM. 'Structure-from-Motion' photogrammetry: A low-cost, effective tool for geoscience applications. Geomorphology. 2012; 179:300–314. https://doi.org/10.1016/j.geomorph.2012.08.021

28. Javernick L, Brasington J, Caruso B. Modeling the topography of shallow braided rivers using Structure-from-Motion photogrammetry. Geomorphology. 2014; 213:166–182. https://doi.org/10.1016/j.geomorph.2014.01.006

29. Hu H, Ferrari R, Mckinnon D, Roff Ga, Smith R, Mumby PJ, et al. Measuring reef complexity and rugosity from monocular video bathymetric reconstruction. International Coral Reef Symposium. 2012; 12 (July):9–13.

30. Lavy A, Eyal G, Neal B, Keren R, Loya Y, Ilan M. A quick, easy and non-intrusive method for underwater volume and surface area evaluation of benthic organisms by 3D computer modelling. Methods in Ecology and Evolution. 2015; p. n/a–n/a. https://doi.org/10.1111/2041-210X.12331

31. Leon JX, Roelfsema CM, Saunders MI, Phinn SR. Measuring Coral reef Rerrain Roughness using 'Structure-from-Motion' Close-Range Photogrammetry. Geomorphology. 2015; 242:21–28. https://doi.org/10.1016/j.geomorph.2015.01.030

32. Storlazzi CD, Dartnell P, Hatcher GA, Gibbs AE. End of the chain? Rugosity and fine-scale bathymetry from existing underwater digital imagery using structure-from-motion (SfM) technology. Coral Reefs. 2016;. https://doi.org/10.1007/s00338-016-1462-8

33. Ferrari R, McKinnon D, He H, Smith RN, Corke P, Gonzalez-Rivero M, et al. Quantifying multiscale habitat structural complexity: A cost-effective framework for underwater 3D modelling. Remote Sensing. 2016; 8(2). https://doi.org/10.3390/rs8020113

34. Dandois JP, Ellis EC. High spatial resolution three-dimensional mapping of vegetation spectral dynamics using computer vision. Remote Sensing of Environment. 2013; 136:259–276. https://doi.org/10.1016/j.rse.2013.04.005

35. Balletti C, Guerra F, Tsioukas V, Vernier P. Calibration of action cameras for photogrammetric purposes. Sensors. 2014; 14(9):17471–17490. https://doi.org/10.3390/s140917471 PMID: 25237898

36. Helmholz P, Long J, Munsie T, Belton D. Accuracy assessment of go pro hero 3 (Black) camera in underwater environment. International Archives of the Photogrammetry, Remote Sensing and Spatial Information Sciences—ISPRS Archives. 2016; 41(July):477–483. https://doi.org/10.5194/isprs-archives-XLI-B5-477-2016

37. Burns J, Delparte D, Gates R, Takabayashi M. Integrating Structure-from-Motion Photogrammetry with Geospatial Software as a Novel Technique for Quantifying 3D Ecological Characteristics of Coral Reefs. PeerJ. 2015; https://doi.org/10.7717/peerj.1077 PMID: 26207190

38. Figueira W, Ferrari R, Weatherby E, Porter A, Hawes S, Byrne M. Accuracy and Precision of Habitat Structural Complexity Metrics Derived from Underwater Photogrammetry. Remote Sensing. 2015; 7 (12):16883–16900. https://doi.org/10.3390/rs71215859

39. Gutierrez-Heredia L, Benzoni F, Murphy E, Reynaud EG. End to End Digitisation and Analysis of Three-Dimensional Coral Models, from Communities to Corallites. PLoS ONE. 2016; 11(2). https://doi.org/10.1371/journal.pone.0149641 PMID: 26901845

40. Bradbury RH, Reichelt E. Fractal Dimension of a Coral Reef. Marine Ecology Progress Series. 1983; 10:169–171. https://doi.org/10.3354/meps010169

41. Mark D. Fractal Dimension of a Coral Reef at Ecological Scales: A Discussion. Marine Ecology Progress Series. 1984; 14:293–294. https://doi.org/10.3354/meps014293

42. Herzfeld UC, Overbeck C. Analysis and simulation of scale-dependent fractal surfaces with application to seafloor morphology. Computers and Geosciences. 1999; 25:979–1007. https://doi.org/10.1016/S0098-3004(99)00062-X

43. Martin-Garin B, Lathuilière B, Verrecchia EP, Geister J. Use of Fractal Dimensions to Quantify Coral Shape. Coral Reefs. 2007; 26(3):541–550. https://doi.org/10.1007/s00338-007-0256-4

44. Mandelbrot BB. The Fractal Geometry of Nature. New York: W.H. Freeman; 1982.

45. Kostylev VE, Erlandsson J, Mak YM, Williams GA. The relative importance of habitat complexity and surface area in assessing biodiversity: Fractal application on rocky shores. Ecological Complexity. 2005; 2(3):272–286. https://doi.org/10.1016/j.ecocom.2005.04.002

46. Zawada DG, Brock JC. A Multiscale Analysis of Coral Reef Topographic Complexity Using Lidar-Derived Bathymetry. Journal of Coastal Research. 2009; 10053:6–15. https://doi.org/10.2112/SI53-002.1

47. Hsui CY, Wang CC. Synergy between fractal dimension and lacunarity index in design of artificial habitat for alternative SCUBA diving site. Ecological Engineering. 2013; 53:6–14. https://doi.org/10.1016/j.ecoleng.2013.01.014

48. Casanova D, Florindo JB, Falvo M, Bruno OM. Texture analysis using fractal descriptors estimated by the mutual interference of color channels. Information Sciences. 2016; 346–347:58–72. https://doi.org/10.1016/j.ins.2016.01.077

49. Novianto S, Suzuki Y, Maeda J. Near optimum estimation of local fractal dimension for image segmentation. Pattern Recognition Letters. 2003; 24(1–3):365–374. https://doi.org/10.1016/S0167-8655(02)00261-1

50. Gneiting T, Ševčíková H, Percival DB. Estimators of Fractal Dimension: Assessing the Roughness of Time Series and Spatial Data. Statistical Science. 2012; 27(2):254–282. https://doi.org/10.1214/11-STS370

51. Klinkenberg B, Goodchild MF. The fractal properties of topography: A comparison of methods. Earth Surface Processes and Landforms. 1992; 17(3):217–234. https://doi.org/10.1002/esp.3290170303

52. Zhou HW, Xie H. Direct Estimation of the Fractal Dimensions of a Fracture Surface of Rock. Surface Review and Letters. 2003; 10(05):751–762. https://doi.org/10.1142/S0218625X03005591

53. Zhou G, Lam NSN. A comparison of fractal dimension estimators based on multiple surface generation algorithms. Computers and Geosciences. 2005; 31(10):1260–1269. https://doi.org/10.1016/j.cageo.2005.03.016

54. Carleton JH, Sammarco PW. Effects of Substratum Irregularity on Success of Coral Settlement: Quantification by Comparative Geomorphological Techniques. Bulletin of Marine Science. 1987; 40(1):85–98.

55. Guo T, Capra A, Troyer M, Gruen A, Brooks AJ, Hench JL, et al. Accuracy Assessment of Underwater Photogrammetric Three Dimensional Modelling for Coral Reefs. ISPRS—International Archives of the Photogrammetry, Remote Sensing and Spatial Information Sciences. 2016; XLI-B5(June):821–828. https://doi.org/10.5194/isprsarchives-XLI-B5-821-2016

56. Friedman A, Pizarro O, Williams SB, Johnson-Roberson M. Multi-Scale Measures of Rugosity, Slope and Aspect from Benthic Stereo Image Reconstructions. PLoS ONE. 2012; 7(12). https://doi.org/10.1371/journal.pone.0050440 PMID: 23251370

57. Casella E, Collin A, Harris D, Ferse S, Bejarano S, Parravicini V, et al. Mapping coral reefs using consumer-grade drones and structure from motion photogrammetry techniques. Coral Reefs. 2016; p. 1–7.

58. Pittman SJ, Brown KA. Multi-Scale Approach for Predicting Fish Species Distributions across Coral Reef Seascapes. PLoS ONE. 2011; 6(5):e20583. https://doi.org/10.1371/journal.pone.0020583 PMID: 21637787

Correction

The following correction was filed with *PLOS ONE* on May 12, 2018:

> Figure 6 (on page 11/18 of the *PLOS ONE* print) should be replaced with the graph below (Fig. 2.3(a)). None of the text changes. The differences between the original and revised Figure 6 are as follows: (a) the horizontal axis label on the right graph is corrected from "Real Distance in X or Y (cm)" to "Real Distance in Z (cm)", (b) three erroneous points are removed from the horizontal axes, and (c) the trendlines are corrected to match correct values which are reports in text.

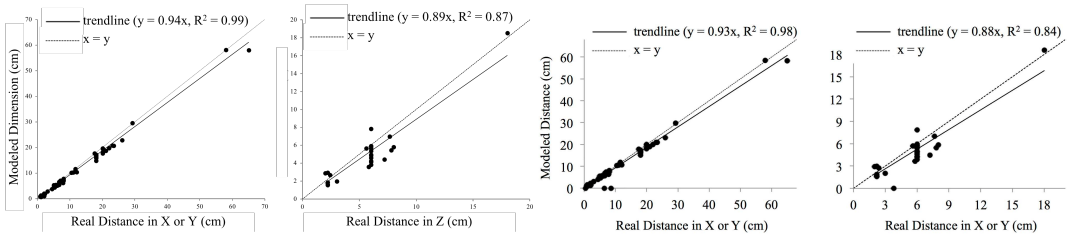

(a) Corrected Figure **(b)** Original Figure

Figure 2.3: Same captions as in the publication: "Figure 6: Accuracy of 3D model in terms of point-to-point distances. The root mean square errors (RMSE) of our models were 1.48 cm in X-Y and 1.35 cm in Z, with models underestimating dimensions in both X-Y and Z."

2.4 Supplementary Material: Teaching Guides

Through 2016-2017 I taught several workshops on how to apply the method presented in this Chapter. After the 3–4 hour workshop, participants were fully competent with software involved. Several participants then went on to teach it to others. The materials I developed for the workshop are hosted online because they are continually updated. They can be found at: `https://github.com/gracecalvertyoung/Underwater-Photogrammetry-Teaching-Material`. Additionally, collaborator Kathryn Whittey and I posted video tutorials on how to compute *R*, *D*, and *1/k* as described in this Chapter; those tutorials are online at `www.graceunderthesea.com`.

2.5 Supplementary Material: Interactive 3D Models

The following direct to interactive versions of 3D models from this Chapter that can be rotated, panned, and made larger/smaller on any web browser, including on a mobile phone. Models are hosted on SketchFab, an online platform for publishing, sharing, and discovering 3D, virtual reality, and artificial reality content. Models are viewable in Google cardboard or other virtual reality headsets as indicated by the orange glasses icon (Creative Commons licence CC0).

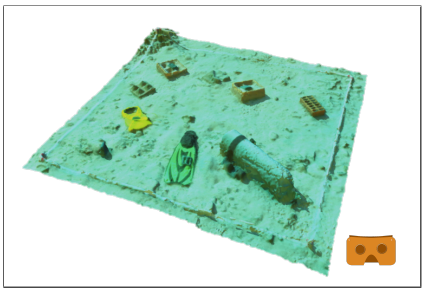

3D model of objects used to measure accuracy of the 3D models (Fig. 2 from the publication in this chapter). Available at `https://skfb.ly/6vvou`, or scan the QR code.

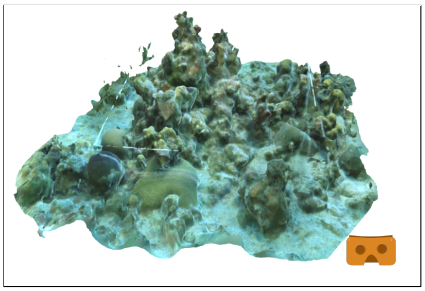

3D model created with the method described in this Chapter. This is a 2 x 2 quadrat of coral reef at the dive site Black Coral Wall, Utila, Honduras filmed 05 August 2016. Available at `https://skfb.ly/6vvoN`, or scan the QR code.

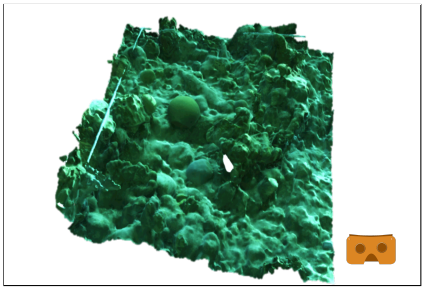

3D model created with the method described in this Chapter. This is a 2 x 2 quadrat of coral reef at the dive site Stingray Point, Utila, Honduras filmed 06 August 2016. Available at `https://skfb.ly/6vvoQ`, or scan the QR code.

I know that the place looks like a bit of a mess, but its actually a very delicate ecosystem.

— The IT Crowd, Season 1, Episode 4

3

Three-Dimensional Models of Coral Reefs Predict Caribbean Fish Abundance and Diversity

Contents

3.1 Context 43
3.2 Author Contributions 45
3.3 Publication: Young, G. C., *et al.* "Three-Dimensional Models of Coral Reefs Predict Caribbean Fish Abundance and Diversity." *In Prep.* 47

3.1 Context

This chapter ties ecological data to reef 3D models created via the method described in the previous chapter. We quantify the structural complexity of the 3D models in terms of the three ecologically relevant metrics described in the previous chapter: linear rugosity, fractal dimension, and vector dispersion. We link these metrics to fish survey variables, although the method could be applied to other correlation studies, such as with urchins, algae, seabed classifications (*e.g.,* rock, muddy sand, mud as in Dartnell and Gardner (2004)), or other ecological features

thought to correlate with structural complexity.

Testament to the timeliness and novelty of this study, in late October 2017, González-Rivero et al. (2017) published a similar study in *Nature Communications* titled "Linking fishes to multiple metrics of coral reef structural complexity using three-dimensional technology." They cite our publication from Chapter 2 of this thesis. Their paper has many similarities to ours and a few key differences as discussed in the paper and summarized here with connections to other sections of this thesis. Like the study we present in this Chapter, they use photogrammetry to create 3D models of a Caribbean reef (Glover's Atoll, Belize). Unlike our study, however, González-Rivero et al. (2017) focus on three damselfish species, whereas we recorded all fish species above the quadrats. González-Rivero et al. (2017) also employed different structural complexity metrics. Their metrics (visual exposure, density of refuges, and substrate availability) correlated more strongly than ours did to the fish data. Differences in site, species, and several other factors apart from methodology could explain this difference, as discussed in our paper. An advantage to their metrics over ours is that theirs have straightforward ecological meaning, whereas fractal dimension and vector dispersion are abstracted mathematically. The drawback to their metrics over ours is that theirs cannot currently be fully automated; theirs require humans to pinpoint refuges and identify algae. While this is acceptable for small data sets, it is not feasible for large swaths of 3D modelled reef, especially if they need to be monitored consistently over years. This topic is further discussed in Chapter 6.3 of this thesis: Limitations and Future Directions. A next step for technology-minded ecologists could be automating the calculation of the metrics used by González-Rivero et al. (2017), or ones similar. This avenue of future research is explored in Chapter 5 and 6.1.4.

This Chapter spawned two follow-up studies that are already underway as publications in preparation (Appendices A & B). Their relations to this chapter are briefly described below.

A Ninety 2x2 m quadrats were 3D modelled on a reef off Bonaire in the Caribbean and tied to fish survey variables — same size quadrats, same 3D modelling

methods, and same fish variables as this chapter, so the different sites could be compared. Only rugosity at the 2 cm scale was calculated from the 3D models to simplify analysis and because this chapter showed that rugosity alone predicted fish survey variables as well as all the other metrics (or visual assessment) combined. As described in Appendix A, there were significant linear relationships between rugosity and species richness ($R^2 = 0.43$), Simpson diversity index ($R^2 = 0.31$), and Shannon diversity index ($R^2 = 0.27$), with R^2 values higher than reported in the present chapter. The study also shows that position on the reef profile (either terrace, drop-off, or slope) effected fish survey variables and rugosity.

B Fifty-six 2x2 m quadrats were 3D modelled on a reef off Utila, Honduras, the same study site as this chapter. Again, the methodology was the same as this chapter — same size quadrats, same 3D modelling methods, and same fish variables — except that fish surveys were conducted by video surveys instead of diver surveys. Contrary to the findings of the present study and others, only total fish abundance significantly correlated with complexity metrics and only with fractal dimension at the scale 5–15 cm ($D_{5-15\,cm}$) and vector dispersion ($1/k$). Further contrary to other studies' findings, the correlations were negative (ρ=-0.41 and -0.29 with $D_{5-15\,cm}$ and $1/k$ respectively). This contrasting result could be the result of the video surveys not capturing as many cryptic fish species as the diver surveys. Moreover, more complex structures (with higher $D_{5-15\,cm}$ and $1/k$) may have occluded more cryptic species in video footage than relatively flat structures did.

3.2 Author Contributions

The authors of this publication, in order, are: G. C. Young, D. A. Exton, S. Burch, E. Page, E. E. Purdue, B. Van Doren, and A. D. Rogers. Author contributions are listed in CRediT taxonomy in Table 3.1 on page 46 following Brand et al. (2015).

Table 3.1: Author contributions for Chapter 3 listed in CRediT taxonomy (Brand et al., 2015). Initials refer to the authors of the paper; in order, they are: G. C. Young, D. A. Exton, S. Burch, E. Page, E. E. Purdue, B. Van Doren, and A. D. Rogers.

Role	Author(s)
Conceptualization – Ideas; formulation or evolution of overarching research goals and aims.	GCY, DAE
Data Curation – Management activities to annotate (produce metadata), scrub data and maintain research data (including software code, where it is necessary for interpreting the data itself) for initial use and later reuse.	GCY
Formal Analysis – Application of statistical, mathematical, computational, or other formal techniques to analyze or synthesize study data.	GCY, SB, EEP, EP, BVD
Funding Acquisition – Acquisition of the financial support for the project leading to this publication.	GCY, DAE, ADR
Investigation – Conducting a research and investigation process, specifically performing the experiments, or data/evidence collection.	GCY, SB, EEP, EP
Methodology – Development or design of methodology; creation of models	GCY
Project Administration – Management and coordination responsibility for the research activity planning and execution.	GCY, DAE
Resources – Provision of study materials, reagents, materials, patients, laboratory samples, animals, instrumentation, computing resources, or other analysis tools.	GCY, DAE, ADR
Software – Programming, software development; designing computer programs; implementation of the computer code and supporting algorithms; testing of existing code components.	GCY
Supervision – Oversight and leadership responsibility for the research activity planning and execution, including mentorship external to the core team.	GCY, DAE, ADR
Validation – Verification, whether as a part of the activity or separate, of the overall replication/reproducibility of results/experiments and other research outputs.	GCY
Visualization – Preparation, creation and/or presentation of the published work, specifically visualization/data presentation.	GCY
Writing - Original Draft Preparation – Creation and/or presentation of the published work, specifically writing the initial draft (including substantive translation).	GCY

Continued on next page

Table 3.1 – *Continued from previous page*

Role	Author(s)
Writing - Review & Editing – Preparation, creation and/or presentation of the published work by those from the original research group, specifically critical review, commentary or revision - including pre- or post-publication stages.	GCY, BVD, DAE, ADR

3.3 Publication: Young, G. C., *et al.* "Three-Dimensional Models of Coral Reefs Predict Caribbean Fish Abundance and Diversity." *In Prep.*

Pages 48–88 of this thesis include the publication as it was formatted for submission to a journal. This formatting choice is consistent with the University's Examination Regulations for Research Degrees in Biological Sciences (Plant Sciences and Zoology).

Three-dimensional models of coral reefs predict Caribbean fish abundance and diversity

G. C. Young[1,2]*, D. A. Exton[2], S. Burch[1,2], E. Page[1,2], E. E. Purdue[1,2], B. M. Van Doren[1], A. D. Rogers[1]

Submission to *Marine Ecology Progress Series*

Running page head (3–6 words): 3D Models Predict Fish

Last edited May 27, 2018

---

[1]Department of Zoology, University of Oxford, Oxford, OX1 3PS, UK

[2]Operation Wallacea, Wallace House, Old Bolingbroke, Spilsby, Lincolnshire, PE23 4EX, UK

ffl*Corresponding author email <grace@robots.ox.ac.uk>

Abstract

Coral reef structural complexity has been shown to positively correlate with fish abundance and diversity. Most correlative studies have measured structural complexity with two-dimensional or visual metrics, such as chain-and-tape rugosity or the Habitat Assessment Score (HAS). In this study, we create three-dimensional (3D) models of 85 2x2 m quadrats of reefs around the Caribbean island of Utila. We show how metrics of structural complexity from the 3D models have the same predictive power for fish abundance and diversity as the more traditional metrics of chain-and-tape rugosity or HAS. The 3D metrics were linear rugosity (R), fractal dimension (D), and vector dispersion ($1/k$). R was the best predictor of fish variables, followed by $1/k$, with the highest significant Spearman's rank correlation coefficients with all fish variables. D measured between 15–30 cm and 5–15 cm also correlated with fish variables, but D measured at other scales 1–120 cm did not. We suggest 3D models become a standard approach for measuring reef structural complexity. Not only can they explain as much variation as traditional measurements for fish abundance and diversity, but also they can non-destructively produce a variety of 3D metrics at numerous spatial scales and keep a permanent record of reef structure over time.

Keywords: underwater photogrammetry · coral reefs · fish · damselfish · structural complexity · habitat complexity · rugosity · fractal dimension

1 Introduction

Studies spanning decades have identified structural complexity as a key factor enabling coral reefs to provide their unique ecosystem functions (Hiatt et al., 1960, McCormick, 1994, Knudby & LeDrew, 2007, Graham & Nash, 2013). Broadly those ecosystem functions include hosting some of the planet's highest levels of biodiversity (Moberg & Folke, 1999), harbouring a third of all marine species (Fisher et al., 2014), and protecting shorelines against storms and erosion (Ferrario et al., 2014). In this context, structural complexity describes reefs' physical, three-dimensional (3D) geometry. The geometry provides essential habitat features associated with ecosystem engineers, such as shelter from predators (Hixon & Beets, 1993, Rogers et al., 2014), places to spawn (Bourget et al., 1994, Coker et al., 2012), surface areas for grazing (Vergés et al., 2011), and differential regions of light (Obura, 2005) and turbulence (Hearn et al., 2001, Johansen et al., 2008).

A smorgasbord of metrics can quantify reef structural complexity. The most popular metric is chain-and-tape or linear rugosity (R). To measure R, a SCUBA diver lays a chain on a reef and measures the end-to-end distance that the chain falls. The chain's full length divided by its draped length equals R, meaning that R increases with structural complexity (Risk, 1972, Luckhurst & Luckhurst, 1978). Other metrics derive from profile gauges (Carleton & Sammarco, 1987, McCormick, 1994), digital level gauges (Dustan et al., 2013), visual assessments by divers (Gratwicke & Speight, 2005, Wilson, Graham & Polunin, 2007), or vectorizations of reef 3D models (also termed 'surface descriptors' or 'terrain descriptors;' *e.g.,* Wilson, O'Connell, Brown, Guinan & Grehan (2007), Friedman et al. (2012), Figueira et al. (2015)).

Most structural complexity metrics correlate with other indicators of reef health such as fish abundance, species richness, coral cover, and macroalgal cover, although relationships can vary from strong to weak or be inconsistent

(McCormick, 1994, Lingo & Szedlmayer, 2006, Komyakova et al., 2013). The relationship between structural complexity and fish is of particular interest to not only ecologists who want to understand relationships between structure and function (Lingo & Szedlmayer, 2006), but also to fisheries managers who want to maximise yields (Rogers et al., 2014). While correlations do not imply causations, the correlations are particularly useful in the context of reef studies because (a) structural complexity may be an easy-to-measure proxy for other indicators of reef health and (b) they hint at possible underlying ecological principals that could, for example, enhance reef restoration.

Relying on R alone as the metric of structural complexity, as many studies do, leaves much unanswered about correlations' ecological underpinnings. Although relatively easy to calculate, R is a simplistic measure that can mask nuances in reef structure (Friedlander & Parrish, 1998, Goatley & Bellwood, 2011, Plaisance et al., 2011, Graham & Nash, 2013). Moreover, measuring it with the chain-and-tape method can damage the reef and yields R only at the spatial resolution of the chain link. This can be problematic because it is often unclear which spatial scales are ecologically meaningful for organisms of interest (Knudby & LeDrew, 2007, Mellin et al., 2009).

Metrics from reef 3D models are particularly promising for structural complexity assessments because the 3D models can be preserved over time, analysed automatically at several scales, and yield a wide variety of metrics (including, but not limited to, R). 3D metrics' precision and accuracy are limited only by a 3D model's spatial resolution, and 3D reef models can be generated with arbitrarily fine or large spacial resolutions (mm to km scales), dependent upon the modelling method. Thanks to technological advancements in the last decade, there are several underwater 3D modelling methods, including photogrammetry (Burns et al., 2015, Leon et al., 2015), LiDAR (Pittman & Brown, 2011), sonar (Huvenne et al., 2002, Wilson, O'Connell, Brown, Guinan & Grehan, 2007, Zawada et al., 2010), satellite remote sensing with acoustic depth sounding (Purkis et al., 2008), stereo

imagery with underwater vehicle position (Johnson-Roberson et al., 2010), and combinations thereof (Costa et al., 2009, Pizarro et al., 2009, Robert et al., 2017).

Several studies worldwide have demonstrated that structural complexity positively correlates with fish abundance and/or diversity through structural complexity metrics *not* derived from 3D models: *e.g.,* in the Caribbean (Almany, 2004, Gratwicke & Speight, 2005, Grober-Dunsmore et al., 2007, Rogers et al., 2014), on the Great Barrier Reef (Beukers & Jones, 1997, Komyakova et al., 2013), off Western Australia (Vergés et al., 2011), off New Zealand (Willis & Anderson, 2003), in the Gulf of California (Aburto-Oropeza & Balart, 2001), and in the Red Sea (Roberts & Ormond, 1987). Far fewer studies have demonstrated that structural complexity correlates with fish assemblages through metrics derived from 3D models. Mellin et al. (2009) review the nine studies available at the time of publication that used remote sensing data, which can produce a type of 3D model, to predict coral reef fish abundances and diversities. The author notes that these studies generally did not corroborate each other. In the Caribbean, Agudo-Adriani et al. (2016) showed that length, volume, number of peripheral branches, and average number of branches from photogrammetry 3D models of the coral *Acropora cervicornis* predicted fish abundance and richness. Bejarano et al. (2011) showed that acoustic roughness from ecosounder 3D models predicted fish abundance. Pittman & Brown (2011) showed that metrics from LiDAR 3D models (scales 5-300 m) could predict fish species distributions. Off the Florida coast, Walker et al. (2009) showed that surface and linear R from LiDAR 3D models predicted fish populations. González-Rivero et al. (2017) found that metrics from photogrammetric 3D models of reef explained damselfish abundance distribution better than the traditional measure of rugosity.

This study is one of the first to tie ecological data to a suite of structural complexity metrics that are only possible to compute from 3D models. It uses a suite of 3D metrics from photogrammetric 3D models to attempt to predict fish assemblages at the meter scale. Fish surveys and 3D models (accurate to ≈1.3 cm)

were completed over 2x2 m quadrats on a Caribbean reef. Structural complexity was quantified by 3D metrics that could be automatically calculated from the 3D models by software: rugosity (R), fractal dimension (D) measured at five different scales 1–120 cm, and vector dispersion ($1/k$). Additionally, structural complexity was quantified by Habitat Assessment Score (HAS), a metric derived from in-water diver surveys. HAS was chosen as a baseline to compare with 3D metrics because it is a popular means of capturing a range of habitat features that has been shown to correlate significantly and positively with fish abundance and species richness (Gratwicke & Speight, 2005).

This paper addresses several research questions. The first relates to the 3D models' predictive abilities: *Are 3D metrics able to predict fish abundance, species richness, and diversity as well as or better than HAS?* The second research question attempts to better understand: *Does the 3D metric fractal dimension correspond to what divers perceive as refuges (holes or crevices) at the same size categories?* This would suggest that if fish prefer structures with high fractal dimension, it could be because the high fractal dimension indicates the presence of refuges, a feature already shown to affect fish (Willis & Anderson, 2003, Gratwicke & Speight, 2005). Finally, *is damselfish (Pomacentridae family) abundance greater for fractal dimensions at scales close to their body sizes?* Damselfish were highlighted because they have demonstrated preferences for high structural complexity at the scales measured in this study (Holbrook et al., 2000, Precht et al., 2010), although not in terms of 3D metrics.

2 Materials and methods

2.1 Study sites

This study took place at five reef sites on the southern coast of the Caribbean island of Utila, Honduras (Fig. 1). Each site was surveyed in both the morning and afternoon and over several days to counter potential bias from weather or

time of day. Data were collected over 17 days between 18 July 2016 and 9 August 2016. Eighty-five 2x2 m quadrats were surveyed, at least 15 at each dive site. Research commenced under permit from the Instituto de Conservación Forestal (#ICF-DE-MP-080-2016).

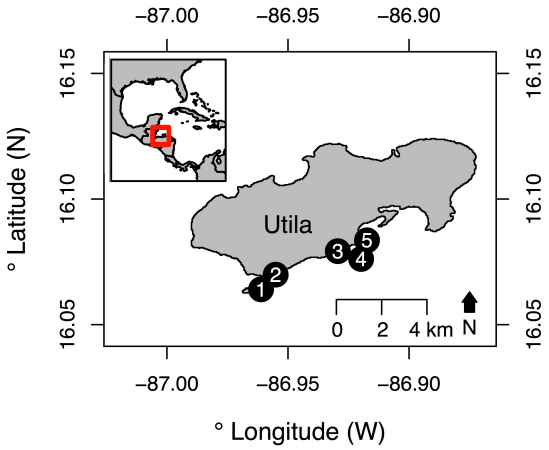

Figure 1: Study sites around the Caribbean island of Utila, Honduras. Inset shows Utila (boxed in red) relative to the rest of Central America and the Caribbean. Reef sites labelled as follows: (1) Diamond Cay (DC), (2) Stingray Point (SP), (3) Little Bight (LB), (4) Pretty Bush (PB), and (5) Black Coral Wall (BW). Map generated with permission from the GADM database of Global Administrative Areas.

2.2 Quadrat placement

Quadrats were placed in a semi-random fashion. Firstly, SCUBA divers laid a 20 m transect tape along the reef, starting near a site's mooring buoy and continuing along a depth contour at 5±2 m. Each time a site was surveyed, the transect was placed on a different area of reef at the same depth (5±2 m). Secondly, divers placed quadrats equidistantly along the transect (5 m apart). Two considerations made quadrat placement not truly random: (1) When placing a quadrat, a diver did not include moving structures that would obscure other parts of the seabed; this was because moving structures cannot be rendered by SfM photogrammetry, as they do not have a static position in 3D space. In practice, this meant repositioning some quadrats on nearby suitable reef to avoid sea fans and sea whips (most commonly *Gorgonia flabellum* or *Ellisella barbadensis*).

(2) Quadrats were positioned such that they could lay flat, approximately parallel to the ocean surface, to ensure consistency in slope across the data.

2.3 In-water data collection

2.3.1 Underwater filming

Divers filmed each quadrat with a GoPro camera (either Hero 3, 3+ or 4) in a GoPro flat port underwater housing. They followed exactly the method described in Young et al. (2017); *i.e.,* they swam over the quadrat in a lawnmower pattern while pointing the camera directly down at the seabed. The camera was in video mode with all default settings except: resolution 1080p, field-of-view narrow, sharpness medium, capture rate 24-30 frames per second, and white balance 6500K. Only ambient light illuminated scenes. Divers spent 2-5 minutes filming each quadrat. Filming was stopped if there were any movements that would hinder the quality of the 3D model (*e.g.,* if a school of fish swam between the camera and the quadrat), and divers restarted filming once the disturbance passed.

2.3.2 Recording Habitat Assessment Scores (HAS)

Two divers separately estimated the Habitat Assessment Score (HAS) of a quadrat. They followed the method of Gratwicke & Speight (2005), whereby divers score the reef from 1 to 5 in six categories: (1) rugosity, (2) variety of growth forms, (3) approximate height, (4) number of refuge size categories, (5) approximate percentage of live cover, and (6) approximate percentage of hard substratum. HAS is the sum of those scores, where a low value indicates low habitat complexity while a high value indicates high habitat complexity.

Divers were not expected to always record the exact same score, as HAS is partially subjective. Two divers' scores were therefore averaged as the best estimate for the quadrat. Additionally, divers recorded which of the refuge size categories they observed for HAS. They recorded "present" if they observed holes or gaps

in habitat architecture or substratum at a given size category, or "absent" if they did not. The size categories were 1-5, 6-15, 16-30, 31-50 and >50 cm, following Gratwicke & Speight (2005).

2.3.3 Surveying fish

The method for surveying fish was the same as Gratwicke & Speight (2005), the study that devised HAS. For nine minutes divers recorded all fish passing within the ∼2x2x2 m space over the quadrat boundaries; they did this while hovering at least 1 m away from the quadrat. A final minute was spent looking closer at the quadrat, actively searching for fish previously unnoticed because they were camouflaged or hiding in the structure.

From the fish survey data, the following summary metrics were computed for each quadrat: total fish abundance, species richness (*i.e.,* number of distinct species), Shannon diversity index (Shannon, 1948), Simpson diversity index (Simpson, 1949), and damselfish abundance. These metrics were chosen based on similarities with other publications of fish survey results, in particular Gratwicke & Speight (2005) and Belmaker (2009). Note that total fish abundance was the sum of the residential and transient fish abundances.

2.4 3D model generation

Video footage of a quadrat was converted into an image sequence at 3 frames per second using the open source program FFmpeg (www.ffmpeg.org). Images were then loaded into the structure-from-motion software PhotoScan Standard (Agisoft LLC, St. Petersburg, Russia), where 3D models rendered with the same settings as Young et al. (2017). Models were then imported into the 3D modelling software Rhinoceros 3D ("Rhino"; Robert McNeel & Associates, Seattle, WA, USA), where each was scaled such that a quadrat's edge length was 2 m. All models were rotated so that the quadrat laid parallel to the X-Y plane, as this is how quadrats were placed in-water. Figure 2 shows two example 3D models with

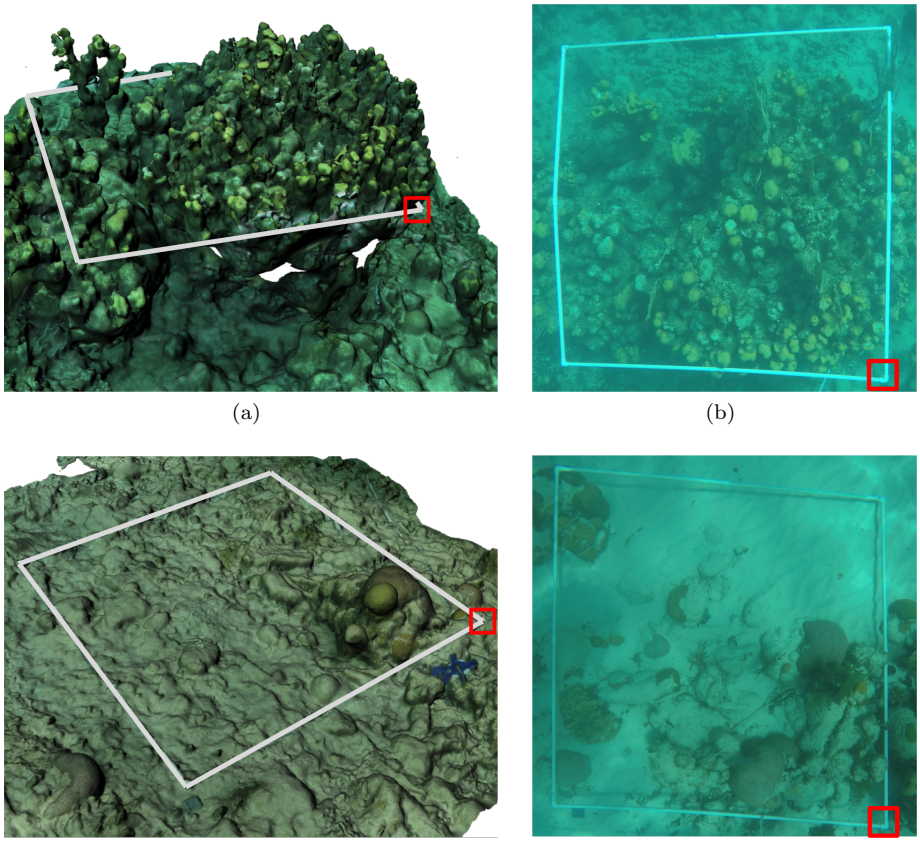

Figure 2: 3D models from photogrammetry and photos of 2x2 m quadrats with contrasting structural complexity. Images are shown with true colours, no RGB correction. (a) 3D model of quadrat with high structural complexity (*i.e.,* all 3D metrics greater than median values); quadrat highlighted for visual clarity. Corner boxed in red corresponds to corner in (b), a birds-eye-view photo of the same quadrat. (c) 3D model of quadrat with low structural complexity (*i.e.,* all 3D metrics lower than median values); quadrat highlighted for visual clarity. Corner boxed in red corresponds to corner in (d), a birds-eye-view photo of the same quadrat.

different structural complexities. Because the filming and rendering method was the same as in Young et al. (2017), it is assumed that these 3D models were also precise and accurate to 1.48 cm in X-Y and 1.35 cm in Z.

Quadrat data were discarded if quadrat edges in the 3D model were not clear enough to indicate scale. Seven quadrats (from an original 92 rendered) were removed from the dataset for this reason.

2.5 3D metrics computation

All 3D models' structural complexity metrics were computed using the scripts available from Young et al. (2017); scripts were written in the Python program-

ming language for use within the Rhino 3D modelling software. The structural complexity metrics from the 3D models are hereafter referred to as the 3D metrics and should not be confused with HAS, which is a habitat complexity metric from in-water diver surveys. The following 3D metrics were chosen for their ecological relevance, as described in Young et al. (2017): linear rugosity (R), fractal dimension (D), and vector dispersion ($1/k$).

To compute R, six virtual chains were laid on the 3D model as depicted in Fig. 3(a). Virtual chains traced the contours of the 3D model, as would a physical chain laid upon the sea floor. They were laid via the extendible-chain method of Young et al. (2017). Values of R computed this way from 3D models correlate positively and tightly with those measured *in-situ* via the chain-and-tape method Young et al. (2017), the most widely used structural complexity metric among marine researchers (Graham & Nash, 2013). Equation 1 gives R for a quadrat, where R is the average from six virtual chains.

$$R = \frac{1}{6}\left(\sum_{i=0}^{N=6} \frac{\text{undraped length of chain}_i}{\text{draped length of chain}_i}\right), \tag{1}$$

where all chains in this study had a draped length 1.75 m and undraped lengths > 1.75 m. The draped length of 1.75 m was used instead of the theoretical maximum of 2 m (the length of the quadrat), because it allowed chains to cover as much of the quadrat area as possible while consistently and comfortably avoiding the PVC pipes of the quadrat itself.

Fractal dimension (D) was computed at five scales: 60–120, 30–60, 15–30, 5–15, and 1–5 cm. These ranges were chosen to follow the refuge size categories chosen for HAS by Gratwicke & Speight (2005), although some modifications were needed as the upper bound of D must be divisible by the lower bound, and because D requires set boundaries. D is a unitless number between 2 and 3, where 2 indicates a flat plane (2D) and 3 indicates a very complex surface (close to 3D). Ecologically, if $D_{15-30\,cm}$ is high ($D_{15-30\,cm} > \approx 2.25$), then there is likely

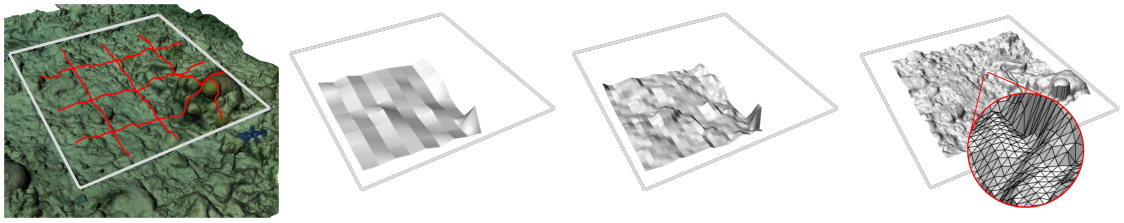

(a) (b) (c) (d)

Figure 3: Intermediate steps in the calculation of structural complexity metrics from the 3D models. (a) Six virtual chains (shown in red) laid in a grid pattern over the reef 3D model to calculate linear rugosity (R). For the same quadrat, a 1.20 x 1.20 m patch of quadrat rendered at (b) the 15 cm resolution and (c) the finer resolution of 5 cm. Fractal dimension (D) describes how the surface area changes with resolution. (d) A 1.60 x 1.60 m patch of the quadrat rendered from a grid of points (spaced 1 cm apart) projected onto the reef 3D model; close-up shows how triangles connected adjacent points. Vector dispersion ($1/k$) describes relationships between the angles of triangle's normal vectors. For all 3D metrics, higher values indicate higher structural complexity.

to be many crevices suitable for animals with body sizes 15–30 cm (Tokeshi & Arakaki, 2012). Conversely, if $D_{15-30\,cm} = 2.00$, then the surface is a flat plane and does not offer shelter to animals of those body sizes. To further develop an ecological understanding of D, in this study values of D were compared with divers' perceptions of the refuge size categories for HAS.

Finally, $1/k$ was computed by the script available from Young et al. (2017) and originally by Carleton & Sammarco (1987). Whereas Carleton & Sammarco (1987) calculated $1/k$ from points they measured with a profile gauge on coral samples, in this study a virtual grid of points was projected onto the 3D models. The script projected a 1.60 x 1.60 m grid of points within the 3D model quadrat. Grid points were evenly spaced apart by 0.01 m. The script then created a surface from the points by connecting adjacent points with triangles as depicted in Fig. 3(d). It then computed $1/k$ for each 0.20 x 0.20 m area. Values from all areas (*i.e.,* the 64 areas, each 0.20 x 0.20 m, which composed the total 1.60 x 1.60 m grid) were averaged to estimate $1/k$ for the quadrat.

2.6 Statistical analysis

All statistical analysis was conducted in R 3.3.3 (R Core Team, 2017). Statistical significance was considered at $\alpha = 0.05$. The fish variables were considered

dependent variables, while the structural complexity metrics were considered independent variables.

Firstly, Spearman rank correlation coefficients (ρ) determined the strength and significance of monotonic relationships between variables. ρ was more suitable than linear models for assessing trends because the data were heavily skewed. The False Discovery Rate correction adjusted P-values to avoid Type I errors from multiple testing. Before combining data from the different sites and days, analysis of variance (ANOVA) tests determined whether or not site, day, or interactions between the two significantly affected any of the fish variables. Post-hoc pairwise t-tests probed any differences between individual sites. If two variables significantly correlated with $|\rho| > 0.80$, then they were considered collinear, and only one was carried forward in analysis to avoid redundancy. To elucidate possible ecological interpretations of D, it was plotted against the refuge size categories that divers observed for HAS so that any patterns that might explain correlations between those two variables could be visually inspected. A Principal Component Analysis (PCA) also assessed relationships between the 3D metrics and consolidated them into fewer variables or principal components (Jolliffe, 1986). The function 'PCA' from the 'FactoMineR' library (Lê et al., 2008) performed the PCA; it automatically scaled values to unit variance prior to PCA.

Secondly, linear models fit the relationships between fish variables and structural complexity metrics and compared the predictive powers of the models with HAS and 3D metrics. One set of linear models had HAS as the independent variable. Another set had 3D metrics (represented by the first principal component, PC1) as the independent variable. A final set, created post-hoc, had R as the independent variable. The models with R were created post-hoc because R alone had highly significant correlations in terms of ρ with all fish variables. The fish variables were transformed by either natural logarithm, square, or square root to meet model assumptions (diagnostics in Fig. S1-S2). Initial models included site as a fixed effect and day as random effects using the 'lmer' function of the

R library 'lme4' (Bates et al., 2015). Site was a fixed rather than random effect because (a) we had only five sites, and (b) because the ANOVA revealed sites' effects were not random (with one site, PB, had a stronger effect on fish variables than the other sites). A random effect was removed if its 95% confidence interval contained zero, and a fixed effect was removed from a model if non-significant. Vuong tests compared non-nested models (Vuong, 1989). They were implemented with the 'vuongtest' function in the R library 'nonnest2' (Merkle et al., 2015). If Vuong's variance test established that two models were distinguishable, then Vuong's non-nested likelihood ratio test evaluated the null hypothesis that the two models fit equally well to the focal population. The null hypothesis could be rejected in favour of either model fitting better than the other (Merkle et al., 2015). If model fits were equal (null hypothesis accepted), then we concluded that the independent variables of the two models have the same predictive power. Differences in models' Akaike Information Criterion (AIC) corroborated Vuong test results.

3 Results

3.1 Effects of site and day

Neither site nor day (nor interactions between the two) significantly affected any of the fish variables ($P \geq 0.05$; two-way ANOVAs). Data from all sites and days were therefore combined in further analysis in terms of ρ.

3.2 Relationships between fish variables

Some fish variables correlated very strongly (Fig. S3). The following were removed from further statistical analyses because they were colinear with at least one other variable (Table 1): (1) species richness in favour of total abundance and (2) Simpson diversity index in favour of Shannon diversity index. Therefore

312 the only fish variables carried forward in analysis were: (1) total fish abundance,
313 (2) Shannon diversity index, and (3) damselfish abundance.

Table 1: Summary of variables. Those noted as being very strongly correlated had Spearman's rank correlation coefficient of $|\rho| \geq 0.80$.

Structural Complexity Metrics	Fish Variables
From 3D models:	Total abundance
R	*Very strongly correlated with:*
$D_{60-120\ cm}$	Species richness
$D_{30-60\ cm}$	Shannon index
$D_{15-30\ cm}$	*Very strongly correlated with:*
$D_{5-15\ cm}$	Simpson index
$D_{1-5\ cm}$	Species richness
$1/k$	Damselfish abundance
From diver surveys:	
HAS	

314 A total of 1645 fish were observed across the 85 quadrats. The six most ob-
315 served species (encompassing 52% of observations) were *Stegastes partitus, Tha-*
316 *lassoma bifasciatum, Scarus iserti, Halichoeres garnoti, Stegastes adustus,* and
317 *Scarus taeniopterus*, and 54 other distinct species were recorded. Thirty-five per-
318 cent of fish recorded were damselfish (Pomacentridae family). The majority of
319 damselfish were *Stegastes partitus* and *S. adustus*, which comprised 32% and 20%
320 of damselfish respectively, followed by *S. planifrons* (17%) and *Chromis cyanea*
321 (12%). Table S1 lists each species and its observed frequency. The average
322 quadrat had 19 ± 10 individual fish (mean $\pm$ standard deviation), a Shannon
323 index of 0.78 ± 0.18, and 7 ± 4 damselfish (Fig. S3).

324 3.3 Relationships between structural complexity metrics

325 All 3D metrics significantly correlated with each other and with HAS (Fig.
326 S4), but none were collinear and therefore all were included in further statistical
327 analysis (Table 1).

328 3.3.1 Relationships between D and HAS refuge size categories

329 Divers reported observing refuge size categories 1-5, 5-15, 15-30, 30-60, and
330 60-120 cm in 97%, 86%, 40%, 9%, and 1% of quadrats, respectively. Their per-

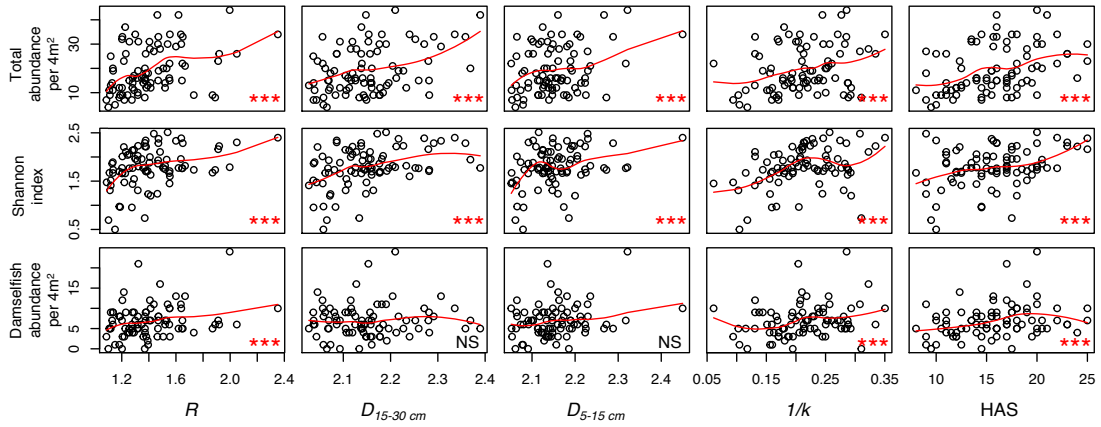

Figure 4: Relationships between fish variables and structural complexity metrics. LOESS smoothing lines in red. All correlations are weak ($0.20 \leq |\rho| \leq 0.39$), except the moderately strong relationship between R and total abundance ($0.40 \leq |\rho| \leq 0.59$). $N = 85$ for all correlations. P-values adjusted by the False Discovery Rate correction. (***) ρ significant with P-adjusted ≤ 0.05. (NS) ρ non-significant.

ceptions showed no relation to D at any scale (Fig. S5), except that for categories 30-60 and 60-120 cm, where divers almost never observed refuges, D was heavily skewed towards low values (Fig. S4).

3.3.2 3D metrics in Principal Component Analysis (PCA)

The PCA consolidated the 3D metrics into one variable. The first principal component (PC1) captured the majority of variation in the 3D metrics (62.5%). Other principal components only marginally increased the proportion of variance captured (Fig. S6). PC1 strongly correlated with HAS, but not strongly enough to be considered collinear ($\rho = 0.64$, $P \ll 0.05$).

3.4 Relationships between structural complexity metrics and fish variables

R and *1/k* were the only 3D metrics that significantly correlated with all fish variables (Table 2; Fig. 4). HAS also significantly correlated with all fish variables (Table 2; Fig. 4). $D_{15-30\,cm}$ and $D_{5-15\,cm}$ significantly correlated with fish variables except damselfish abundance (Table 2; Fig. 4). $D_{30-60\,cm}$ and $D_{1-5\,cm}$ significantly correlated with total abundance, but not any of the other fish vari-

Table 2: Spearman's rank correlation coefficients (ρ) between structural complexity metrics and fish survey variables. $D_{60-120\ cm}$ is not listed because none of its correlations were significant, but it was included in the P-value correction. P-values adjusted by the False Discovery Rate correction to avoid errors from multiple testing (adjusted for 32 tests). Significant P-values bolded.

	N	ρ	P-adjusted
Rugosity			
Total abundance	85	0.42	**< 0.001**
Shannon index	85	0.38	**< 0.001**
Damselfish abundance	85	0.24	**0.042**
Fractal Dimension 30-60 cm			
Total abundance	85	0.25	**0.040**
Shannon index	85	0.20	0.097
Damselfish abundance	85	-0.03	0.819
Fractal Dimension 15-30 cm			
Total abundance	85	0.32	**0.011**
Shannon index	85	0.39	**< 0.001**
Damselfish abundance	85	0.01	0.950
Fractal Dimension 5-15 cm			
Total abundance	85	0.25	**0.040**
Shannon index	85	0.29	**0.017**
Damselfish abundance	85	0.20	0.097
Fractal Dimension 1-5 cm			
Total abundance	85	0.24	**0.040**
Shannon index	85	0.17	0.160
Damselfish abundance	85	0.16	0.164
Vector Dispersion			
Total abundance	85	0.28	**0.027**
Shannon index	85	0.34	**0.006**
Damselfish abundance	85	0.27	**0.028**
HAS			
Total abundance	85	0.43	**< 0.001**tbf
Shannon index	85	0.32	**0.011**
Damselfish abundance	85	0.29	**0.017**

ables (Table 2). $D_{60-120\,cm}$ did not significantly correlate with any fish variables. All relationships between structural complexity metrics and fish variables were weak ($0.20 \leq |\rho| \leq 0.39$; Table 2), except for the moderately strong relationship between R and total abundance ($0.40 \leq |\rho| \leq 0.59$; Table 2).

Although D did not correlate with damselfish abundance at any scale, plots of the data revealed a notable outlier (Fig. S7). The outlier quadrat had D 2–4 standard deviations (SD) above mean values in four of the five size categories and hosted damselfish abundance more than five SD above the mean (Fig. S7–S8).

3.5 Did 3D models predict fish survey results as well as or better than HAS?

The 3D metrics (represented by PC1) predicted fish survey results no better and no worse than HAS (Table 3; full Vuong results in Table S2). R alone also predicted fish survey results with the same predictive power as PC1 (full Vuong results in Table S2; linear model in Table S3). In all linear models, the variance explained by day as a random effect did not significantly differ from zero. Day was therefore removed as a random effect in all linear models. Similarly, the variance explained by site did not significantly differ from zero for total fish abundance or Shannon index. Site was therefore removed as a random effect from those two linear models.

4 Discussion

The automated 3D modelling method had the same predictive power as HAS (Table 3). R alone from the 3D models, which is collinear with chain-and-tape measurements(Young et al., 2017), also had the same predictive power as HAS. This study recommends that future studies employ 3D metrics over HAS or other traditional methods for a number of reasons: (1) 3D metrics are purely quantitative and therefore can be more objectively compared across sites, times, and data

Table 3: Linear models for the fish survey metrics: natural logarithm of total abundance (log(t. abundance)) and Shannon diversity index squared (Shannon^2). Linear models contained only fixed effects, listed as coefficients. Abbreviations as follows: dependent variable (Dependent Var.), coefficients (Coeff.), estimate of coefficient (Est.) standard error of coefficient (SE), Akaike Information Criterion (AIC), first principal component (PC1), and Habitat Assessment Score (HAS). Significant P-values bolded.

	Model Summary					Goodness of Fit				Vuong Test Result
Dependent Var.	Coeff.	Est.	SE	t-value	Pr($>\|t\|$)	AIC	R^2	F	P	
log(t. abundance)	(Inter.)	0.64	0.03	24.22	**2E-16**	125	0.15	$F_{1,83}$	**2E-04**	Model fits equal
	PC1	0.04	0.01	3.35	**0.001**			= 15.11		$P \gg 0.05$
	(Inter.)	1.90	0.22	8.78	**2E-13**	120	0.20	$F_{1,83}$	**2E-05**	
	HAS	0.06	0.01	4.50	**2E-05**			= 20.25		
Shannon^2	(Inter.)	3.37	0.14	24.17	**2E-16**	289	0.12	$F_{1,83}$	**0.001**	Model fits equal
	PC1	0.22	0.07	3.35	**0.001**			= 11.25		$P \gg 0.05$
	(Inter.)	1.47	0.58	2.55	**0.013**	288	0.12	$F_{1,83}$	**0.001**	
	HAS	0.12	0.04	3.39	**0.001**			= 11.44		

collectors; (2) unlike HAS and other *in-situ* measurements, 3D metrics can be relied upon on sites where it is not possible for divers to visit; (3) as it is becoming increasingly feasible to repeatedly 3D model large swaths of reef (km scale), an automated data analysis method can keep up with the data much better than a labour-intensive method; (4) the 3D models are a permanent record of the reef's 3D structure that can be analysed with several metrics across spatial scales.

The equal predictive abilities of PC1 and HAS could be explained in part by the strong correlations between them ($\rho = 0.64$, $P \ll 0.05$). This was surprising because PC1 and HAS derived from different measurement techniques: one purely quantitative and one partially subjective. Moreover, HAS contained an estimate of live cover, which does not necessarily correlate with structural complexity (Alvarez-Filip et al., 2011) let alone any of the 3D metrics. The correlation between PC1 and HAS could stem from them both containing R, even though R was precisely measured from the 3D models and "eyeballed" by divers for HAS. While R is only one-sixth of a HAS score, it is likely doubly weighted in HAS because Gratwicke & Speight (2005) found it to be colinear with another of the six variables in HAS: percentage hard substratum. It was therefore unsurprising that R strongly correlated with HAS ($\rho = 0.72$; Fig. S4). It would also be ecologically

391 feasible to assume that D related to the refuge size categories in HAS; however,
392 this study found no evidence of such a relationship (Fig. S5).

393 R alone predicted fish variables as well as the suite of 3D metrics represented
394 by PC1. Studies wishing to save time or simplify analysis might therefore choose
395 to measure only R from the models. After all, R is generally highly correlated
396 with other metrics (Fig. S4 and Wilson, O'Connell, Brown, Guinan & Grehan
397 (2007)) and the easiest to understand conceptually. That said, once a 3D model
398 is generated, it is not much extra computational time to compute all the 3D
399 metrics, and they may yield greater ecological understanding. In this study R
400 may have been the best predictor because it covered close to the full width of
401 the quadrat (1.75/2.00 m), whereas D and *1/k* covered less (1.20/2.00 m and
402 1.60/2.00 m, respectively); further study would be needed to confirm patterns.

403 It is still unclear how to interpret D ecologically in the context of reef fishes.
404 D did not correspond to the presence or absence of refuge size categories divers
405 observed for HAS (Fig. S5), nor did it relate significantly to damselfish abundance
406 (Fig. S7). It was expected that damselfish would prefer habitats with high fractal
407 dimension at the scales near their body sizes, but this study did not observe
408 significant trends. There was a notable outlier quadrat (Fig. S7; Fig.S8), and
409 future studies might probe this effect by sampling surfaces with a wider range
410 of D, rather than randomly placing quadrats. All fish were smaller than the
411 body sizes in the category 60–120 cm, which might explain why no correlations
412 with $D_{60-120\,cm}$ were significant. However, this explanation is not likely given
413 that there is still not evidence that fish prefer D near their body size. $D_{1-5\,cm}$
414 significantly correlated with total abundance but not the other fish variables
415 (Table 2), even though many fish were in this body size category. Curiously, this
416 was true even though $D_{1-5\,cm}$ strongly correlated with $D_{5-15\,cm}$ and *1/k* ($\rho = 0.71$
417 and 0.73, respectively; Fig. S4), which each significantly correlated with all or
418 most fish variables.

There are a few possible explanations for why PC1 or HAS explained a low proportion of variance compared to other studies (less than one-third; Table 3). Firstly, it is difficult to benchmark this study against others from different regions and time periods. Possibly the only other comparable baseline is from Gratwicke & Speight (2005), the paper that devised HAS. Like the present study, Gratwicke & Speight (2005) took place on a Caribbean reef (British Virgin Islands) and over similarly sized quadrats (2.5x2.5 m quadrats vs this study, which used 2x2 m). Their study was over a decade ago, however, when Caribbean reefs may have been more structurally complex (Alvarez-Filip et al., 2009) and had more fish (Paddack et al., 2009). In their study, HAS correlated with the square root of total fish abundance with $R^2 = 0.17$ and with number of species with $R^2 = 0.55$. While the data could not be directly compared, the present study found correlations with similar R^2 values for total fish abundance (R^2=0.20; Table 3), but not for number of species (which was collinear with total abundance in this study, so R^2=0.20 again). Our relationship is also less strong than that measured by Agudo-Adriani et al. (2016) from their photogrammetry 3D models of a Caribbean reef off the central coast of Venezuela. They found that the length, volume, number of peripheral branches, and average number of branches of the coral *Acropora cervicornis* colonies explained 61% and 69% of abundance and richness of fish assemblage, respectively. Differences in region and metrics may account for these differences. Secondly, the relatively small observed ranges in abundance (4–44 fish over 4m^2) and 3D may have muted trends in the data. Thirdly, including singleton fish species may also have biased the diversity indices, but this bias would have been consistent in the comparison between the 3D metrics and HAS predictive abilities. Future studies might modify the fish observing method by collecting data over larger periods of time to create species accumulation curves before choosing the idea amount of time to watch fish. Fourthly and finally, habitat structural complexity, however it is measured, cannot explain all or even most variations in fish populations. There are several other ecological and

448 random effects at play not captured by 3D metrics, such as latitude, temperature,
449 interspecies interactions, and stability of the environment (Newman et al., 2015).

450 Corroborating support for photogrammetric 3D modelling as a tool for struc-
451 tural complexity analysis, González-Rivero et al. (2017) found that their measures
452 of structural complexity from 3D models of reefs around Belize predicted dam-
453 selfish abundance *better* than surface rugosity (ratio of the surface area of the
454 convoluted terrain to the surface area of the projected flat plane). González-
455 Rivero et al. (2017) used 3D metrics different from those in this study, namely
456 visual exposure to predators and competitors, density of predation refuges, and
457 substrate-related food availability. Their metrics correlated more strongly than
458 ours did to damselfish abundance. Differences in site, species, and several other
459 factors apart from methodology could explain this difference. Their metrics have
460 more straightforward ecological meanings than R, D, or $1/k$, which are more ab-
461 stracted mathematically. The only drawback to their metrics is that they are
462 not yet fully automated; they require a human to count crevices and outline turf
463 algae. It would be worthwhile to develop means of fully automating their mea-
464 surements so that they can be quantified repeatedly across large swaths of reef
465 with minimal effort.

466 Structural complexity, measured by HAS or PC1, explained more variation in
467 residential fish abundance than it did in total fish abundance or transient abun-
468 dance (Table 3). This could have a number of ecological explanations, although
469 further study is needed to imply causation. Residential fish may have included
470 a higher proportion of juveniles than did transient fish, and juvenile fish tend to
471 depend upon structural complexity more strongly than do adult fish: Beukers &
472 Jones (1997) found juvenile fish survivorship to be significantly higher on com-
473 plex corals compared to open-structures. Similarly, Almany (2004) found that
474 damselfish recruitment was greater on highly complex reefs compared to lower
475 complexity reefs. It could also be possible that residential fish included more
476 prey to piscivorous predators than did transient fish. As Almany (2004) dis-

cuss, predation risk is often lower in complex habitats for a wide range of taxa. Moreover, prey often increase their use of high complexity habitats as refugia in the presence of predators, and predators may be less efficient foragers in high complexity habitats.

5 Conclusion

This study adds to a growing body of evidence showing how 3D models can be an effective tool for monitoring marine ecosystems. Not only do metrics from 3D models correlate with more traditional metrics of complexity such as chain-and-tape rugosity and HAS, but they also have the same ability to predict fish abundance and diversity. Unlike more traditional means of measuring structural complexity, the 3D models can be analysed automatically and infinitely for many metrics at a range of spatial scales. We therefore suggest other studies use 3D modelling as a tool for measuring underwater structural complexity.

6 Acknowledgements

The authors would like to acknowledge the Marshall Aid Commemoration Commission for funding authors GCY and BMVD, Operation Wallacea for facilitating fieldwork, and the following people for their assistance: Dominic Andradi-Brown, Faye-Marie Crooke, Caitlin Fowler, Natalie Lubbock, Sam Lungari, Jess Mellito, and Grace Williams.

References

Aburto-Oropeza, O. & Balart, E. (2001), 'Community Structure of Reef Fish in Several Habitats of a Rocky Reef in the Gulf of California', *Marine Ecology* **22**(4), 283–305.

Agudo-Adriani, E. A., Cappelletto, J., Cavada-Blanco, F. & Croquer, A. (2016), 'Colony geometry and structural complexity of the endangered species Acropora cervicornis partly explains the structure of their associated fish assemblage', *PeerJ* **4**(e1861).

Almany, G. (2004), 'Does increasing habitat complexity reduce predation and competition in coral reef fish assemblages?', *Oikos* **106**(2), 275–284.

Alvarez-Filip, L., Côté, I. M., Gill, J. A., Watkinson, A. R. & Dulvy, N. K. (2011), 'Region-wide temporal and spatial variation in Caribbean reef architecture: Is coral cover the whole story?', *Global Change Biology* **17**(7), 2470–2477.

Alvarez-Filip, L., Dulvy, N. K., Gill, J. a., Cote, I. M. & Watkinson, a. R. (2009), 'Flattening of Caribbean Coral Reefs: Region-Wide Declines in Architectural Complexity', *Proceedings of the Royal Society B: Biological Sciences* **276**(1669), 3019–3025.

Baldwin, C. C., Weigt, L. A., Smith, D. G. & Mounts, J. H. (2009), 'Reconciling Genetic Lineages with Species in Western Atlantic Coryphopterus (Teleostei: Gobiidae)', *Smithsonian Contributions to the Marine Sciences* **38**, 111–138.

Bates, D., Mächler, M., Bolker, B. & Walker, S. (2015), 'Fitting Linear Mixed-Effects Models Using {lme4}', *Journal of Statistical Software* **67**(1).

Bejarano, S., Mumby, P. J. & Sotheran, I. (2011), 'Predicting structural complexity of reefs and fish abundance using acoustic remote sensing (RoxAnn)', *Marine Biology* **158**(3), 489–504.

Belmaker, J. (2009), 'Species richness of resident and transient coral-dwelling fish responds differentially to regional diversity', *Global Ecology and Biogeography* **18**(4), 426–436.

Beukers, J. S. & Jones, G. P. (1997), 'Habitat Complexity Modifies the Impact of Piscivores on a Coral Reef Fish Population', *Oecologia* **114**(1), 50–59.

Bourget, E., DeGuise, J. & Daigle, G. (1994), 'Scales of substratum heterogeneity, structural complexity, and the early establishment of a marine epibenthic community', *Journal of Experimental Marine Biology and Ecology* **181**(1), 31–51.

Burns, J., Delparte, D., Gates, R. & Takabayashi, M. (2015), 'Integrating Structure-from-Motion Photogrammetry with Geospatial Software as a Novel Technique for Quantifying 3D Ecological Characteristics of Coral Reefs', *PeerJ* **3**(e1077).

Carleton, J. H. & Sammarco, P. W. (1987), 'Effects of Substratum Irregularity on Success of Coral Settlement: Quantification by Comparative Geomorphological Techniques', *Bulletin of Marine Science* **40**(1), 85–98.

Coker, D. J., Graham, N. A. J. & Pratchett, M. S. (2012), 'Interactive effects of live coral and structural complexity on the recruitment of reef fishes', *Coral Reefs* **31**(4), 919–927.

Costa, B. M., Battista, T. A. & Pittman, S. J. (2009), 'Comparative evaluation of airborne LiDAR and ship-based multibeam SoNAR bathymetry and intensity for mapping coral reef ecosystems', *Remote Sensing of Environment* **113**(5), 1082–1100.

Dustan, P., Doherty, O. & Pardede, S. (2013), 'Digital Reef Rugosity Estimates Coral Reef Habitat Complexity', *PLoS ONE* **8**(2).

Ferrario, F., Beck, M. W., Storlazzi, C. D., Micheli, F., Shepard, C. C. & Airoldi, L. (2014), 'The effectiveness of coral reefs for coastal hazard risk reduction and adaptation', *Nature Communications* **5**(3794).

Figueira, W., Ferrari, R., Weatherby, E., Porter, A., Hawes, S. & Byrne, M. (2015), 'Accuracy and Precision of Habitat Structural Complexity Metrics Derived from Underwater Photogrammetry', *Remote Sensing* **7**(12), 16883–16900.

Fisher, R., Leary, R. A. O., Brainard, R. E., Caley, M. J., Fisher, R., Leary, R. A. O., Low-choy, S., Mengersen, K., Knowlton, N. & Brainard, R. E. (2014), 'Report Species Richness on Coral Reefs and the Pursuit of Convergent Global Estimates Species Richness on Coral Reefs and the Pursuit of Convergent Global Estimates', *Current Biology* **25**(4), 500–505.

Friedlander, A. M. & Parrish, J. D. (1998), 'Habitat Characteristics Affecting Fish Assemblages on a Hawaiian Coral Reef', *Journal of Experimental Marine Biology and Ecology* **224**(1).

Friedman, A., Pizarro, O., Williams, S. B. & Johnson-Roberson, M. (2012), 'Multi-Scale Measures of Rugosity, Slope and Aspect from Benthic Stereo Image Reconstructions', *PLoS ONE* **7**(12).

Goatley, C. H. R. & Bellwood, D. R. (2011), 'The Roles of Dimensionality, Canopies and Complexity in Ecosystem Monitoring', *PLoS ONE* **6**(11).

González-Rivero, M., Harborne, A. R., Herrera-Reveles, A., Bozec, Y.-M., Rogers, A., Friedman, A., Ganase, A. & Hoegh-Guldberg, O. (2017), 'Linking fishes to multiple metrics of coral reef structural complexity using three-dimensional technology', *Scientific Reports* **7**(1), 13965.

Graham, N. A. J. & Nash, K. L. (2013), 'The Importance of Structural Complexity in Coral Reef Ecosystems', *Coral Reefs* **32**, 315–326.

Gratwicke, B. & Speight, M. R. (2005), 'The Relationship Between Fish Species Richness, Abundance and Habitat Complexity in a Range of Shallow Tropical Marine Habitats', *Journal of Fish Biology* **66**(3), 650–667.

Grober-Dunsmore, R., Frazer, T. K., Lindberg, W. J. & Beets, J. (2007), 'Reef fish and habitat relationships in a Caribbean seascape: The importance of reef context', *Coral Reefs* **26**(1), 201–216.

Hearn, C., Atkinson, M. & Falter, J. (2001), 'A physical derivation of nutrient-uptake rates in coral reefs: Effects of roughness and waves', *Coral Reefs* **20**(4), 347–356.

Hiatt, R. W., Strasburg, D. W., Monographs, S. E. & Jan, N. (1960), 'Ecological Relationships of the Fish Fauna on Coral Reefs of the Marshall Islands', *Ecological Monographs* **30**(1), 65–127.

Hixon, M. A. & Beets, J. P. (1993), 'Predation, Prey Refuges, and the Structure of Coral-Reef Fish Assemblages', *Ecological Monographs* **63**(1), 77–101.

Holbrook, S. J., Forrester, G. E. & Schmitt, R. J. (2000), 'Spatial patterns in abundance of a damselfish reflect availability of suitable habitat', *Oecologia* **122**(1), 109–120.

Huvenne, V. a. I., Blondel, P. & Henriet, J. P. (2002), 'Textural analyses of sidescan sonar imagery from two mound provinces in the Porcupine Seabight', *Marine Geology* **189**(3-4), 323–341.

Johansen, J. L., Bellwood, D. R. & Fulton, C. J. (2008), 'Coral reef fishes exploit flow refuges in high-flow habitats', *Marine Ecology Progress Series* **360**, 219–226.

Johnson-Roberson, M., Pizarro, O., Williams, S. B. & Mahon, I. (2010), 'Generation and Visualization of Large-Scale Three-Dimensional Reconstructions from Underwater Robotic Surveys', *Journal of Field Robotics* **21**(1).

Jolliffe, I. (1986), *Principal Component Analysis and Factor Analysis*, second edn, Springer New York.

Knudby, A. & LeDrew, E. (2007), 'Measuring Structural Complexity on Coral Reefs', *Proceedings of the American Acadamy of Underwater Sciences 26th Symposium* pp. 181–188.

602 Komyakova, V., Munday, P. L. & Jones, G. P. (2013), 'Relative Importance of
603 Coral Cover, Habitat Complexity and Diversity in Determining the Structure
604 of Reef Fish Communities', *PLoS ONE* **8**(12), e83178.

605 Lê, S., Josse, J. & Husson, F. (2008), '{FactoMineR}: A Package for Multivariate
606 Analysis', *Journal of Statistical Software* **25**(1), 1–18.

607 Leon, J., Roelfsema, C. M., Saunders, M. I. & Phinn, S. R. (2015), 'Measur-
608 ing Coral Reef Terrain Roughness using 'Structure-from-Motion' Close-Range
609 Photogrammetry', *Geomorphology* **242**, 21–28.

610 Lingo, M. E. & Szedlmayer, S. T. (2006), 'The influence of habitat complexity
611 on reef fish communities in the northeastern Gulf of Mexico', *Environmental
612 Biology of Fishes* **76**(1), 71–80.

613 Luckhurst, E. & Luckhurst, K. (1978), 'Analysis of the Influence of Substrate
614 Variables on Coral Reef Fish Communities', *Marine Biology* **323**(49), 317–323.

615 McCormick, M. I. (1994), 'Comparison of Field Methods for Measuring Surface
616 Topography and their Associations with a Tropical Reef Fish Assemblage', *Ma-
617 rine Ecology Progress Series* **112**, 87–96.

618 Mellin, C., Andréfouët, S., Kulbicki, M., Dalleau, M. & Vigliola, L. (2009), 'Re-
619 mote sensing and fish-habitat relationships in coral reef ecosystems: Review
620 and pathways for multi-scale hierarchical research', *Marine Pollution Bulletin*
621 **58**(1), 11–19.

622 Merkle, E. C., You, D. & Preacher, K. J. (2015), 'Testing non-nested structural
623 equation models', *Psychological Methods* **21**(2).

624 Moberg, F. & Folke, C. (1999), 'Ecological Goods and Services of Coral Reef
625 Ecosystems', *Ecol Econ* **29**(2), 215–233.

626 Newman, S. P., Meesters, E. H., Dryden, C. S., Williams, S. M., Sanchez, C.,
627 Mumby, P. J. & Polunin, N. V. C. (2015), 'Reef Flattening Effects on Total

628 Richness and Species Responses in the Caribbean', *Journal of Animal Ecology*
629 **84**(6), 1678–1689.

630 Obura, D. O. (2005), 'Resilience and climate change: Lessons from coral reefs and
631 bleaching in the Western Indian Ocean', *Estuarine, Coastal and Shelf Science*
632 **63**(3), 353–372.

633 Paddack, M. J., Reynolds, J. D., Aguilar, C., Appeldoorn, R. S., Beets, J., Bur-
634 kett, E. W., Chittaro, P. M., Clarke, K., Esteves, R., Fonseca, A. C., Forrester,
635 G. E., Friedlander, A. M., García-Sais, J., González-Sansón, G., Jordan, L.
636 K. B., McClellan, D. B., Miller, M. W., Molloy, P. P., Mumby, P. J., Nagelk-
637 erken, I., Nemeth, M., Navas-Camacho, R., Pitt, J., Polunin, N. V. C., Reyes-
638 Nivia, M. C., Robertson, D. R., Rodríguez-Ramírez, A., Salas, E., Smith, S. R.,
639 Spieler, R. E., Steele, M. A., Williams, I. D., Wormald, C. L., Watkinson, A. R.
640 & Côté, I. M. (2009), 'Recent Region-wide Declines in Caribbean Reef Fish
641 Abundance', *Current Biology* **19**(7), 590–595.

642 Pittman, S. J. & Brown, K. A. (2011), 'Multi-Scale Approach for Predicting Fish
643 Species Distributions across Coral Reef Seascapes', *PLoS ONE* **6**(5), e20583.

644 Pizarro, O., Eustice, R. M. & Singh, H. (2009), 'Large area 3D reconstructions
645 from underwater surveys', *IEEE Journal of Oceanic Engineering* **34**(2), 150–
646 169.

647 Plaisance, L., Caley, M. J., Brainard, R. E. & Knowlton, N. (2011), 'The Diversity
648 of Coral Reefs: What are We Missing?', *PLoS ONE* **6**(10).

649 Precht, W. F., Aronson, R. B., Moody, R. M. & Kaufman, L. (2010), 'Changing
650 Patterns of Microhabitat Utilization by the Threespot Damselfish, Stegastes
651 Planifrons, on Caribbean Reefs', *PLoS ONE* **5**(5).

652 Purkis, S. J., Graham, N. A. J. & Riegl, B. M. (2008), 'Predictability of reef fish
653 diversity and abundance using remote sensing data in Diego Garcia (Chagos
654 Archipelago)', *Coral Reefs* **27**(1), 167–178.

655 R Core Team (2017), *R: A Language and Environment for Statistical Computing*,
656 R Foundation for Statistical Computing, Vienna, Austria.

657 Risk, M. J. (1972), 'Fish Diversity on a Coral Reef in The Virgin Islands', *Atoll*
658 *Research Bulletin* **153**.

659 Robert, K., Huvenne, V. A. I., Georgiopoulou, A., Jones, D. O. B., Marsh, L.,
660 D. O. Carter, G. & Chaumillon, L. (2017), 'New approaches to high-resolution
661 mapping of marine vertical structures', *Scientific Reports* **7**(1), 9005.

662 Roberts, C. M. & Ormond, R. F. G. (1987), 'Habitat complexity and coral reef fish
663 diversity and abundance on Red Sea fringing reefs', *Marine Ecology Progress*
664 *Series* **41**(1972), 1–8.

665 Rogers, A., Blanchard, J. L. & Mumby, P. J. (2014), 'Vulnerability of coral reef
666 fisheries to a loss of structural complexity', *Current Biology* **24**(9), 1000–1005.

667 Shannon, C. E. (1948), 'A mathematical theory of communication', *The Bell*
668 *System Technical Journal* **27**(July 1928), 379–423.

669 Simpson, E. H. (1949), 'Measurement of Diversity', *Nature* **163**(4148), 688–688.

670 Tokeshi, M. & Arakaki, S. (2012), 'Habitat complexity in aquatic systems: Frac-
671 tals and beyond', *Hydrobiologia* **685**(1), 27–47.

672 Vergés, A., Vanderklift, M. A., Doropoulos, C. & Hyndes, G. A. (2011), 'Spatial
673 patterns in herbivory on a coral reef are influenced by structural complexity
674 but not by algal traits', *PLoS ONE* **6**(2).

675 Vuong, Q. (1989), 'Likelihood Ratio Tests for Model Selection and Non-Nested
676 Hypotheses', *Econometrica* **57**(2), 307–333.

677 Walker, B. K., Jordan, L. K. B. & Spieler, R. E. (2009), 'Relationship of Reef
678 Fish Assemblages and Topographic Complexity on Southeastern Florida Coral
679 Reef Habitats', *Journal of Coastal Research* **10053**, 39–48.

Willis, T. J. & Anderson, M. J. (2003), 'Structure of cryptic reef fish assemblages: Relationships with habitat characteristics and predator density', *Marine Ecology Progress Series* **257**(2000), 209–221.

Wilson, M. F. J., O'Connell, B., Brown, C., Guinan, J. C. & Grehan, A. J. (2007), 'Multiscale Terrain Analysis of Multibeam Bathymetry Data for Habitat Mapping on the Continental Slope', *Marine Geodesy* **30**(1-2), 3–35.

Wilson, S., Graham, N. A. J. & Polunin, N. V. C. (2007), 'Appraisal of Visual Assessments of Habitat Complexity and Benthic Composition on Coral Reefs', *Marine Biology* **151**, 1069–1076.

Young, G. C., Dey, S., Rogers, A. D. & Exton, D. (2017), 'Cost and time-effective method for multi-scale measures of rugosity, fractal dimension, and vector dispersion from coral reef 3D models', *Plos One* **12**(4), e0175341.

Zawada, D. G., Piniak, G. A. & Hearn, C. J. (2010), 'Topographic complexity and roughness of a tropical benthic seascape', *Geophysical Research Letters* **37**(14).

A Electronic Supplementary Material

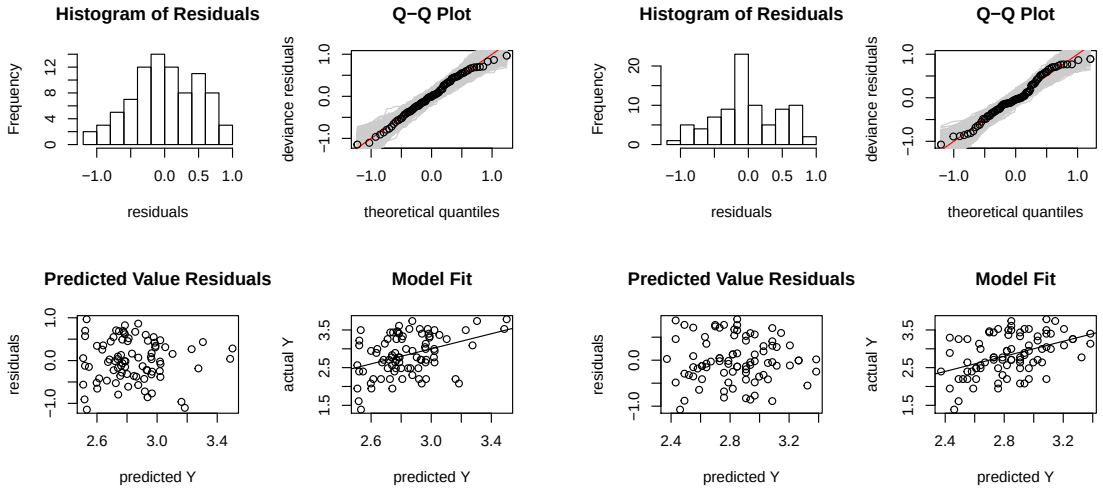

(a) log(total abundance) ∼ PC1

(b) log(total abundance) ∼ HAS

Figure S1: Diagnostic plots for the linear models of the natural logarithm of total abundance as predicted by (a) the 3D models and (b) Habitat Assessment Scores (HAS). Full model details in Table 3. The Q-Q plot shows in grey 2000 replicate data sets simulated over one quantile of the residual distribution; the Q-Q plot was generated by the "qq.gam" function of the R library "mgcv" (R Core Team, 2017).

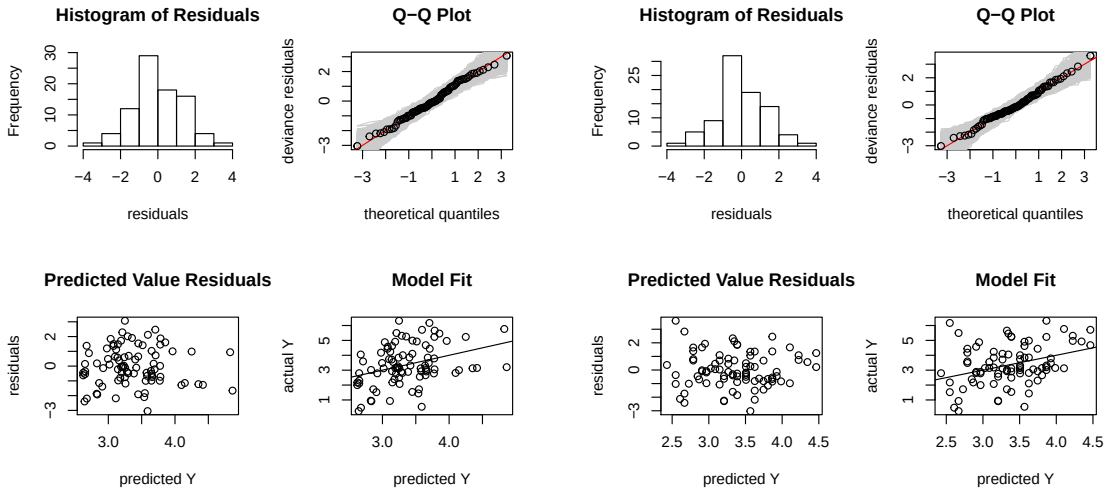

(a) Shannon^2 $\sim$ PC1

(b) Shannon^2 $\sim$ HAS

Figure S2: Diagnostic plots for the linear models of the Shannon diversity index squared as predicted by (a) the 3D models and (b) Habitat Assessment Scores (HAS). Full model details in Table 3. The Q-Q plot shows in grey 2000 replicate data sets simulated over one quantile of the residual distribution; the Q-Q plot was generated by the "qq.gam" function of the R library "mgcv" (R Core Team, 2017).

Table S1: Fish species abundances (N) observed across all 85 quadrats. Note that species were visually identified (following the method of (Gratwicke & Speight, 2005)), and so there may be instances where taxonomically similar species were recorded as the same species. In particular, some gobies recorded as *Coryphopterus personatus* may have been *C. hyalinus*, an equally common species in the region that is nearly identical taxonomically but distinct genetically (Baldwin et al., 2009).

Family	Species	N
Acanthuridae	*Acanthurus chirurgus*	9
	Acanthurus coeruleus	13
	Acanthurus tractus	2
Aulostomidae	*Aulostomus maculatus*	6
Carangidae	*Caranx crysos*	3
	Caranx ruber	29
Chaetodontidae	*Chaetodon capistratus*	39
	Chaetodon ocellatus	9
	Chaetodon striatus	3
Gobiidae	*Coryphopterus glaucofraenum*	4
	Coryphopterus personatus	63
	Elacatinus lobeli	10
Grammatidae	*Gramma loreto*	9
Haemulidae	*Haemulon flavolineatum*	2
	Haemulon scriurus	1
Holocentridae	*Sargocentron coruscum*	2
Labridae	*Bodianus rufus*	9
	Clepticus parrae	1
	Halichoeres bivittatus	30
	Halichoeres garnoti	131
	Halichoeres radiatus	1
	Thalassoma bifasciatum	156
Lutjanidae	*Lutjanus mahogoni*	6

Continued on next page

Table S1 – *Continued from previous page*

Family	Species	*N*
	Ocyurus chrysurus	5
Megalopidae	*Megalops atlanticus*	1
Monacanthidae	*Cantherhines pullus*	1
Mullidae	*Pseudupeneus maculatus*	2
Ostraciidae	*Acanthostracion polygonius*	1
	Lactophrys triqueter	9
Pomacanthidae	*Holacanthus ciliaris*	2
	Holacanthus tricolor	1
	Pomacanthus arcuatus	11
Pomacentridae	*Abudefduf saxatilis*	8
	Chromis cyanea	71
	Chromis multilineata	8
	Microspathodon chrysurus	17
	Stegastes adustus	115
	Stegastes diencaeus	15
	Stegastes leucostictus	22
	Stegastes partitus	198
	Stegastes planifrons	97
	Stegastes variabilis	31
Scaridae	*Scarus iserti*	143
	Scarus taeniopterus	111
	Scarus vetula	8
	Sparisoma aurofrenatum	43
	Sparisoma chrysopterum	16
	Sparisoma radians	1
	Sparisoma rubripinne	8
	Sparisoma viride	35
Serranidae	*Cephalopholis cruentata*	7
	Hypoplectrus indigo	10
	Hypoplectrus nigricans	2
	Hypoplectrus puella	2
	Serranus tabcarius	1
	Serranus tigrinus	7
Sparidae	*Calamus calamus*	1
Synodontidae	*Synodus intermedius*	1
	Synodus saurus	23
Tetraodontidae	*Canthigaster rostrata*	73
	TOTAL	1645

695

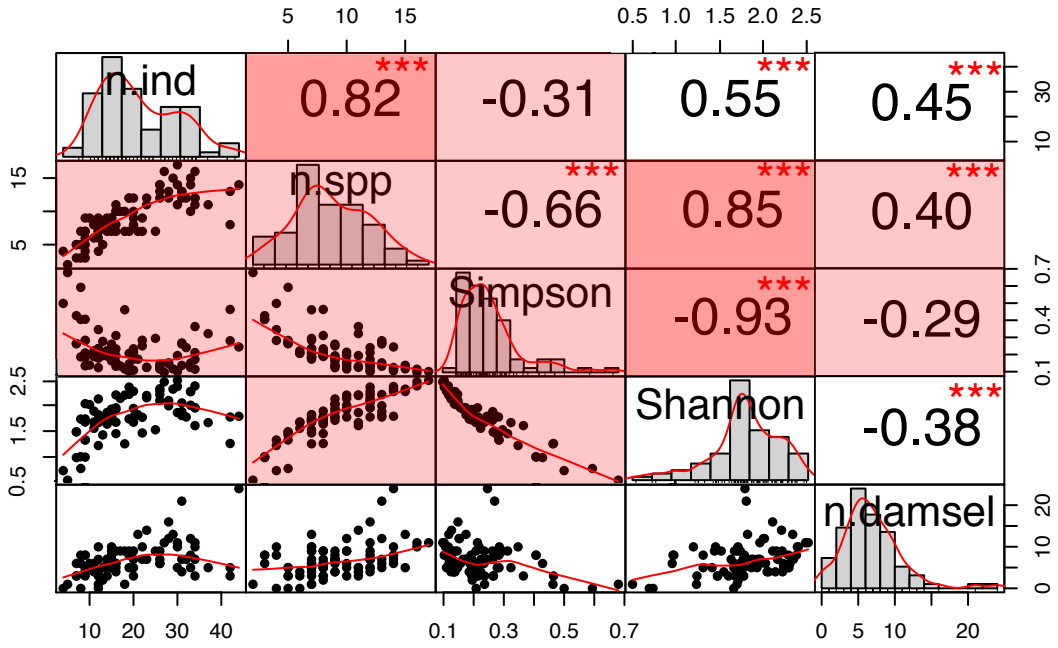

Figure S3: Correlations between fish survey variables. From top to bottom along the diagonal, abbreviations include: total fish abundance (n.ind), species richness (n.spp), Simpson diversity index (Simpson), Shannon diversity index (Shannon), and damselfish abundance (n.damsel). Lower diagonal contains scatter plots with Loess curves. Diagonal contains histograms of data with probability density curves. Upper diagonal contains Spearman's rank correlation coefficients (ρ) and significances ($P \leq 0.002^{***}$). With a Bonferroni correction, the significance threshold was $0.050/21 = 0.002$. Those highlighted in red were removed from further analysis because of collinearities with other variables ($|\rho| > 0.80$).

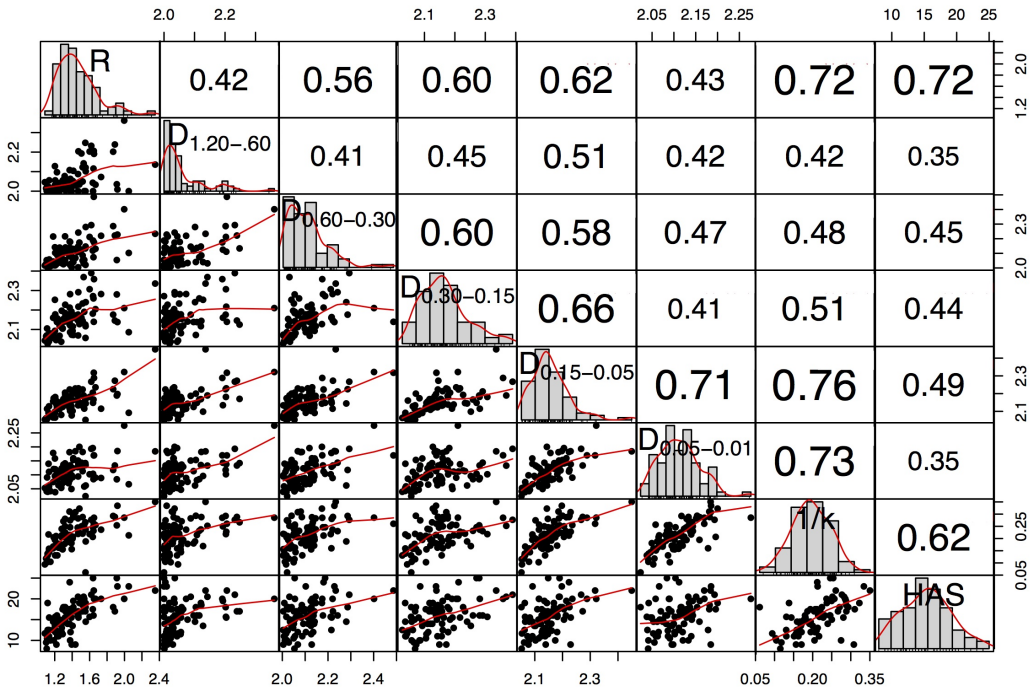

Figure S4: Correlations between structural complexity metrics: linear rugosity (R), fractal dimension (D) at varying resolutions (*e.g.*, between 1.20-0.60 m), vector dispersion ($1/k$), and Habitat Assessment Score (HAS). Lower diagonal contains scatter plots with Loess curves. Diagonal contains histograms of data with probability density curves. Upper diagonal contains Spearman's rank correlations coefficients. All correlations were significant. Text size in upper diagonal corresponds to significance level. With a Bonferroni correction, the significance threshold was $0.050/28 = 0.002$. All variables were carried forward in analysis.

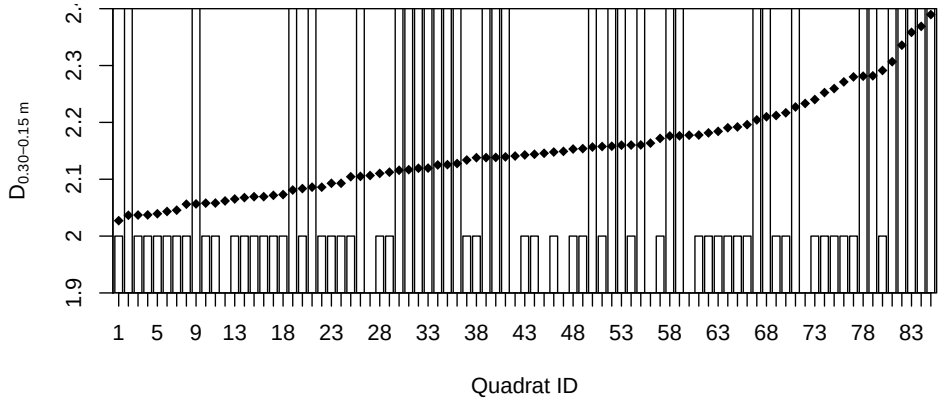

(a) Refuge size category 16-30 cm; D between 15-30 cm

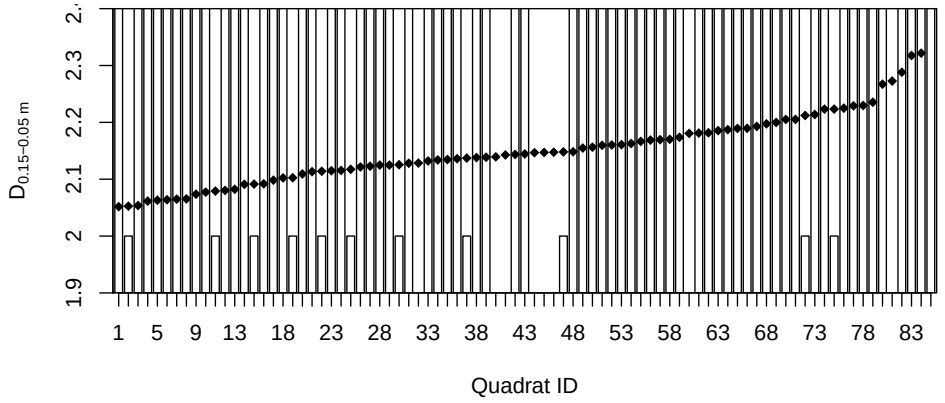

(b) Refuge size category 6-15 cm; D between 5-15 cm

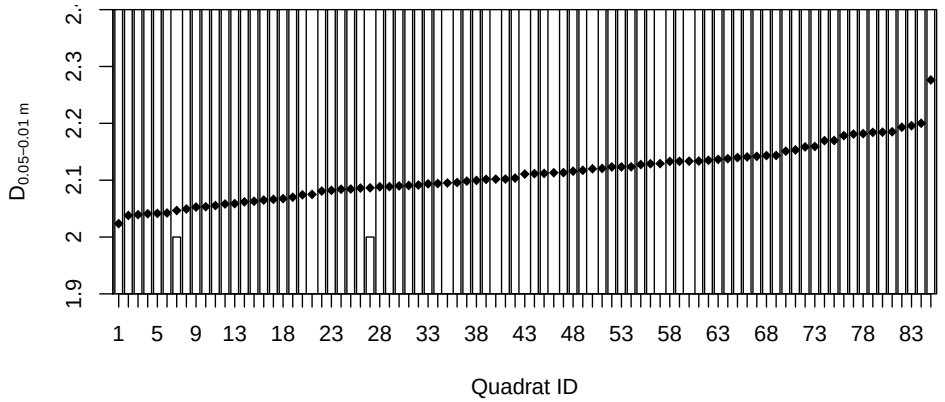

(c) Refuge size category 1-5 cm; D between 1-5 cm

Figure S5: Comparison between fractal dimension (D) and diver's judgement of whether or not refuges existed at given size categories. Bars show diver's judgment: $D > 2.4$ if the diver observed a refuge at the given size category, and $D = 2.0$ if the diver did not. Absent bars indicate missing data (n=77 for diver's judgments and n=85 for D). On the X-axis, quadrats are ordered from lowest to highest fractal dimension, and therefore quadrat identification numbers do not correspond between plots (a)-(c). The size categories of 50-30 or >50cm are not presented because divers observed them too infrequently (on <5 quadrats). There appears to be no pattern relating D to diver's judgement.

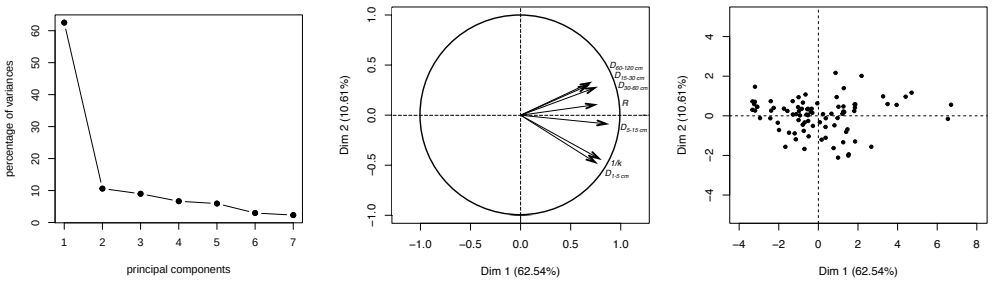

(a) Scree plot (b) Variables factor map (c) Individuals factor map

Figure S6: Principal Component Analysis (PCA) of the 3D metrics. (a) Scree plot showing variance explained by principal components. The first principal component (PC1) captured the majority of the variance (62.54%), and other components only marginally increased the proportion of variance. (b) Variables factor map with labelled structural complexity metrics; all vectors point in similar directions with similar strengths along Dim 1 (PC1). (c) Individual factors map showing a fairly even spread over Dim 1 among the 85 data points.

Table S2: Vuong test results. M_{PC1}, M_{HAS} and M_R respectively refer to the linear model with PC1, HAS, and R as their independent variable. Dependent variable abbreviations include: natural logarithm of total abundance (log(t. abundance)) and Shannon diversity index squared (Shannon^2). The test statistic ω^2 characterizes population variance in the likelihood ratios of the two models being compared (Merkle et al., 2015). The test statistic z (fully $z_{1-\alpha/2}$) is the variate at which the cumulative distribution function of the standard normal distribution equals $1 - \alpha/2$. The significance threshold was $\alpha = 0.05$. Significant P-values bolded.

Dependent Variable	Vuong Test Results
	Variance tests
	H0: M_{PC1} and M_{HAS} are indistinguishable
	H1: M_{PC1} and M_{HAS} are distinguishable
log(t. abundance)	$\omega^2 = 0.149$, $P =$ **5e-05**
Shannon^2	$\omega^2 = 0.158$, $P = 0.421$
	H0: M_{PC1} and M_R are indistinguishable
	H1: M_{PC1} and M_R are distinguishable
log(t. abundance)	$\omega^2 = 0.046$, $P =$ **7e-05**
Shannon^2	$\omega^2 = 0.058$, $P = 0.348$
	Non-nested likelihood ratio tests
	H0: M_{PC1} and M_{HAS} fit equally to the focal population
	H1A: M_{PC1} fits better than M_{HAS}
log(t. abundance)	z = -0.610, $P = 0.729$
Shannon^2	NA (models indistinguishable)
	H1B: M_{HAS} fits better than M_{PC1}
log(t. abundance)	z = -0.610, $P = 0.271$
Shannon^2	NA (models indistinguishable)
	H0: M_{PC1} and M_R fit equally to the focal population
	H1A: M_{PC1} fits better than M_R
log(t. abundance)	z = -0.255, $P = 0.601$
Shannon^2	NA (models indistinguishable)
	H1B: M_R fits better than M_{PC1}
log(t. abundance)	z = -0.255, $P = 0.399$
Shannon^2	NA (models indistinguishable)

Full linear model details in Table 3 (M_{PC1} and M_{HAS}) and Table S3 (M_R).

Table S3: Linear models for fish survey metrics with linear rugosity (R) as the dependent variable. Abbreviations as in Table 3. Significant P-values bolded.

	Model Summary					Goodness of Fit			
Dependent Var.	Coeff.	Est.	SE	t-value	Pr($>\|t\|$)	AIC	R^2	F	P
log(t. abundance)	(Inter.)	1.662	0.3194	5.203	**1E-06**	125.544	0.1439	$F_{1,83}$	**3E-04**
	R	0.8333	0.2231	3.735	**3E-04**			= 13.95	
Shannon^2	(Inter.)	0.30	0.82	0.38	0.707	285	0.15	$F_{1,83}$	**3E-04**
	R	2.16	0.57	3.81	**3E-04**			= 14.48	

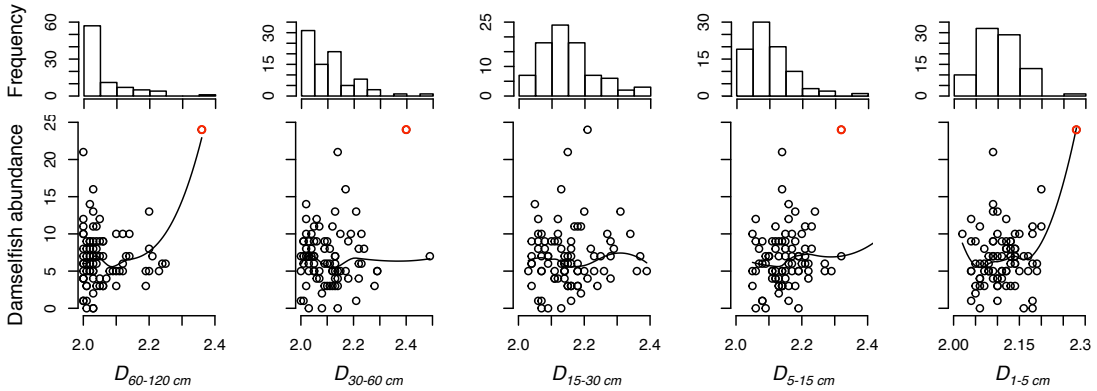

Figure S7: Damselfish (*Pomacentridae* family) abundance plotted against fractal dimension (D) at five scales. Plots include a Loess smoothing line (2nd degree local polynomial with smoothness parameter at 2/3). Top row contains histograms of the values of D. Outlier point highlighted in red; it is 2–4 standard deviations above mean values of $D_{60-120\ cm}$, $D_{30-60\ cm}$, $D_{5-15\ cm}$, and $D_{1-5\ cm}$ and contained a damselfish abundance more than five standard deviations above the mean. Figure S8 depicts this unique quadrat.

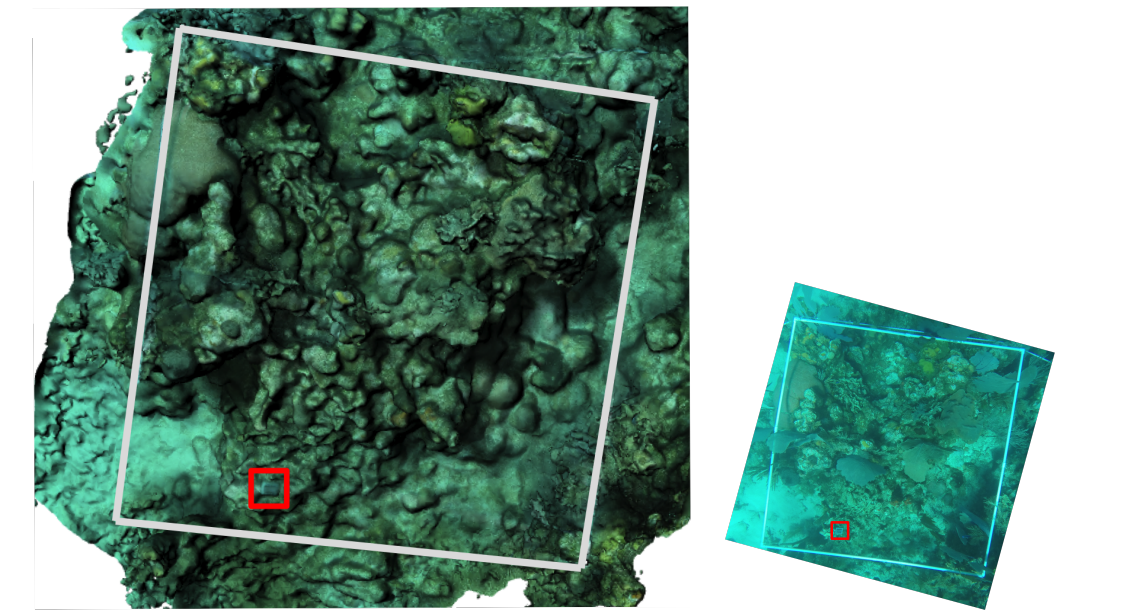

(a) Quadrat 3D model (b) Quadrat photograph

(c) 576 squares (d) 64 squares (e) 16 squares (f) 4 squares (g) 1 square

Figure S8: Outlier quadrat in terms of its high fractal dimension (D) at all scales 1–120 cm, except 15-30 cm (Fig. S7). (a) 3D model of the quadrat with the 2 x 2 m outline of the quadrat highlighted for clarity. (b) Photo of the quadrat. Boxed in red is a reference point corresponding indicating the same area in the 3D model and photo. (c-g) Surfaces used to compute the fractal dimensions of the quadrat. Squares of edge length δ are projected onto the 3D model of the reef to generate these surfaces. Surface area increases with finer resolution. Renderings shown at five resolutions: (c) $\delta = 5\ cm$, (d) $\delta = 15\ cm$, (e) $\delta = 30\ cm$, (f) $\delta = 60\ cm$, (f) $\delta = 120\ cm$.

Electronic Supplementary Material—References

Baldwin, C. C., Weigt, L. A., Smith, D. G. & Mounts, J. H. (2009), 'Reconciling Genetic Lineages with Species in Western Atlantic Coryphopterus (Teleostei: Gobiidae)', *Smithsonian Contributions to the Marine Sciences* **38**, 111–138.

Gratwicke, B. & Speight, M. R. (2005), 'The Relationship Between Fish Species Richness, Abundance and Habitat Complexity in a Range of Shallow Tropical Marine Habitats', *Journal of Fish Biology* **66**(3), 650–667.

Merkle, E. C., You, D. & Preacher, K. J. (2015), 'Testing non-nested structural equation models', *Psychological Methods* **21**(2).

R Core Team (2017), *R: A Language and Environment for Statistical Computing*, R Foundation for Statistical Computing, Vienna, Austria.

The older I get, the more I'm conscious of ways very small things can make a change in the world. Tiny little things, but the world is made up of tiny matters, isn't it?

— Sandra Cisneros, Novelist

4

How Centimetre-Scale Structural Complexity Affects Sessile Epibenthic Organism Settlement on a Caribbean Reef

Contents

4.1 Context 89
4.2 Author Contributions 91
4.3 Publication: Young, G. C., *et al.* "How centimetre-scale structural complexity affects sessile epibenthic organism settlement on a Caribbean reef." *In Prep.* . 93

4.1 Context

This chapter describes a controlled experiment testing the role of structural complexity on sessile epibenthic organism settlement after one year. Structural complexity is measured in terms of vector dispersion (*1/k*), the metric described in Chapter 2 and mentioned in Chapters 1 and 3. The work has broad applications in artificial reef (AR) design. There is some debate as to whether an AR needs to appear natural (*i.e.,* mimicking the appearance of a natural reef; Fig. 4.1)

(a) **(b)** **(c)**

Figure 4.1: Examples of reef restoration modules with "natural shapes," *i.e.,* shapes designed to be structurally as similar as possible to natural reefs. (a) Dr. Harold Hudson by reef restoration module designed to replicate reef topography and create habitat for cryptic biota. Module fabricated in 2002 by Florida Keys National Marine Sanctuary from poured concrete, fibreglass-reinforced rod, and oolitic-limestone (Hopley, 2011). Source: Jeff Anderson with permission. (b) Module on Molasses Reef, Key Largo four years after deployment. Source: Jeff Anderson with permission. (c) 3D printed surface for reef restoration and organism settlement. Source: Jessica Gregory at Fabien Cousteau Ocean Learning Center with permission.

or if it can appear artificial (*i.e.*, composed of man-made shapes; Fig. 4.2) for effective reef restoration (Carr and Hixon, 1997; Perkol-Finkel et al., 2006). This chapter measures effectiveness specifically in terms of how the surface recruits sessile epibenthic organisms after one year. Scleractinian coral spats are the main organism of interest, as they are key ecosystem engineers (Chapter 1). Sponges, algae, polychaetes, and bryozoans are also included in the study, as they settled with coral spats. Descriptions of surface appearances as "natural" or "artificial-shaped" are re-interpreted in terms of the structural complexity metric *1/k*.

Our conclusion that the availability of sheltered area affected coral spat settlement locations more than *1/k* or other variables was not surprising based on other studies' results (*e.g.,* Edmunds et al. (2014); Whalan et al. (2015)). Instead, the takeaway message is that metrics like *1/k* alone are inadequate to predict coral spat settlement (or other epibenthic organism settlement apart from algae). Rather than persevering with *1/k*, a modern approach should be applied to identify surface characteristics that influence settlement patterns. That modern approach is likely machine learning. For example, a 3D model of a coral reef could feed into a machine learning algorithm along with associated ecosystem information such as settlement densities, fish abundance, or coral cover. The algorithm could

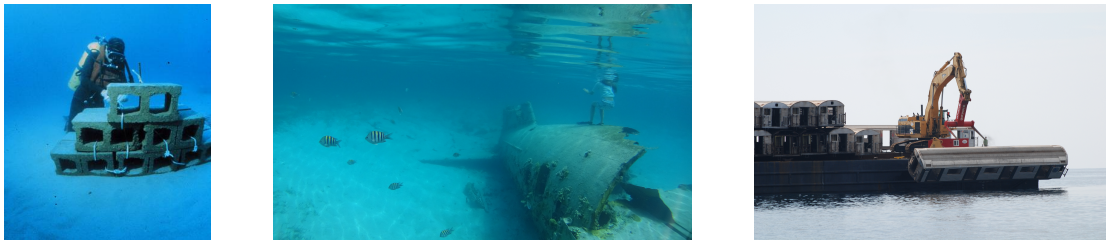

(a) (b) (c)

Figure 4.2: Examples of artificial reefs with "artificial shapes," *i.e.,* shapes not designed to resemble natural reef structure. *Could adding holes or slightly modifying their texture (1/k) improve coral spat settlement rates onto these structures?* (a) Diver constructs artificial reef from cinder blocks. Source: United States Department of Commerce, public domain (CC-0 1.0). (b) Sunken aircraft serves as artificial reef off Norman's Cay, Bahamas. Source: Daniel Piraino, public domain (CC-0 1.0). (c) Retired subway cars on a barge before being sunk to form an artificial reef. Source: South Carolina Department of Natural Resource, available through Creative Commons licence (CC BY-SA 3.0).

test all possible permutations of angles, scales, and complexity measures from the 3D models and learn the patterns that tie those features to the ecosystem data. Once able to predict ecosystem variables, the algorithm could yield insight into the precision role of 3D structure in shaping a marine ecosystem and thereby inform AR designs. The following chapter (Chapter 5) takes this idea further by presenting a preliminary assessment of a machine learning approach.

4.2 Author Contributions

The authors of this publication, in order, are: G. C. Young, D. A. Exton, D. Andradi-Browna, K. Shepherd, J. van der Grient, A. D. Rogers. Author contributions are listed in CRediT taxonomy in Table 4.1 on page 91 following Brand et al. (2015).

Table 4.1: Author contributions for Chapter 4 listed in CRediT taxonomy (Brand et al., 2015). Initials refer to the authors of the paper; in order, they are: G. C. Young, D. A. Exton, D. Andradi-Browna, K. Shepherd, J. van der Grient, A. D. Rogers.

Role	Author(s)
Conceptualization – Ideas; formulation or evolution of overarching research goals and aims.	GCY, ADR, DAB

Continued on next page

Table 4.1 – *Continued from previous page*

Role	Author(s)
Data Curation – Management activities to annotate (produce metadata), scrub data and maintain research data (including software code, where it is necessary for interpreting the data itself) for initial use and later reuse.	GCY, KS
Formal Analysis – Application of statistical, mathematical, computational, or other formal techniques to analyze or synthesize study data.	GCY, KS, JvG, ADR
Funding Acquisition – Acquisition of the financial support for the project leading to this publication.	GCY, DAE, ADR
Investigation – Conducting a research and investigation process, specifically performing the experiments, or data/evidence collection.	GCY, KS
Methodology – Development or design of methodology; creation of models	GCY, DAB, ADR
Project Administration – Management and coordination responsibility for the research activity planning and execution.	GCY, DAE, DAB, KS
Resources – Provision of study materials, reagents, materials, patients, laboratory samples, animals, instrumentation, computing resources, or other analysis tools.	GCY, DAE
Software – Programming, software development; designing computer programs; implementation of the computer code and supporting algorithms; testing of existing code components.	GCY
Supervision – Oversight and leadership responsibility for the research activity planning and execution, including mentorship external to the core team.	GCY
Validation – Verification, whether as a part of the activity or separate, of the overall replication/reproducibility of results/experiments and other research outputs.	GCY
Visualization – Preparation, creation and/or presentation of the published work, specifically visualization/data presentation.	GCY
Writing - Original Draft Preparation – Creation and/or presentation of the published work, specifically writing the initial draft (including substantive translation).	GCY
Writing - Review & Editing – Preparation, creation and/or presentation of the published work by those from the original research group, specifically critical review, commentary or revision - including pre- or post-publication stages.	GCY, JvG, ADR, DAB, DAE

4.3 Publication: Young, G. C., *et al.* "How centimetre-scale structural complexity affects sessile epibenthic organism settlement on a Caribbean reef." *In Prep.*

Pages 94–128 of this thesis include the publication as it was formatted for submission to the *Marine Ecology Progress Series*. This formatting choice is consistent with the University's Examination Regulations for Research Degrees in Biological Sciences (Plant Sciences and Zoology).

How centimetre-scale structural complexity affects sessile epibenthic organisms on a Caribbean reef

G. C. Young[1,2*], D. A. Exton[2], D. A. Andradi-Brown[1,2,¶], K. Shepherd[1,2], J. van der Grient[1], A. D. Rogers[1]

Last edited May 27, 2018

---

[1]Department of Zoology, University of Oxford, Oxford, OX1 3PS, UK

[2]Operation Wallacea, Wallace House, Old Bolingbroke, Spilsby, Lincolnshire, PE23 4EX, UK

[¶]Present Address: Oceans Conservation, World Wildlife Fund-US, 1250 24th St. NW, Washington, D.C., 20037 USA

ffl*Corresponding author email <grace@robots.ox.ac.uk>

Abstract

With coral reefs facing global decline, conservationists are increasingly constructing artificial reefs (ARs) to aid reef recovery. Many studies have found correlations between reef health and metrics of three-dimensional (3D) reef structural complexity, such as vector dispersion (*1/k*). Fewer studies have experimentally tested the role of structural complexity in promoting early organism recruitment. For this study, approximately 200 recruitment tiles were produced from 3D prints and placed for one year on a shallow Caribbean reef around Utila, Bay Islands, Honduras. Recruitment tiles had two contrasting designs; one based on a 3D modelled natural reef and the other based on artificial shapes. Despite differing shapes, both designs had identical structural complexity at the 1 cm scale ($1/k = 0.25$). Additionally, flat control surfaces had $1/k = 0.00$. Contrary to expectation, *1/k* affected algae, but not corals, sponges, polychaetes, or bryozoans. While there were no differences in recruitment densities between the natural and artificial-shaped tile designs, algae and coral spat densities were higher on horizontal tiles (parallel to the ocean surface) compared to vertical tiles. All organisms, except algae, settled in higher densities on sheltered, reef-facing regions than on exposed regions. It was surprising was that cryptic textured surfaces did not increase organism densities compared to flat cryptic surfaces. This is likely a result of the release agent applied to tiles' textured and edge faces. This pilot study highlighted the promise of controlling algae settlement with 1 cm surfaces, but also highlights methodological improvements for future studies that create 3D settlement tiles.

Keywords: structural complexity - habitat complexity - substratum heterogeneity - coral spat - coral recruitment - coral settlement - coral reefs - algae - sponge - polychaete - bryozoans - 3D modelling - artificial reefs

1 Introduction

Global coral reef health is rapidly declining (Hughes et al., 2017), with the combined effects of climate change, overfishing, pollution and disease putting up to 90% of the world's reefs in danger of total collapse by 2030 (Burke et al., 2011). Reef loss negatively impacts fish biomass (Paddack et al., 2009), shoreline protection (Cambers, 1997), tourism (Burke & Maidens, 2004), and other ecosystem services of high economic and intrinsic value (Conservation International, 2008, Burke et al., 2011).

There are significant efforts worldwide to create artificial reefs (ARs) that mitigate the effects of reef loss and/or enhance fisheries yield (Baine, 2001). An AR is defined as any submerged structure placed deliberately on the seabed to mimic some characteristics of a natural reef (Baine, 2001). ARs deployed for reef restoration have ranged from concrete replicas of existing corals (Hopley, 2011), to breeze-blocks (Gratwicke & Speight, 2005) and other concrete shapes (Sherman et al., 2002, Al-Horani & Khalaf, 2013), to shipwrecks (Walker & Schlacher, 2014), to piles of tires (Baine, 2001). While some ARs have higher coral cover and fish abundance than adjacent natural reefs (Burt et al., 2009), most are not so successful and/or have not existed long enough to realise significant benefits (Walker & Schlacher, 2014).

The structural complexity (or "shape") of substratum creates refuges and niches for organisms that colonise a natural reef (Graham & Nash, 2013) or AR (Al-Horani & Khalaf, 2013, Edmunds et al., 2014). In this context, the term structural complexity can be used interchangeably with other descriptors of geometry, including texture, roughness, rugosity, or substratum heterogeneity. There is no consensus as to what type or scale of structural complexity optimally increases organism settlement onto an AR. Several studies conclude that natural shapes improve an AR's ability to mimic ecosystems on adjacent reefs (Perkol-Finkel et al., 2006) or mitigate further reef degradation (Carr & Hixon, 1997), where

natural shapes are defined as those that are structurally as similar as possible to a natural reef (Carr & Hixon, 1997). This qualitative description of shape is not readily captured by quantitative metrics for mathematical models or cross-site comparisons, however.

Structural complexity requires a suite of metrics for it to be fully evaluated and understood. Different structural complexity metrics have correlated with a range of ecosystem features (coral spat settlement (Carleton & Sammarco, 1987, Petersen et al., 2005), live coral cover (Graham & Nash, 2013), algae cover (Johnson, 1994, Graham & Nash, 2013), invertebrate density and diversity (Beck, 1998, Idjadi & Edmunds, 2006, Graham & Nash, 2013, Martins et al., 2016), and fish density and biomass (Graham & Nash, 2013). Conventionally, structural complexity is measured as linear or chain-and-tape rugosity (Graham & Nash, 2013), which is the ratio of the draped length of a chain to its straight-line length. Rugosity is therefore often used by ecologists as a synonym for structural complexity (Beck, 1998). Rugosity has its limitations, as it can be misleading because it reduces a 3D structure to 2D (Goatley & Bellwood, 2011). Several other metrics exist that capture 3D surface characteristics, such as: surface rugosity (the ratio of surface area to planar area, not to be confused with linear rugosity) (Ferrari et al., 2016), fractal dimension (Beck, 1998), vector properties (Carleton & Sammarco, 1987, Beck, 1998), or less computationally intense measures such as the count and sizes of pits and crevasses (Petersen et al., 2005, Martins et al., 2016) or whether a surface is flat or textured (Johnson, 1994).

From the broad suite of structural complexity metrics, we have chosen to investigate vector dispersion (*1/k*), a unitless value between 0 and 1 that is greater with the variety of angles on a surface. We choose $1/k$ over other metrics because (i) it generally correlates with other metrics of structural complexity (Carleton & Sammarco, 1987, McCormick, 1994, Beck, 2000); (ii) it can be measured computationally on a continuous scale; and (iii) because there is already evidence suggesting that it strongly correlates with coral spat settlement (Carleton & Sammarco,

1987). In their 1979-1980 study in the Great Barrier Reef, Australia, Carleton & Sammarco (1987) found that $1/k$ measured at the 1 cm scale correlated positively and linearly with coral spat density after four months; they specifically recorded scleractinian corals (several genera).

This paper reports a controlled experiment that tests the effect of natural versus artificial structural complexity upon epibenthic organism settlement on a Caribbean reef. We precisely control the structural complexity of settlement surfaces in terms of *1/k* through structure-from-motion 3D modelling and 3D printing. Scleractinian coral spat (juvenile, newly recruited corals) were the primary organism of focus, although other organisms on the surface were also recorded (algae, sponges, polychaetes, and bryozoans). Our primary hypothesis was: The natural-shaped surface will harbour higher densities of sessile epibenthic organisms after one year compared to an artificial-shaped surface, even with structural complexity controlled in terms of *1/k*. If true, the hypothesis would suggest that the qualitative descriptions of a surface as either natural and artificial capture an important feature that *1/k* misses. As a control we also compared settlement densities between the surfaces with $1/k = 0.25$ and $1/k = 0.00$.

2 Methods

2.1 Study site

Tiles were placed at Coral View (16.09°'N, −86.91°'W; GPS coordinates in WGS84 format), on the south shore of Utila, Honduras, a Caribbean island at the southern end of the Mesoamerican Barrier Reef (Fig. 1). We conducted research under a permit from the Instituto de Conservación Forestal (#ICF-DE-MP-080-2016). At Coral View, the reef exists as a spur and groove system that transitions into a gentle reef slope down to approximately 40 m depth (Andradi-Brown et al., 2016). Tiles were placed at 15 m depth at Coral View, where there is an average hard coral cover of 15-20 % (Andradi-Brown et al., 2016). The west

112 end of Coral View is adjacent to a boat channel opening into a mangrove lagoon,
113 which can cause sediment levels greater than those on the east end of the dive
114 site [*personal observation*].

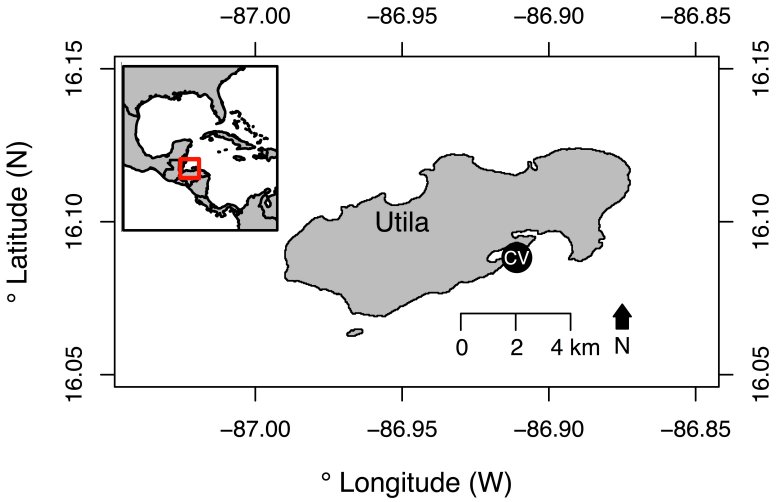

Figure 1: Map shows the dive site Coral View (marked "CV"), where 192 tiles were placed 15±2 m deep on the reef. Inset map shows Utila's location relative to the rest of the Caribbean. Map sourced from GADM database of Global Administrative Areas under a CC BY licence.

115 2.2 Tile designs

116 Vector dispersion was calculated following Young et al. (2017): *i.e.,* a grid of
117 points spaced 1 cm apart was projected onto the 3D model, and adjacent points
118 were connected by triangles to form a surface with *1/k* defined as:

$$R = \sqrt{\left(\sum_{1}^{i} cos_x\right)^2 + \left(\sum_{1}^{i} cos_y\right)^2 + \left(\sum_{1}^{i} cos_z\right)^2} \quad (1)$$

$$1/k = (i - R)/(i - 1), \quad (2)$$

119 where i is the number of triangles forming the surface; cos_x is the directional
120 cosine of a triangle's normal vector with respect to the X-axis; cos_y is the direc-
121 tional cosine with respect to the Y-axis, and cos_z is the directional cosine with
122 respect to the Z-axis (Fig. 2(a)).

123 The surface areas of the natural and artificial-shaped differed, as detailed in

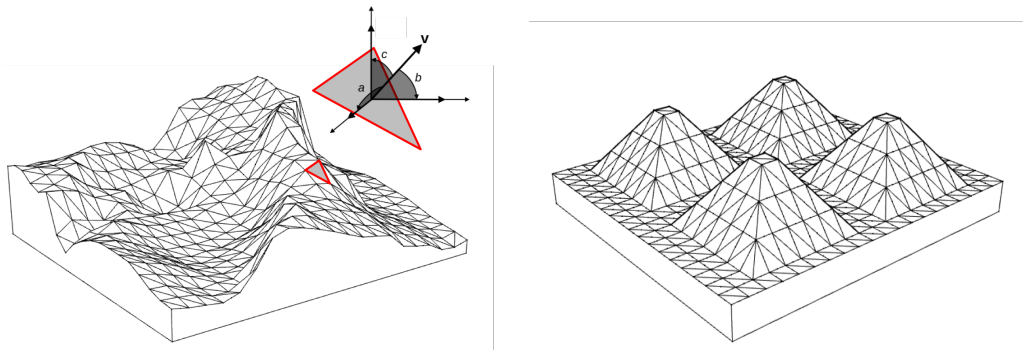

(a) Natural-shaped tile (b) Artificial-shaped tile

Figure 2: Designs for (a) natural-shaped tile and (b) artificial-shaped tile. Each tile is 18 x 20 cm at its base with a maximum height of 8 cm (natural-shaped) or 6 cm (artificial-shaped). Despite different appearances, both designs' textured faces (720 triangles) have the same vector dispersion (*1/k*). Their opposite faces are flat ($1/k = 0$). Inset on (a) shows the normal vectors used to compute $1/k$ for a surface triangle.

Fig. 3. This was accounted for during analysis by comparing densities rather than counts of settled organisms.

2.2.1 Natural-shaped tile

The textured face of the natural-shaped tile (Fig. 2(a) & 3) was designed by cropping a 3D model of the reef 10 m deep at Coral View to an 18 x 20 cm patch. The 3D model was generated from structure-from-motion photogrammetry following (Young et al., 2017). The section was chosen for its relatively high vector dispersion, $1/k = 0.25$ (Carleton & Sammarco (1987) measured $1/k$ from 0.04–0.26). Because $1/k$ was calculated at the 1 cm resolution, the resolution of the tile was normalized to 1 cm by keeping the surface as the set of triangles used to compute $1/k$ (Fig. 2(a)). The tile's textured face was therefore composed of 720 triangles covering a 18 x 20 cm grid.

2.2.2 Artificial-shaped tile

The textured face of the artificial-shaped tile (Fig. 2(b) & Fig. 3) was designed from four pyramids to have the same $1/k$ as the natural-shaped tile. Pyramids were chosen as the artificial shape for ease of calculation of $1/k$ using the triangle-based method of Carleton & Sammarco (1987). The tips of the pyramids

	Natural-Shaped Tile			Artificial-Shaped Tile		
Tile Face	Depiction	Area (cm^2)	*1/k*	Depiction	Area (cm^2)	*1/k*
Textured (T)		500	0.25		490	0.25
Edge (E)		216	NA		152	NA
Flat (F)		360	0.00		360	0.00
Total	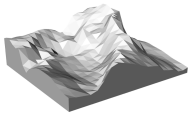	1076	0.25	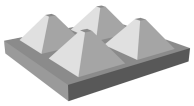	1002	0.25

Figure 3: Surface areas of decomposed natural and artificial-shaped tiles. Both tile design had three faces, labelled Textured (T), Edge (E), and Flat (F). The structural complexity metric vector dispersion (*1/k*) is compared between the T and F faces because they diametrically opposed each other.

were dulled to avoid sharp points that may chip during manufacturing. Like the natural-shaped tile, the textured face was composed of 720 triangles covering a 18 x 20 cm grid (Fig. 2(b)).

2.3 Tile manufacturing

Tile designs were 3D printed on a MakerBot Replicator 2 (MakerBot, Brooklyn, NY). Moulds were then formed around the 3D prints from *VytaFlex 30* (Smooth-On, Inc.; Macungie, PA). Moulds were then used to cast concrete replicas of the 3D prints (Fig. 4). Moulds were coated in a release agent, *AquaCon* (Smooth-On, Inc.), to allow for easy removal of the concrete tiles. The release agent's effect on organisms is unknown, but it was applied equally over all textured and edge faces, so its effect was assumed to be constant.

Concrete was chosen as the tile material because it was inexpensive, available at the study site, and a recommended material for an AR (Fitzhardinge, 1989).

(a) (b)

Figure 4: Manufactured tiles prior to underwater deployment. Each tile is cast concrete, 20×18 cm at its base. (a) Overhead view of two natural-shaped tiles and two artificial-shaped tiles. (b) Angled view of tiles.

Concrete can host ecological community development similar to natural coral reefs, and is durable in seawater (Fitzhardinge, 1989). Each batch of concrete was made with the same 4:3:8 ratio of cement, water, and fine aggregate by volume. Chicken wire was embedded within each tile to ensure structural soundness. A mark embedded in the underside face of each tile indicated which orientation it would have underwater. This mark and other irregularities in the concrete meant that tiles' flat "faces" were not perfectly flat, but still $1/k \approx 0$. Importantly, any shape variations from the original 3D prints were consistent between tile designs (natural or artificial) because imperfections came from the same batches of concrete. The concrete tiles were unconditioned before they were placed on the reef.

2.4 Tile placement and retrieval

The natural and artificial-shaped tiles were placed in equal proportions on the reef and retrieved after one year. All tiles were placed between late-July and early-August 2015 along a 160 m transect 15 ± 2 m deep. To control for effects of placement angles, tiles were placed in three different orientations (down (D), up (U), and side (S)) such that tile's textured face either touched the reef or faced away from the reef (Fig. 5 & A1). To control for effects of placement along the

reef, six tiles were grouped close together in a block. Each block contained a representative of each shape in each orientation. Tiles rested on the reef, held in place by their own weight.

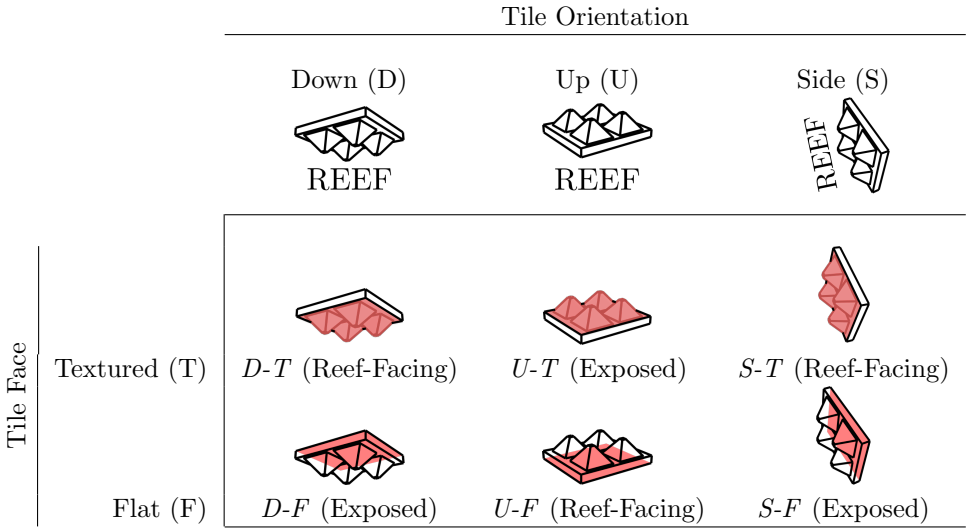

Figure 5: How tile faces touched the reef. In any orientation, one tile face touched the reef (reef-facing) and an opposite face pointed away from the reef (exposed). Reef-facing regions were in shade, while exposed regions were in light. Edges fell into neither classification, as they partially touched the reef and partially were exposed. Orientation-face combinations are referred to as Down-Textured (D-T), Up-Textured (U-T), *etc.*

Tiles were retrieved from the reef exactly one year after placement. To check if a tile had shifted orientation during placement, its orientation was compared to the mark embedded into the tile indicating its original orientation To ensure that no organisms detached during retrieval, divers wrapped each tile in a labelled plastic bag before it was brought to the surface.

All tiles were scored on-land within 24 hours of retrieval. Organisms were visually classified and counted without the aid of microscopes, which limited identification. Surface areas were estimated by placing a transparent sheet marked with 1 cm^2 grid squares over the tile and counting the number of squares filled more than half by the organism. The sheet was pressed flat over the algae and sponge.

2.5 Statistical analysis

Organisms were assessed in terms of density so they could be compared across tile shapes and faces.

Permutational analysis of variance (PERMANOVA) was well suited to the multi-factor, zero-inflated nature of the data and it benefited from the experiment's balanced design (Anderson et al., 2008). Models were stratified by block to control for any spatial variation in recruitment rates along the fore-reef slope. All PERMANOVAs ran for 99,999 permutations based on Euclidean distances using the "adonis" function from the "vegan" package (Oksanen et al., 2016) of R (R Development Core Team, 2017). Initial models included all possible interaction terms, and non-significant ($P \geq 0.05$) interaction terms were removed in a hierarchical manner to simplify the models. Each taxonomic group was analysed in a separate PERMANOVA because groups did not have the same degrees of freedom: While coral spat were counted on all retrieved tiles, other organisms were counted on most, but not all, tiles because of time constraints (see degrees of freedom in Table 1). The "betadisper" function, also from the "vegan" package of R, checked that data satisfied the PERMANOVA assumption that groups had the same multivariate homogeneity in their dispersions (Anderson et al., 2008); this assumption is hereafter refereed to as "the PERMANOVA assumption" or "same multivariate spread."

To study the effects of tile shape (natural vs artificial) and orientation (D vs U vs S) on organism settlement through PERMANOVA, settlement densities were computed over total tile areas in order to satisfy the PERMANOVA assumption. Testing over individual tile faces (D-T vs U-F vs S-T *etc.*) did not satisfy the assumption for all combinations. A pairwise PERMANOVA tested differences between the three orientations (D vs U vs S), with P values adjusted by the False Discovery Rate correction to avoid Type I errors from multiple testing.

To study the effect of vector dispersion on organism settlement, tiles' textured faces (where $1/k = 0.25$) were compared to flat faces (where $1/k \approx 0$) for orien-

tations where the PERMANOVA assumption was met. For coral spat, sponges, polychaetes, and bryozoans, reef-facing textured faces (D-T) could be compared to the reef-facing flat (U-F), but other combinations of orientation-faces violated the PERMANOVA assumption. For algae, the effect of vector dispersion on exposed faces could also be tested because groupings satisfied the assumption. Data from S-oriented tiles were not included in comparisons of *1/k* because data from these tiles had different multivariate spread than data from D-T or U-F. Tile shape (natural vs artificial) was retained in models, regardless of its significance previous PERMANOVAs, because it was the main focus of this study.

To identify significant differences between the reef-facing, exposed, and edge tile regions, Mann-Whitney-Wilcoxon tests compared organism densities. Tiles' unique identification numbers were included in an initial PERMANOVA, where they were non-significant; this confirmed the assumption of Mann-Whitney-Wilcoxon that samples be independent.

Finally, to assess correlations between organisms, Spearman's rank correlation coefficients (ρ) described significant relationships between organism densities.

3 Results

Of the 192 tiles placed, 173 (90%) were retrieved and analysed. All retrieved tiles maintained their orientations during placement. In total, there were 1,130 coral spat that settled on the 7.924 m^2 of reef-facing tile areas (142.6 spat/m^2 over reef-facing area). Only 10% of all recorded coral spat settled on non-reef-facing tile areas (12.96 spat/m^2 over exposed and edge areas).

There was a significant linear trend with coral spat density increasing by 6.9 coral spat per m^2 every 5 m from east to west along the 160 m transect at Coral View (Fig. A3). This effect was accounted for in the statistical analysis by stratifying PERMANOVAs by block numbers.

Table 1: PERMANOVA results testing the effects of tile shape (natural (N) or artificial (A)) and orientation (down (D), up (U), or side (S)) upon organism settlement. Organism densities were computed over total tile areas, which met the PERMANOVA assumption. Significant P-values bolded ($P \leq 0.050$). PERMANOVAs based on Euclidean distances and stratified by tiles' block numbers.

Organism ∼ Source of Variation	*df*	MeanSqs	Pseudo-F	P
Coral spat/m^2 over total tile area ∼				
Shape (N vs A)	1	2144.0	0.2	0.660
Orientation (D vs U vs S)	2	31460.0	2.9	0.054*
Residuals	169	10680.0		
Algae % cover over total tile area ∼				
Shape (N vs A)	1	55.9	0.3	0.575
Orientation (D vs U vs S)	2	851.5	4.1	**0.009**
Residuals	147	207.0		
Sponges % cover over total tile area ∼				
Shape (N vs A)	1	0.3	0.3	0.584
Orientation (D vs U vs S)	2	0.6	0.6	0.510
Residuals	156	1.0		
Polychaetes/m^2 over total tile area ∼				
Shape (N vs A)	1	289.5	0.1	0.800
Orientation (D vs U vs S)	2	2770.7	0.6	0.553
Residuals	156	4703.0		
Bryozoans/m^2 over whole tile area ∼				
Shape (N vs A)	1	7075.7	1.8	0.070
Orientation (D vs U vs S)	2	7219.6	1.8	0.227
Residuals	152	3960.9		

* Borderline significance.

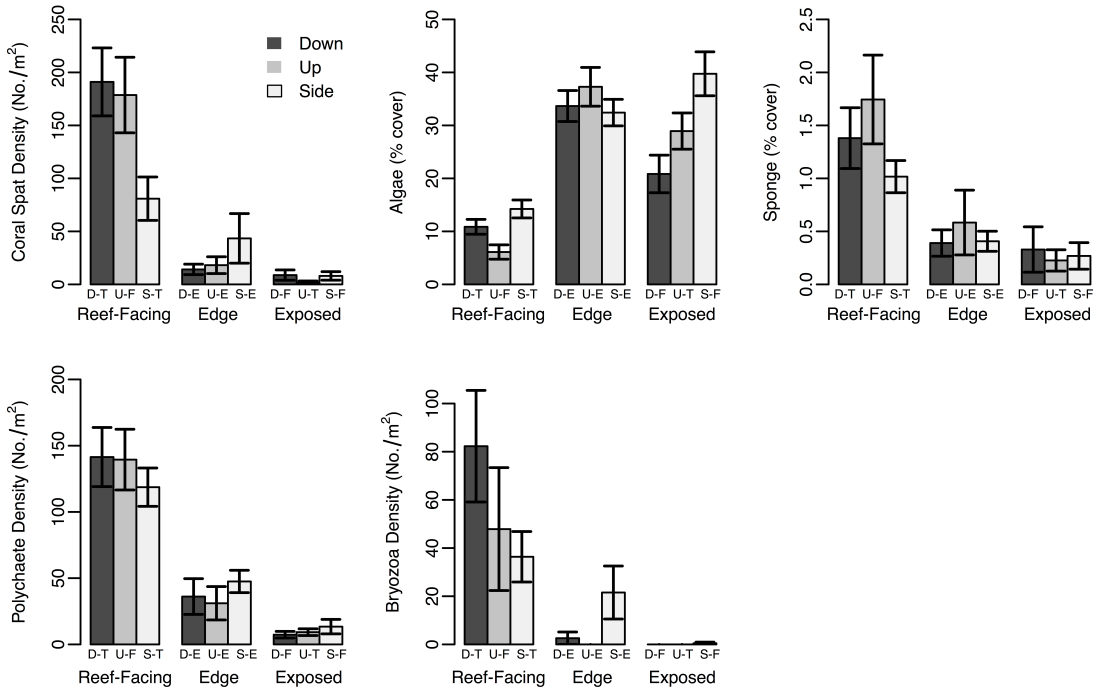

Figure 6: Mean settlement densities on each orientation-face ± one standard error for (a) coral spat, (b) algae, (c) sponges, (d) polychaetes, and (e) bryozoans. All differences between reef-facing and exposed regions were highly significant (Mann-Whitney-Wilcoxon tests; Table A1). Down-Textured (D-T), Up-Flat (U-F), Side-Textured (S-T), *etc.* refer to orientation-face combinations.

3.1 Did tile shape and/or orientation influence settlement?

Tile shape (natural vs artificial) did not significantly influence the settlement of any of the organisms studied (Table 1; Fig. A4). Tile orientation (D vs U vs S) also did not significantly influence the settlement of any organism except algae (Table 1). Orientation's effect on coral spat was only slightly above the significance threshold ($P = 0.054$; Table 1). The difference between S and the other orientations in terms of coral spat settlement appears stark in Fig. 6. Although the difference is not statistically significant (P-adjusted ≥ 0.110; pairwise PERMANOVA), on S tiles coral spat densities (computed over total tile area) were 1.9x lower in terms of mean and 5.3x lower in terms of median than on D tiles. Tile orientation affected algae in that S tiles had significantly higher algae cover than D tiles (Fig. 6). S tiles had 26.14 ± 2.06 % algae cover (mean ± one standard error), while D tiles had 18.03 ± 1.85 % algae cover (computed over total tile area).

Table 2: PERMANOVA results testing the effect of tile shape (natural (N) or artificial (A)) and vector dispersion ($1/k$) upon organism settlement over reef-facing areas. Tile faces were never compared between the same tile, preserving samples' independence. Only down (D) and up (U) tiles were included, because data from side (S) tiles violated the PERMANOVA assumption. Algae was the only organism that settlement sufficiently on exposed tile regions for the data to meet the PERMANOVA assumption. Significant P-values bolded ($P \leq 0.05$). PERMANOVAs based on Euclidean distances and stratified by tiles' block numbers.

Organism ∼ Source of Variation	*df*	MeanSqs	Pseudo-F	P
Coral spat/m^2 over reef-facing area ∼				
Shape (N vs A)	1	37196.0	0.6	0.421
$1/k$=0.25 vs 0.00	1	3805.0	0.1	0.785
Residuals	105	61686.0		
Algae % cover over reef-facing areas ∼				
Shape (N vs A)	1	16.2	0.2	0.705
$1/k$=0.25 vs 0.00	1	346.0	3.7	**0.021**
Residuals	93	93.4		
Algae % cover over exposed area ∼				
Shape (N vs A)	1	20.0	0.0	0.838
$1/k$=0.25 vs 0.00	1	1925.0	3.2	0.057*
Residuals	93	593.0		
Sponge % cover over reef-facing area ∼				
Shape (N vs A)	1	15.0	2.5	0.107
$1/k$=0.25 vs 0.00	1	3.7	0.6	0.472
Residuals	97	6.1		
Polychaetes/m^2 over reef-facing area ∼				
Shape (N vs A)	1	5582.7	0.2	0.695
$1/k$=0.25 vs 0.00	1	6.6	0.0	0.988
Residuals	97	25672.9		
Bryozoans/m^2 over reef-facing area ∼				
Shape (N vs A)	1	13222.0	0.5	0.301
$1/k$=0.25 vs 0.00	1	29961.0	1.0	0.360
Residuals	96	29365.0		

* Borderline significance.

3.2 Did vector dispersion influence settlement?

There is no evidence that $1/k$ influenced any of the organisms except algae (Table 2; Fig. 6). $1/k$ influenced algae, with $1/k = 0.25$ attracting 10.43 ± 1.36 % algae cover on reef-facing areas (median 7.96 %) and $1/k = 0.00$ attracting 6.62 ± 1.42 % algae cover on reef-facing areas (median 3.61 %). The effect of $1/k$ on algae on exposed areas was borderline significant ($P = 0.057$; Table 2), with again $1/k = 0.25$ attracting higher algae cover than $1/k = 0.00$ (Fig. 6).

3.3 Did organisms settle on the reef-facing, edge, or exposed tile regions?

All organisms except algae settled almost exclusively on reef-facing regions (Fig. 6). Conversely, algae cover was greatest on edge regions (Fig. 6). Differences between reef-facing, edge, and exposed regions were highly significant, except the difference for bryozoans between edge and exposed regions (Mann-Whitney-Wilcoxon tests; Table A1).

Notably the reef-facing region of S-oriented tiles differed in its multivariate spread compared to the reef-facing regions of D and U tiles. This difference can be seen in Fig 6, where the reef-facing regions of S tiles attracted 80.85 $\pm$ 20.47 coral spat per m^2 (median 20.41 coral spat per m^2) and the reef-facing regions of D and U tiles attracted 183 $\pm$ 23.75 coral spat per m^2 (median 83.33 coral spat per m^2)—more than double the density.

3.4 Did coral spat settlement differ with settlement of other taxa?

All relationships between organisms were positive. Spearman's ranks correlation coefficients (ρ) revealed significant relationships between coral spat and all other all organisms that varied in strength from weak ($0.20 \leq |\rho| \leq 0.39$; Table 3) to moderate ($0.40 \leq |\rho| \leq 0.59$; Table 3). Sponges and polychaetes correlated very strongly ($\rho = 0.87$; Table 3). Bryozoans correlated significantly with both algae and sponges, although the relationships were weak ($0.20 \leq |\rho| \leq 0.39$) to very weak ($0.00 \leq |\rho| \leq 0.19$). Algae's correlations with organisms besides bryozoans were non-significant, perhaps because algae settled on edge and exposed tile regions, while the other organisms almost exclusively settled upon reef-facing tile regions (Fig. 6).

Table 3: Spearman's rank correlation coefficients (ρ) between recorded organisms. Only densities over reef-facing regions are compared; data on coral and algae were only compared for D and U tiles because of difference with S tiles observed in PERMANOVA and in Fig. 6. P-values adjusted by the False Discovery Rate correction. Significant P-adjusted values bolded (P-adjusted ≤ 0.050).

	Coral	Algae	Sponges	Polychaets	Bryozoans
Coral spat/m^2	1.00	**0.36**	**0.49**	**0.47**	**0.44**
Algae (% cover)		1.00	0.11	0.09	**0.21**
Sponges (% cover)			1.00	**0.87**	**0.17**
Polychaetes/m^2				1.00	0.15
Bryozoans/m^2					1.00

4 Discussion

There was no evidence that any of the organism densities differed between the natural and artificial-shaped surfaces. Additionally, for organisms except algae, there was no evidence that densities differed between the textured and flat surfaces, where $1/k = 0.25$ and $1/k \approx 0.00$, respectively. Algae had a higher percent cover on textured surfaces compared to flat surfaces. This study therefore suggests that ARs with similar *1/k* to natural reefs at the 1 cm scale will not be more effective for organism recruitment after one year compared to artificial shapes.

While results show that building an artificial reef with $1/k > 0$ may not enhance the density of settling coral spat, increasing $1/k$ also increases surface area, and in this study resulted in a higher total number of living organisms. Artificial reefs with higher surface area (perhaps as a result of $1/k$) should therefore be expected to have higher settlement and survivorship rates.

This was a pilot study that pioneered a method for using 3D printed designs in recruitment tile designs. We suggest several improvements to the method for future studies.

1. **Scoring method.** The method for identifying organisms should be more rigid to allow genus and species-level classifications. With 200 tiles, such an effort would be likely require ≥30 minutes per tile. It could be condensed by only searching reef-facing tile areas. Finally, using a microscope to iden-

tify organisms would detail species identification, including distinguishing between algal functional groups, and allow detection of smaller organisms. Bleaching tiles prior to counts of polychaetes, bryozoans, or coral would likely have made counts more accurate. Identification of images is tempting, but many creatures were under layers of algae so counting by-hand does seem to be the best route forward. Researchers commonly soak the tiles in bleach for 24-48 hours. The bleach removes organic material but the skeletons of individual corals and bryozoans remain and can be counted.

2. **Tile elevation.** Elevating the tiles would reduce sedimentation. By blocking tiles we were able to assume that sedimentation rates were the same between tiles of the same block. That said, controlling for sedimentation would better facilitate cross-site comparisons.

3. **Tile conditioning.** Conditioning the tiles by leaving them in seawater for more than two weeks and eliminating the release agent, or using a different release agent, will likely lower the tile's acidity and allow more organisms to settle on the tiles (Fitzhardinge, 1989, Goh & Lee, 2008).

With only one study site, this experiment was unable to piece apart influence of environmental conditions specific to the study site, such as sedimentation, eutrophication, and local biota. It did, however, account for any changes in environmental conditions at the site by placing tiles in blocks equally spaced along 180 m at the study site and controlling for the blocks in the statistical analysis.

4.1 Effects of tile shape

The natural and artificial-shaped tiles did not differ in terms of organism settlement. This conclusion fits with that of Carleton & Sammarco (1987), who found that coral spat density correlated positively and tightly with $1/k$ (with Pearson's correlation coefficient of 0.688, $P < 0.05$), because $1/k$ was the same

on both tile shapes. However, contrary to Carleton & Sammarco (1987), there were no differences between reef-facing tile areas that were flat, where $1/k \approx 0$, and textured, where $1/k = 0.25$, in terms of any of the organisms except algae. These findings suggest that substratum shape, as measured in this study, did not influence settlement. The contrast with Carleton & Sammarco (1987) likely results from time difference between our studies and the Great Barrier Reef having higher coral cover and spat settlement than the Caribbean. In general data acquired on an AR at one site may not be suitable for extrapolation to another (Sherman et al., 2001). Additionally, Carleton & Sammarco (1987) used natural substrate (pieces of platy coral), where every plate had $1/k > 0$. While they found that $1/k$ on the 1 cm scale was a powerful predictor of coral settlement, their tiles would naturally have possessed structural complexity on smaller scales as well, which must be intertwined with the larger scale models and may have enhanced settlement rates (Edmunds et al., 2014).

These results were likely affected by the release agent, which may have left residue on textured and edge faces. For all organisms but algae, cryptic, textured faces had significantly higher organism densities than edge, flat faces. This would suggest that habitat suitability of the textured surfaces was marred by the release agent.

Algae were the only organism that settled significantly differently on either the textured or flat faces. Algae settlement was greater on textured faces (where $1/k = 0.25$) than on flat faces (where $1/k \approx 0$) (Fig. 6). This finding goes against the suggestion of Loke et al. (2016) that algae tend to be affected by topological differences only at scales less than 10 μm (whereas the tiles in the present study showed topological differences at the 1 cm scale). Perhaps the textured faces of the tiles created turbulence that reduced benthic boundary layers leading to high nutrient supply, or was less easy for grazers to cover compared to the flat faces. Curiously, the reduction in algae cover on flat faces did not result in increased densities of coral spat or other sessile organisms.

The question therefore remains, *what aspects of a settlement surface shape influences organism settlement?* Several studies concluded that substratum shape influences the settlement density of coral spat and other marine organisms (Johnson, 1994, Petersen et al., 2005, Idjadi & Edmunds, 2006, Mumby & Steneck, 2008, Chapman & Underwood, 2011, Graham & Nash, 2013, Davies et al., 2013, Martins et al., 2016, Hata et al., 2017), where shape in this context is used interchangeably with the terms roughness, texture, rugosity, complexity, or heterogeneity. Textured cryptic surfaces did not enhance organism settlement densities compared to flat cryptic surfaces. This could be because flat surfaces were closer to the reef, including closer reef chemical cues, whereas textured surfaces had fewer touch points.

Modifications to *1/k* may change its explanatory power. For example, *1/k* could be supplemented with indicators of (a) how graze-able a surface is by herbivores—a factor discussed by Sammarco & Carleton (1981) among others; (b) hydrodynamic effects (such as those discussed by Bourget et al. (1994)); (c) other measures of structural complexity such as rugosity; or, (d) measurements at scales smaller than 1 *cm* (such as those discussed by Roth & Knowlton (2009), Nozawa (2012), Edmunds et al. (2014)).

4.2 Effects of tile orientation

Some studies have found that tile orientation (or "substrate angle") strongly influences coral settlement (Carleton & Sammarco, 1987, Tomascik, 1991, Glasby & Connell, 2001); but also see (Mundy, 2000). The relationship between coral settlement and substrate angle likely depends upon light intensity and/or depth (Birkeland et al., 1981, Maida et al., 1994, Babcock & Mundy, 1996). Although these factors were held constant in this study, *D, U* and *S*-oriented tiles would have received different amounts of light on the textures of their reef-facing, exposed, and edge regions. Therefore differences in settlement between orientations could not be predicted by the results of previous studies.

No significant differences were detected between *D, U*, and *S* tiles in terms of the settlement of any organism except algae when settlement densities were computed over total tile areas (Table 1). When settlement densities were computed exclusively over reef-facing areas, however, *S* tiles exhibited lower mean densities than the other orientations (Fig. 6). That said, the significances of these difference could not be assessed in PERMANOVAs because the reef-facing regions of *S*-oriented tiles differed in multivariate spread compared to the reef-facing regions of the other orientations (Fig. 6). Contrastingly, other studies have observed greater coral settlement on steeper (or vertical) surfaces compared to horizontal ones (Carleton & Sammarco, 1987, Tomascik, 1991, Davies et al., 2013), but these have either assessed only one site (Carleton & Sammarco, 1987, Davies et al., 2013) or found that the trend only held true at four of their six sites (Tomascik, 1991). Moreover, while Sammarco (1991) suggest that 37-45 degrees is the optimal plate angle for coral settlement, Mundy (2000) found no evidence for such an optimal angle in their study of coral settlement on numerous plate angles 0–90 degrees. Together, these results highlight an unclear or inconsistent relationship between orientation and organism settlement, or a relationship masked by other environmental factors influencing settlement.

Algae were the only organisms that orientation significantly affected: S tiles attracted 1.5x higher algae cover than D tiles. This was somewhat surprising because both D and S tiles had the same reef-facing and exposed surface areas. If algae cover had been greater on vertical surfaces compared to horizontal ones (as Virgilio et al. (2006) showed in their study of turf-forming seaweeds), then U and S should also have significantly differed, but they did not. One explanation may be that U, despite being horizontal and therefore less attractive to algae according to Virgilio et al. (2006), had a greater proportion of its surface area exposed (where algae cover was greater than reef-facing regions; Fig. 6), thereby masking orientation's effect.

Coral spats dominance on the reef-facing regions (undersides) of tiles was ex-

pected based on the results of several studies (Carleton & Sammarco, 1987, Babcock & Davies, 1991, Maida et al., 1994, Roth & Knowlton, 2009, Arnold & Steneck, 2011, Brandl et al., 2014). This pattern is likely tied to factors including light intensity, grazing, sedimentation, and hydrodynamics (Maida et al., 1994). Likewise other organisms' proclivities for the reef-facing regions of tiles was predicted by other studies (*e.g.,* sponges (Vermeij, 2006, Arnold & Steneck, 2011); polychaetes (Schwindt & Iribarne, 2000); or bryozoans (Keough & Downes, 1982, Baird & Hughes, 1999)). Vermeij (2006) found on a Caribbean reef that macroalgae dominated the topsides (exposed) regions of their panels. Conversely, Arnold et al. (2010) found that on a Caribbean reef crustose coralline algae (CCA) cover was greatest on the undersides of settlement places.

Oriented *D*, the artificial and natural-shaped tiles had different number of contact points on a flat surface. Natural undulations of the reef meant that the number of contact points varied even more. All tiles were approximately horizontal with the surface, however, and as there were no observed difference between the tile shapes, it is assumed that this had a minor effect. Because the tiles had steep angles built into them, tile orientation did not necessarily indicate the angles of the substrates where organisms settled. Settlement is probably more influenced by the angle of the specific surface of settlement than the angle of the plate as a whole. This could it be a confounding factor in the results. Future studies could also include a sideways tile with the textured surface facing outwards. This may lead to clearer conclusions regarding algal settlement.

4.3 Correlations between organisms

Coral spat settlement correlated positively with all other organisms, with weak to moderate relationship strengths (Table 3). Coral spat may have favoured the same environmental conditions as the other organisms, and competition may not have sufficiently affected the populations yet. If the tiles were left *in-situ* longer than the one year, it is likely that the macroalgae and/or sponges would have

killed many of the coral spat.

4.4 Artificial reef applications

Our results suggest that it may be possible to control algae settlement on an AR by adjusting texture or *1/k*. Ideally, a design could encourage positive ecological interactions and optimise organism settlement and survivorship, in part by thwarting mortality from sponge and macroalgae overgrowth. Our findings also suggest that the availability of sheltered, reef-facing area is likely more important than cm-scale complexity in enhancing settlement. This conclusion aligns with the finding that larval-size crevices, which offer complete shelter, can increase settlement even on exposed surfaces (Edmunds et al., 2014, Whalan et al., 2015). Finally, an AR's resemblance to a natural reef at the 1 cm scale did not affect organism recruitment in this study. This result implies that a structure precisely crafted to match a natural reef should not be expected to have greater settlement rates than a collection of pyramids or other artificial shapes with the same structural complexity.

5 Conclusion

This study has piloted a method for using 3D printed moulds to test different shapes of settlement surfaces underwater. Future studies could improve the method by, for example, conditioning tiles and changing the release agent used on the concrete moulds. Contrary to expectation, we found that *1/k* affected only algae settlement, and not coral spat, sponge, polychaete, or bryozoan settlement. This finding went against the trend reported by Carleton & Sammarco (1987) in their 1986 study on the Great Barrier Reef, Australia. Surprisingly, textured cryptic surfaces (with high *1/k*) did not enhance organism settlement densities compared to flat cryptic surfaces. One possible explanation is that the flat surfaces had more touch points with the reef, and were therefore closer to

reef chemical cues. Another possible explanation is that the textured surfaces had more residue from the release agent, which may have inhibited organism growth. Methodological improvements are needed to better study nuances in structural complexity's role in early organism settlement and moreover, ways to design ARs for maximizing or minimizing certain organisms growth.

Acknowledgements

Thanks to Operation Wallacea for facilitating fieldwork, the Marshall Commission for supporting GCY, the Fisheries Society of the British Isles for supporting DAAB, Richard Smith at University of Oxford Radcliffe Science Library for assistance 3D printing, Erika Gress for feedback on the experimental design, and the following for critical assistance during fieldwork: Jonathon Burroughs, Faye-Marie Crooke, Mary Ellen Fluharty, Shagun Gupta, Tobias Hodnett, Anna Kelly, Jack Laverick, Shorvin Mcfield, Kirsty Porter, Naomi Slator, Prasanna Stephan Wijesinghe, Grace Williams, Calvin Woods, Gina Wright, and Island Construction.

References

Al-Horani, F. A. & Khalaf, M. A. (2013), 'Developing artificial reefs for the mitigation of man-made coral reef damages in the Gulf of Aqaba, Red Sea: coral recruitment after 3.5 years of deployment', *Marine Biology Research* **9**(8), 749–757.

Anderson, M., Gorley, R. & Clarke, K. (2008), *Permanova+ for Primer: Guide to Software and Statistical Methods*, PRIMER-E Ltd., Plymouth, U.K.

Andradi-Brown, D. A., Gress, E., Wright, G., Exton, D. A. & Rogers, A. D. (2016), 'Reef Fish Community Biomass and Trophic Structure Changes across Shallow to Upper-Mesophotic Reefs in the Mesoamerican Barrier Reef, Caribbean', *Plos One* **11**(6), e0156641.

Arnold, S. N. & Steneck, R. S. (2011), 'Settling into an increasingly hostile world: The rapidly closing "recruitment window" for corals', *PLoS ONE* **6**(12).

Arnold, S. N., Steneck, R. S. & Mumby, P. J. (2010), 'Running the gauntlet: Inhibitory effects of algal turfs on the processes of coral recruitment', *Marine Ecology Progress Series* **414**, 91–105.

Babcock, R. & Davies, P. (1991), 'Effects of Sedimentation on Settlement of Acropora Millepora', *Coral Reefs* **9**(4), 205–208.

Babcock, R. & Mundy, C. (1996), 'Coral recruitment: Consequences of settlement choice for early growth and survivorship in two scleractinians', *Journal of Experimental Marine Biology and Ecology* **206**(1-2), 179–201.

Baine, M. (2001), 'Artificial reefs: a review of their design, application, management and performance', *Ocean & Coastal Management* **44**(3-4), 241–259.

Baird, A. H. & Hughes, T. P. (1999), 'Competitive dominance by tabular corals: an experimental analysis of recruitment and survival of understory assemblages'.

Beck, M. W. (1998), 'Comparison of the measurement and effects of habitat structure on gastropods in rocky intertidal and mangrove habitats', *Marine Ecology Progress Series* **169**, 165–178.

Beck, M. W. (2000), 'Separating the elements of habitat structure: Independent effects of habitat complexity and structural components on rocky intertidal gastropods', *Journal of Experimental Marine Biology and Ecology* **249**(1), 29–49.

Birkeland, C., Rowley, D. & Randall, R. H. (1981), Coral recruitment patterns at Guam, *in* 'Proc 4th Int Coral Reef Symp', Vol. 2, pp. 339–344.

Bourget, E., DeGuise, J. & Daigle, G. (1994), 'Scales of substratum heterogeneity, structural complexity, and the early establishment of a marine epibenthic community', *Journal of Experimental Marine Biology and Ecology* **181**(1), 31–51.

Brandl, S. J., Hoey, A. S. & Bellwood, D. R. (2014), 'Micro-topography mediates interactions between corals, algae, and herbivorous fishes on coral reefs', *Coral Reefs* **33**(2), 421–430.

Burke, L. & Maidens, J. (2004), *Reefs at Risk in the Caribbean*, World Resources Institute (WRI).

Burke, L., Reytar, K. & Mark Spalding, A. P. (2011), *Reefs at Risk Revisited*, World Resources Institute (WRI).

Burt, J., Bartholomew, A., Usseglio, P., Bauman, A. & Sale, P. F. (2009), 'Are artificial reefs surrogates of natural habitats for corals and fish in Dubai, United Arab Emirates?', *Coral Reefs* **28**(3), 663–675.

Cambers, G. (1997), 'Beach Changes in the eastern Caribbean Islands: Hurricane Impacts and Implications for Climate Change', *Journal of Coastal Research* **24**, 29–47.

Carleton, J. H. & Sammarco, P. W. (1987), 'Effects of Substratum Irregularity on Success of Coral Settlement: Quantification by Comparative Geomorphological Techniques', *Bulletin of Marine Science* **40**(1), 85–98.

Carr, M. & Hixon, M. (1997), 'Artificial Reefs: The Importance of Comparisons with Natural Reefs', *Fisheries* **22**(4), 28–33.

Chapman, M. G. & Underwood, A. J. (2011), 'Evaluation of ecological engineering of "armoured" shorelines to improve their value as habitat', *Journal of Experimental Marine Biology and Ecology* **400**(1-2), 302–313.

Conservation International (2008), 'Economic Values of Coral Reefs, Mangroves, and Seagrasses: A Global Compilation', *Center for Applied Biodiversity Science, Conservation International* .

Davies, S. W., Matz, M. V. & Vize, P. D. (2013), 'Ecological Complexity of Coral Recruitment Processes: Effects of Invertebrate Herbivores on Coral Recruitment and Growth Depends Upon Substratum Properties and Coral Species', *PLoS ONE* **8**(9).

Edmunds, P. J., Nozawa, Y. & Villanueva, R. D. (2014), 'Refuges modulate coral recruitment in the Caribbean and the Pacific', *Journal of Experimental Marine Biology and Ecology* **454**, 78–84.

Ferrari, R., Bryson, M., Bridge, T., Hustache, J., Williams, S. B., Byrne, M. & Figueira, W. (2016), 'Quantifying the response of structural complexity and community composition to environmental change in marine communities', *Global Change Biology* **22**(5), 1965–1975.

Fitzhardinge, R. C. (1989), 'Colonization of Artificial Reef Materials by Corals and Other Sessile Organisms', *Bulletin of Marine Science* **44**(2), 567–579.

Glasby, T. M. & Connell, S. D. (2001), 'Orientation and position of substrata have large effects on epibiotic assemblages', *Marine Ecology Progress Series* **214**, 127–135.

Goatley, C. H. R. & Bellwood, D. R. (2011), 'The Roles of Dimensionality, Canopies and Complexity in Ecosystem Monitoring', *PLoS ONE* **6**(11).

Goh, B. P. L. & Lee, C. S. (2008), 'A study of the effect of sediment accumulation on the settlement of coral larvae using conditioned tiles.', *Proceedings of the 11th International Coral Reef Symposium* pp. 1235–1239.

Graham, N. A. J. & Nash, K. L. (2013), 'The Importance of Structural Complexity in Coral Reef Ecosystems', *Coral Reefs* **32**, 315–326.

Gratwicke, B. & Speight, M. (2005), 'Effects of Habitat Complexity on Caribbean Marine Fish Assemblages', *Marine Ecology Progress Series* **292**, 301–310.

Hata, T., Madin, J. S., Cumbo, V. R., Denny, M., Figueiredo, J., Harii, S., Thomas, C. J. & Baird, A. H. (2017), 'Coral larvae are poor swimmers and require fine-scale reef structure to settle', *Scientific Reports* **7**(2249), 1–9.

Hopley, D., ed. (2011), *Encyclopedia of Modern Coral Reefs: Structure, Form and Process*, Springer, Dordrecht, The Netherlands.

582 Hughes, T. P., Barnes, M. L., Bellwood, D. R., Cinner, J. E., Cumming, G. S.,
583 Jackson, J. B., Kleypas, J., Van De Leemput, I. A., Lough, J. M., Morrison,
584 T. H., Palumbi, S. R., Van Nes, E. H. & Scheffer, M. (2017), 'Coral reefs in the
585 Anthropocene', *Nature* **546**(7656), 82–90.

586 Idjadi, J. A. & Edmunds, P. J. (2006), 'Scleractinian corals as facilitators for other
587 invertebrates on a Caribbean reef', *Marine Ecology Progress Series* **319**, 117–
588 127.

589 Johnson, L. E. (1994), 'Enhanced settlement on microtopographical high points
590 by the intertidal red alga Halosaccion glandiforme', *Limnology and Oceanogra-*
591 *phy* **39**(8), 1893–1902.

592 Keough, M. J. & Downes, B. J. (1982), 'Recruitment of marine invertebrates: the
593 role of active larval choices and early mortality', *Oecologia* **54**(3), 348–352.

594 Loke, L. H. L., Liao, L. M., Bouma, T. J. & Todd, P. A. (2016), 'Succession of
595 seawall algal communities on artificial substrates', *Raffles Bulletin of Zoology*
596 **2016**(32), 1–10.

597 Maida, M., Coll, J. & Sammarco, P. (1994), 'Shedding New Light on Sclerac-
598 tinian Coral Recruitment', *Journal of Experimental Marine Biology and Ecology*
599 **180**(2), 189–202.

600 Martins, G. M., Jenkins, S. R., Neto, A. I., Hawkins, S. J. & Thompson, R. C.
601 (2016), 'Long-term modifications of coastal defences enhance marine biodiver-
602 sity', *Environmental Conservation* **43**(2), 109–116.

603 McCormick, M. I. (1994), 'Comparison of Field Methods for Measuring Surface
604 Topography and their Associations with a Tropical Reef Fish Assemblage', *Ma-*
605 *rine Ecology Progress Series* **112**, 87–96.

606 Mumby, P. J. & Steneck, R. S. (2008), 'Coral reef management and conservation in
607 light of rapidly evolving ecological paradigms', *Trends in Ecology and Evolution*
608 **23**(10), 555–563.

Mundy, C. N. (2000), 'An Appraisal of Methods Used in Coral Recruitment Studies', *Coral Reefs* **19**(2), 124–131.

Nozawa, Y. (2012), 'Effective size of refugia for coral spat survival', *Journal of Experimental Marine Biology and Ecology* **413**, 145–149.

Oksanen, J., Blanchet, F. G., Friendly, M., Kindt, R., Legendre, P., McGlinn, D., Minchin, P. R., O'Hara, R. B., Simpson, G. L., Solymos, P., Stevens, M. H. H., Szoecs, E. & Wagner, H. (2016), 'vegan: Community Ecology Package'.

Paddack, M. J., Reynolds, J. D., Aguilar, C., Appeldoorn, R. S., Beets, J., Burkett, E. W., Chittaro, P. M., Clarke, K., Esteves, R., Fonseca, A. C., Forrester, G. E., Friedlander, A. M., García-Sais, J., González-Sansón, G., Jordan, L. K. B., McClellan, D. B., Miller, M. W., Molloy, P. P., Mumby, P. J., Nagelkerken, I., Nemeth, M., Navas-Camacho, R., Pitt, J., Polunin, N. V. C., Reyes-Nivia, M. C., Robertson, D. R., Rodríguez-Ramírez, A., Salas, E., Smith, S. R., Spieler, R. E., Steele, M. A., Williams, I. D., Wormald, C. L., Watkinson, A. R. & Côté, I. M. (2009), 'Recent Region-wide Declines in Caribbean Reef Fish Abundance', *Current Biology* **19**(7), 590–595.

Perkol-Finkel, S., Shashar, N. & Benayahu, Y. (2006), 'Can artificial reefs mimic natural reef communities? The roles of structural features and age', *Marine Environmental Research* **61**(2), 121–135.

Petersen, D., Laterveer, M. & Schuhmacher, H. (2005), 'Innovative substrate tiles to spatially control larval settlement in coral culture', *Marine Biology* **146**(5), 937–942.

R Development Core Team (2017), 'R: A language and environment for statistical computing.'.

Roth, M. S. & Knowlton, N. (2009), 'Distribution, abundance, and microhabitat characterization of small juvenile corals at Palmyra Atoll', *Marine Ecology Progress Series* **376**, 133–142.

Sammarco, P. W. (1991), 'Geographically specific recruitment and postsettlement mortality as influences on coral communities: The cross-continental shelf transplant experiment.', *Limnology and Oceanography* **36**(3), 496–514.

Sammarco, P. W. & Carleton, J. H. (1981), Damselfish territoriality and coral community structure: reduced grazing, coral recruitment and effects on coral spat, *in* 'Proceedings of the 4th International Coral Reef Symposium', Vol. 2, pp. 525–535.

Schwindt, E. & Iribarne, O. O. (2000), 'Settlement sites, survival and effects on benthos of an introduced reef-building polychaete in a SW Atlantic coastal lagoon', *Bulletin of Marine Science* **67**(1), 73–82.

Sherman, R. L., Gilliam, D. S. & Spieler, R. E. (2001), 'Site-Dependent Differences in Artificial Reef Function: Implications for Coral Reef Restoration NSUWorks Citation', *Bulletin of Marine Science* **2**, 1053–1056.

Sherman, R. L., Gilliam, D. S. & Spieler, R. E. (2002), 'Artificial reef design: void space, complexity, and attractants', *ICES Journal of Marine Science* **59**(1994), S196–S200.

Tomascik, T. (1991), 'Settlement patterns of Caribbean scleractinian corals on artificial substrata along a eutrophication gradient, Barbados, West Indies', *Marine Ecology Progress Series* **77**(2-3), 261–269.

Vermeij, M. J. A. (2006), 'Early life-history dynamics of Caribbean coral species on artificial substratum: The importance of competition, growth and variation in life-history strategy', *Coral Reefs* **25**(1), 59–71.

Virgilio, M., Airoldi, L. & Abbiati, M. (2006), 'Spatial and temporal variations of assemblages in a Mediterranean coralligenous reef and relationships with surface orientation', *Coral Reefs* **25**(2), 265–272.

Walker, S. J. & Schlacher, T. A. (2014), 'Limited habitat and conservation value of a young artificial reef', *Biodiversity and Conservation* **23**(2), 433–447.

Whalan, S., Abdul Wahab, M. A., Sprungala, S., Poole, A. J. & De Nys, R. (2015), 'Larval settlement: The role of surface topography for sessile coral reef invertebrates', *PLoS ONE* **10**(2), 1–17.

Young, G. C., Dey, S., Rogers, A. D. & Exton, D. (2017), 'Cost and time-effective method for multi-scale measures of rugosity, fractal dimension, and vector dispersion from coral reef 3D models', *Plos One* **12**(4), e0175341.

A Electronic Supplementary Material

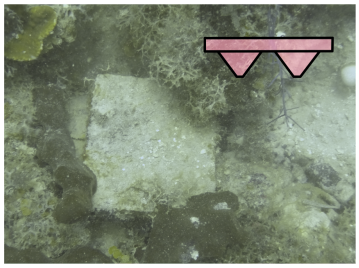

(a) Down orientation

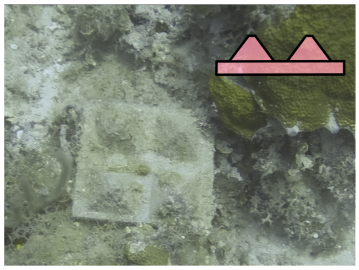

(b) Up orientation

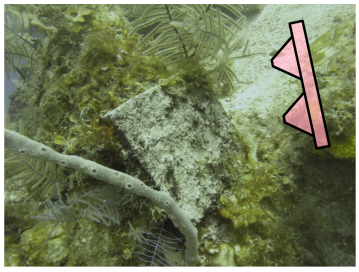

(c) Side orientation

Figure A1: Tile orientations. Photographs are of an artificial-shaped tile after a year of placement on the reef. (a) Overhead photo of down (D) tile: the tile's textured face touched the reef, approximately parallel with the ocean surface. (b) Overhead photo of up (U) tile: the tile's textured face faced away from the reef, approximately parallel with the ocean surface. (c) Angled photo of side (S) tile: the tile was propped against the reef with its textured face touching the reef, approximately perpendicular to the ocean surface.

Figure A2: Coral spat (circled in red) on retrieved tiles. Algae and polycheats also in photos.

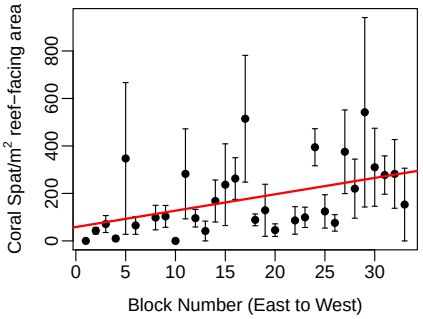

Figure A3: There was a significant linear increase in coral spat density from east to west along the 160 m transect at Coral View. The trend is modelled by $y = 58.5 + 6.9x$ (P=0.006, $R^2 = 0.07$). Density are computed over tiles' reef-facing area, where 90% of coral spat settled. Tiles of all orientations and shapes are included, as these factors did not significantly affect recruitment.

Table A1: Comparing reef-facing, edge, and exposed tile regions in terms of organism settlement. Reef-facing and exposed regions included both textured and flat faces, dependent upon tiles' orientations. Orientation is ignored except in the case of algae, because it was non-significant in the PERMANOVAs. P-values are from Mann-Whitney-Wilcoxon tests. Significant P-values are bolded ($P \leq 0.01\bar{6}$ with Bonferroni correction).

	Reef-Facing vs Edge			Reef-Facing vs Exposed			Edge vs Exposed		
Organism	df	W	P	df	W	P	df	W	P
Coral spat/m^2	347	22,964	$\ll$ **0.0001**	348	24,597	$\ll$ **0.0001**	347	13,517	**0.0049**
Algae (% cover)*	192	1,086	$\ll$ **0.0001**	192	2,294	$\ll$ **0.0001**	192	3,170	**0.0002**
Sponge (% cover)	320	19,169	$\ll$ **0.0001**	320	20,824	$\ll$ **0.0001**	320	11,048	**0.0069**
Polychaetes/m^2	320	19,446	$\ll$ **0.0001**	320	21,748	$\ll$ **0.0001**	320	10,652	**0.0008**
Bryozoans/m^2	313	16,307	$\ll$ **0.0001**	314	16,963	$\ll$ **0.0001**	313	11,770	0.0512

*Only algae over D and U tiles included because of the differences between D and S observed in Table 1.

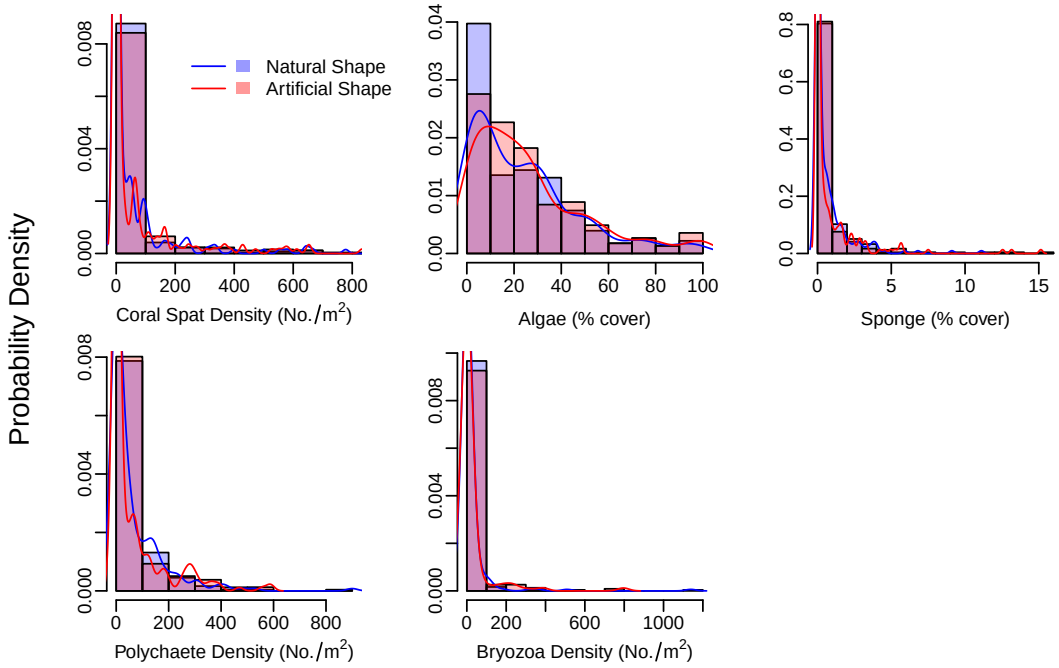

Figure A4: Densities of recruited organisms on the tiles by shape. Histogram bars are left edge-aligned over labels. There is no evidence that tile shape influenced recruitment in terms of any of the organisms studied (Tables 1-2).

Ecology is not, and should not be, the sole preserve of biologists.

— Professor Michael Risk quoted in Hopley et al. (2007)

5

Convolutional Neural Networks Predict Fish Abundance from Underlying Coral Reef Texture

Contents

5.1 Context 129
5.2 Author Contributions 130
5.3 Publication: Young, G. C., *et al.* "Convolutional Neural Networks Predict Fish Abundance from Underlying Coral Reef Texture." *In prep.* 131

5.1 Context

This chapter applies state-of-the-art machine-learning methods to the data from Chapter 3. Instead of assuming rugosity (R), fractal dimension (D), or vector dispersion ($1/k$) describe the relationship between fish and the 3D structure of the reef, the whole 3D model is input into a convolutional neural network that learns patterns with the fish data.

5.2 Author Contributions

The authors of this publication, in order, are: G. C. Young, V. Balntas, and V. A. Prisacariu. Author contributions are listed in CRediT taxonomy in Table 5.1 on page 130 following Brand et al. (2015).

Table 5.1: Author contributions for Chapter 5 listed in CRediT taxonomy (Brand et al., 2015). Initials refer to the authors of the paper; in order, they are: G. C. Young, V. Balntas, and V. A. Prisacariu.

Role	Author(s)
Conceptualization – Ideas; formulation or evolution of overarching research goals and aims.	GCY, VAP
Data Curation – Management activities to annotate (produce metadata), scrub data and maintain research data (including software code, where it is necessary for interpreting the data itself) for initial use and later reuse.	GCY
Formal Analysis – Application of statistical, mathematical, computational, or other formal techniques to analyze or synthesize study data.	GCY, VB
Funding Acquisition – Acquisition of the financial support for the project leading to this publication.	GCY
Investigation – Conducting a research and investigation process, specifically performing the experiments, or data/evidence collection.	GCY
Methodology – Development or design of methodology; creation of models	GCY, VB
Project Administration – Management and coordination responsibility for the research activity planning and execution.	GCY
Resources – Provision of study materials, reagents, materials, patients, laboratory samples, animals, instrumentation, computing resources, or other analysis tools.	GCY, VAP
Software – Programming, software development; designing computer programs; implementation of the computer code and supporting algorithms; testing of existing code components.	GCY, VB
Supervision – Oversight and leadership responsibility for the research activity planning and execution, including mentorship external to the core team.	VAP
Validation – Verification, whether as a part of the activity or separate, of the overall replication/reproducibility of results/experiments and other research outputs.	GCY

Continued on next page

Table 5.1 – *Continued from previous page*

Role	Author(s)
Visualization – Preparation, creation and/or presentation of the published work, specifically visualization/data presentation.	GCY
Writing - Original Draft Preparation – Creation and/or presentation of the published work, specifically writing the initial draft (including substantive translation).	GCY
Writing - Review & Editing – Preparation, creation and/or presentation of the published work by those from the original research group, specifically critical review, commentary or revision - including pre- or post-publication stages.	GCY, VAP

5.3 Publication: Young, G. C., *et al.* "Convolutional Neural Networks Predict Fish Abundance from Underlying Coral Reef Texture." *In prep.*

Pages 132–150 of this thesis include the publication as it was formatted for submission to a journal. This formatting choice is consistent with the University's Examination Regulations for Research Degrees in Biological Sciences (Plant Sciences and Zoology).

Convolutional Neural Networks Predict Fish Abundance from Underlying Coral Reef Texture

G. C. Young[1,2,3]*, V. Balntas[3], V. A. Prisacariu[3]

Last edited May 25, 2018

---

[1]Department of Zoology, University of Oxford, Oxford, OX1 3PS, UK

[2]Department of Engineering Science, University of Oxford, Oxford, OX1 3PJ

[3]Operation Wallacea, Old Bolingbroke, Spilsby, Lincolnshire, PE23 4EX, UK

*Corresponding author email <grace@robots.ox.ac.uk>

Abstract

Coral reefs are among the most biodiverse ecosystems on Earth in large part owing to their unique three-dimensional (3D) structure, which provides niches for a variety of species. Metrics of structural complexity have been shown to correlate with the abundance and diversity of fish and other marine organisms, but they are imperfect representations of a surface that can oversimplify key structural elements and bias discoveries. Moreover, they require researchers to make relatively uninformed guesses about the features and spatial scales relevant to species of interest. This paper introduces a machine-learning method for automating inferences about fish abundance from reef 3D models. It demonstrates the capacity of a convolutional neural network (ConvNet) to learn ecological patterns that are extremely subtle, if not invisible, to the human eye. It is the first time in the literature that no *a priori* assumptions are made about the bathymetry–fish relationship.

Keywords: neural networks, structural complexity, habitat complexity, habitat heterogeneity, fish, coral reef, machine learning, artificial intelligence, ecology

1 Introduction

Like forests, coral reefs have high structural complexity enabling them to maintain some of the greatest levels of biodiversity on Earth [1]. Reefs' unique three-dimensional (3D) structure provides organisms refuges from predators [2], places to spawn [3], surface areas for grazing [4], and niches with optimal light [5], sound [6], or hydrodynamic conditions [7]. Hard corals are the principal architect, but even dead corals or concrete blocks can harbour reef communities [8, 9].

Structural complexity can be measured with a variety of metrics [10], the majority of which significantly correlate with indicators of ecosystem health on land and sea [11, 12]. The most common metric in marine ecology is rugosity, the ratio of a chain's draped length to its fully extended length [13]. It is slowly being replaced with more sophisticated metrics from 3D models, however [14]. 3D models of reef can be created from sonar or LiDAR data [15], areal drone footage if the water is clear enough [16], or structure-from-motion (SfM) photogrammetry [17]. The relationship between fish and structure is of particular interest to not only marine ecologists, but also fisheries managers and conservationists trying to optimise yield or resilience [2, 18]. Terrain descriptors extracted from 3D models have been shown to correlate with fish abundance [19–23], as have more traditional structural complexity metrics [19, 24, 25].

While the basic ecological rationale for these correlations is clear, nuances in the relationship between structure and function are not so clear, and metrics leave much unanswered. They can oversimplify key structural elements [26], bias discoveries [27], and require researchers to make relatively uninformed guessed about which structural features and spatial scales will be relevant to species of interest [10, 19, 28]. Ideally the 3D model is not summarized into a metric, and instead is fed directly into the data analysis pipeline.

Machine-learning (ML) algorithms are a promising approach for this task because they can learn patterns from raw data without *a priori* information and are

not constrained by the assumptions of parametric statistics. Boosted regression trees (BRTs) from ML have successfully modelled bathymetry–fish relationships from variables derived from 3D models at spatial scales 2–300 m [29–31]. The BRTs can reveal variables' relative importance and are robust to extraneous variables, missing values, and interactions, but they still require a researcher to make decisions about which variables to extract from the data; *e.g.,* Costa et al. [31] choose six terrain variables (depth, depth standard deviation, curvature, distance to shelf edge, rugosity, and slope of slope) from their 3D models and measured each at five scales (2, 25, 50, 100, and 300 m). Convolutional neural networks (ConvNets), also known as deep networks, do not require any pre-existing assumptions about which descriptions of the data determine relationships. They can learn patterns (if present) from raw data through layers of linear and non-linear operations. The result is that the network can discover relationships more intricate than what even hundreds of multi-scale variables could predict. Already ConvNets have proven to be a powerful tool in marine ecology for automating image-identification tasks that otherwise require human experts, including annotating coral [32] and identifying polyp activity [33].

This papers introduces a method for learning ecological patterns that are extremely subtle, if not invisible, to the human eye. Our aim is not just to automate inference, but also to let artificial intelligence reveal ecological patterns. We demonstrate the capacity of a neural network to learn fish aggregation patterns from just 85 3D models of the reef. It is the first time in the literature that no *a priori* assumptions are made about the bathymetry–fish relationship.

2 Methods

2.1 Study Area and Data Collection

Data were collected from the south-west coast of the Caribbean island of Utila, Honduras (16.09°N, -86.91°W; GPS coordinates in WGS84 format) under a re-

search permit from the Instituto de Conservación Forestal (#ICF-DE-MP-080-2016). SCUBA divers 3D modelled 85 2 x 2 m patches ("quadrats") of reef 5 ± 2 m deep using underwater photogrammetry (following Young et al. [34]). Additionally, divers recorded the number of fish over each quadrat during a 10-minute fish survey, including 9 minutes spent observing at a distance of $\sim$1 m and 1 minute spent searching up-close for cryptobenthic fish (following Gratwicke and Speight [24]).

For analysis, fish data were binned into 2–8 classes of roughly equal proportions (Fig. 1). We started with the simplest division, low or high amounts of fish, and increased the granularity of classes to test how well the network could cope. We stopped at 8 classes because divisions started to loose ecological meaning (*e.g.,* 12–14 versus 14–16 fish). We formulated our problem as a classification rather than regression problem because ConvNets are generally more robust to classification problems [35].

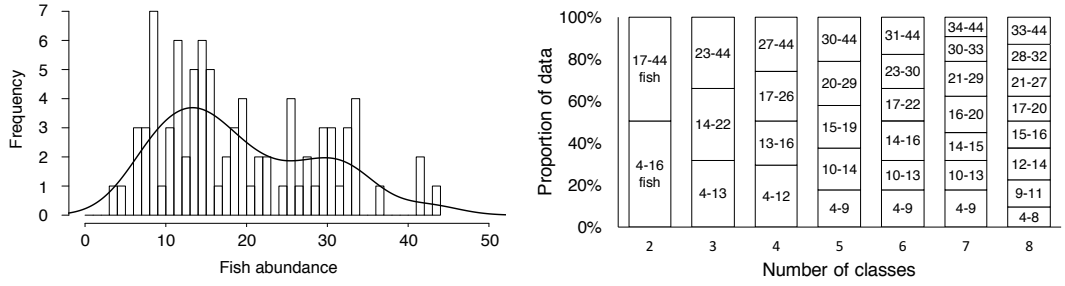

(a) (b)

Figure 1: Fish abundance data. (a) Distribution of fish data (N = 85, minimum = 4 fish, maximum = 44 fish) with Gaussian smoothing kernel density curve. (b) Division of data into classes of roughly equal proportions.

2.2 Conversion of 3D Models into 2D Images

We converted the 3D models into 2D images because ConvNets are presently better at dealing with images than 3D objects. To do so, a grid of points was projected downward onto the 3D model along the Z-axis (Fig. 2(a)–(b)). The grid was 189 x 189 cm rather than the theoretical maximum of 200 x 200 cm,

the size of the quadrat, so that it could consistently avoid the PVC-pipe that demarcated the edges of the quadrat. Grid points were spaced 1.50 cm apart in X and Y (Fig. 2(b)) because the original 3D models had root mean squared spatial accuracy to 1.48 cm in X and Y [34]. X and Y positions corresponded to pixel indexes in the 2D image, while Z positions corresponded to pixel values (Fig. 2(c)). A model's minimum Z-position was assigned a pixel value of 0, and an integer increment in pixel value represented a 1 cm increase in Z-position. Z-positions did not exceed 255 cm, meaning pixel values did not exceed 255 (Fig. 2(c)). The Python script that performed these steps worked with Rhinoceros 3D software ("Rhino"; Robert McNeel & Associates, Seattle, WA, USA) and is available open-source.[1]

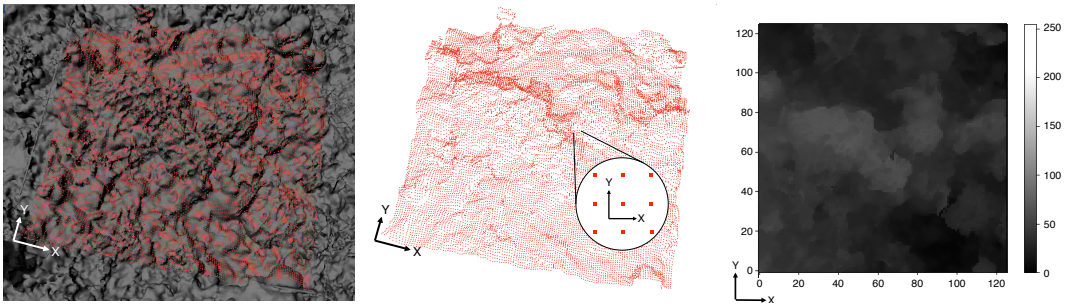

(a) 3D Model (b) Point Cloud (c) Image

Figure 2: Process for converting a 3D model into an image. The X-Y plane is parallel with the ocean surface and the Z-axis points upwards. (a) Points (in red) are projected along the Z-axis onto the uppermost points of the reef 3D model (in grey). (b) Points are extracted from the 3D model. Points cover a 189 x 189 cm grid and each is spaced 1.5 cm from its nearest neighbour. (c) The grid of points is represented as a 126 x 126 pixel greyscale image. Pixel values 0–255 represent Z-positions, each integer representing 1 cm.

The difference between 3D models that hosted high or low fish abundances is extremely subtle to the human eye, and even more so in the image representations (Fig. 3).

2.3 Neural Network Architecture

The 85 images were randomly sorted into a training set containing 60 images and a test set containing 25 images. Three image transformations augmented the

[1] www.github.com/gracecalvertyoung/Rhino-Python-Scripts-for-3D-to-2.5D-Conversion

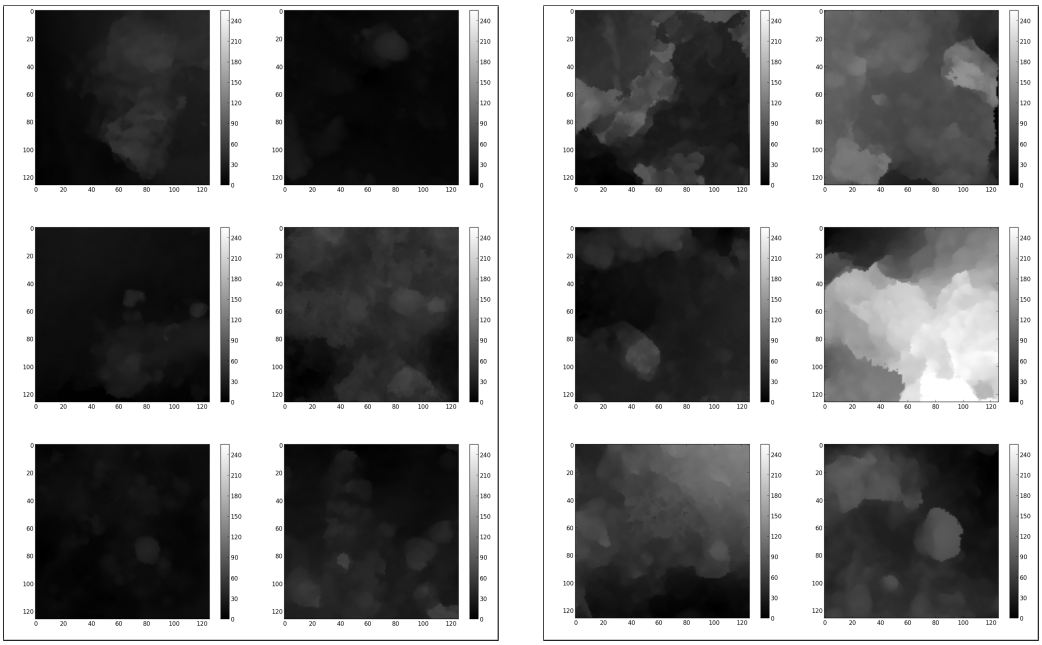

(a) Low fish abundance (b) High fish abundance

Figure 3: Six randomly selected images from (a) the class with the lowest fish abundance (4–8 fish), and (b) the class with the highest fish abundance (33-44 fish).

training dataset: (1) random cropping to 124 x 124 pixels, (2) center cropping to 124 x 124 pixels, and (3) random horizontal flips. These are standard practice in deep learning to increase models' robustness [36, 37]. The image reductions do not affect the validity of the associated fish data, as fish would have moved beyond the 3 x 189 cm cm cropped slivers of the quadrat during surveys. Moreover, this data augmentation is a common practice that improves model accuracy for small training sets [38].

We started with standard network architecture including AlexNet [37] and VGG-16 [39], but these were vastly over parametrised for our limited data set. We therefore implemented our own shallow neural network.

The network contained two layers (Fig. 4). Layer 1 composed of a 2D convolution with 8 channels and a 6x6 pixel kernel. Layer 2 also composed of a 2D convolution, but with 16 channels and a 4x4 pixel kernel. In both layers, the 2D convolution had 2 pixel padding and preceded a rectified linear unit (ReLU) and 2D max pooling with a kernel size of 2 pixels. The network trained using Cross-entropy loss [38] and optimized using the Adam algorithm [40]. The learning

rate was held constant at 0.001. An epoch is an iteration through the network of data that the network has already seen. For each epoch, a random mini-batch of 50 images from the training data fed through the network. The ConvNet was implemented in PyTorch [41].[2]

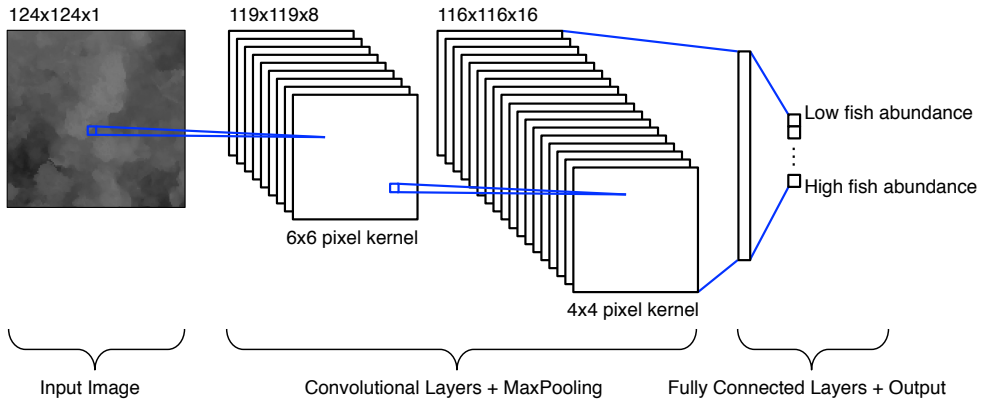

Figure 4: Convolutional neural network (ConvNet) architecture.

We also tested adding a third layer and batch normalization to the network, but they over-fit too quickly to the training set so the more lightweight network was best. We tried dividing the data 50/25/10 into training, validation, and test sets so that we could optimise hyper-parameters such as kernel size, but this only worsened over-fitting.

2.4 Assessment

The accuracy of the ConvNet ($A_{ConvNet}$) was the number of correctly classed images from the training set divided by the total number of images in the training set:

$$A_{ConvNet} = \frac{\#\text{Correctly classified images}}{\#\text{Total test images}} \quad (1)$$

It was compared to the accuracy of a "dumb classifier" (A_{wg}) that classified the test set by making random, weighted guesses based on the proportion of each class in the training set:

[2] www.github.com/gracecalvertyoung/ConvNet-for-Ecology

$$A_{wg} = \frac{1}{\#\text{Total test images}} \sum_{i=1}^{\#\text{ classes}} \left(\frac{\#\text{Training images from class } i}{\#\text{Total training images}} \right)^2 \quad (2)$$

For each number of classes, the data was re-shuffled three times into the training and test sets. The ConvNet was then evaluated once on each shuffling, so $A_{ConvNet}$ was computed three times for each number of class. This helped ensure that results were not determined by a "lucky" division of the data where patterns in the test set closely matched the training set. No parameters changed between evaluations.

2.5 Data & Code Availability

Data and code available on an open GitHub repository upon paper acceptance.

3 Results & Discussion

The ConvNet predicted the correct class of fish with a maximum accuracy of 68% (Table 1), and $A_{ConvNet}$ was consistently greater than A_{wg} for 2–7 classes (Fig. 5 shows $A_{ConvNet} - A_{wg}$). The discrepancy at 8 classes (Fig. 5) likely results from there being insufficient data to generalize trends, as there were only 5–10 images in the training set for each classification at the 8 class granularity. Alternatively, it could be an ecological threshold; *e.g.,* the difference between reef texture for two bins in the 8 class granularity is truly random. In this problem the upper threshold for attainable accuracy is likely considerably lower than 100% because numerous stochastic factors affect fish abundance [42].

Hundreds to thousands more training datum should improve network accuracy. In the coming years, it is indeed expected that there will be vastly more data available, as techniques for creating 3D reef models become evermore time and cost-effective and are adopted by researchers and citizen scientists alike [43]. The underwater 3D models could be generated from any method (*e.g.,* photogram-

Table 1: Accuracy of random weighted guess (A_{wg}) compared to the accuracy of the ConvNet ($A_{ConvNet}$). Averages are from three random shufflings of the data into the training and test sets. Results are reported from the 100-epoch mark, after which the network tended to overfit to the training set.

	Number of Classes						
	2	3	4	5	6	7	8
Average A_{wg}	47%	30%	23%	19%	15%	13%	11%
Average $A_{ConvNet}$	63%	40%	36%	28%	25%	17%	8%
Top A_{wg}	50%	34%	25%	20%	16%	15%	12%
Top $A_{ConvNet}$	68%	44%	44%	32%	28%	20%	12%

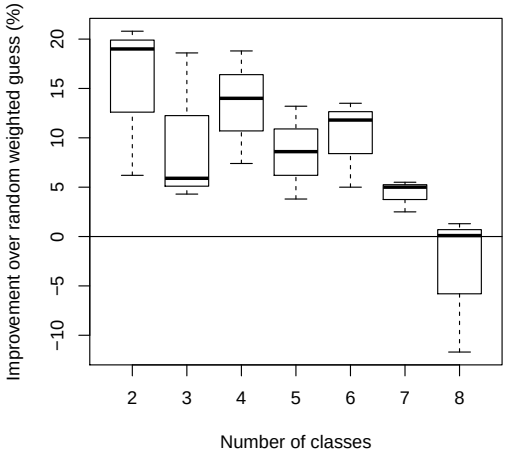

Figure 5: Increase in accuracy of the convolutional nural network (ConvNet) compared to the accuracy of a "dumb classifyer" that makes a random guess about each image in the test set based on the distribution of data in training set. For each number of classes, the ConvNet was tested on three random sortings of the data into the training and test sets.

metry, sonar, LiDAR) and still be applied to the ConvNet framework as long as they are in a standardized format. Additional descriptors could also augment the data, such as site information (if different between inputs) or scaling factors (if quadrats are different sizes); these could be incorporated following what Huang et al. [44] developed for adding text descriptors into their image classification problem. The caveat is that any extra parameters require even more training data [45]. Including the colours of points may also improve accuracy, especially if colour reliably corresponded to algae, coral cover, or other ecological features that help predict fish abundance. To do so, colour fidelity should be consistent across the data, which can be accomplished through modifications to the photogrammetry method [46].

Another way to improve accuracy may be to train the network on 3D rep-

resentations rather than images. A 3D model would contain features that are collapsed in the image representation, such as the canopy structures and crevices that provide creatures refuge. The irregular format of point clouds traditionally poses challenges for deep learning networks, but this hurdle can be overcome by voxel transformations or with more advanced networks [47, 48]. Again, however, training more network parameters requires more data. Additionally, benchmarking the neural network's accuracy against traditional metrics of reef structural complexity, such as rugosity, rather than weighted guesses may be more revealing.

Once it achieves considerable accuracy, this network could be used to validate artificial reef designs aiming to maximize fish abundance, predict hotspots that should be conservation priorities, or conduct a range of other science, conservation, and management tasks. The framework is versatile and could also learn other ecological patterns, from land or sea, that are not obvious to the human eye.

4 Conclusion

This paper has demonstrated that a neural network has the capacity to learn fish abundance patterns from raw representations of the underlying coral reef topography. The results are encouraging considering the small amount of samples used to train the network. The ConvNet achieved an accuracy of 68% from just 85 images, and this accuracy should improve with more data. Once extended with hundreds more data points, this method of learning patterns could reveal insights into how fish use structure and be a tool for making automated predictions of where fish will aggregate. Additionally, the versatile framework could learn other complex ecological patterns, from land or sea.

5 Acknowledgements

The Marshall Aid Commemoration Commission funded author GCY and Operation Wallacea funded and facilitated data collection.

6 Author Contributions

Conceptualization: GCY, VAP; Data curation: GCY; Formal analysis: GCY; Funding acquisition: GCY, VAP.; Methodology: GCY, VB, VAP; Project administration: VAP; Resources: VAP; Software: GCY, VB; Supervision: VAP; Validation: GCY, VB; Visualization: GCY; Writing – original draft: GCY; Writing – review & editing: GCY, VAP.

7 Competing Interests

The authors declare there are no competing interests.

References

[1] Andrew Scott Hoey, Shaun K Wilson, Morgan S Pratchett, Andrew S Hoey, and Shaun K Wilson. Reef degradation and the loss of critical ecosystem goods and services provided by coral reef fishes. *Current Opinion in Environmental Sustainability*, 7:37–43, 2014. ISSN 1877-3435. doi: 10.1016/j.cosust.2013.11.022.

[2] Alice Rogers, Julia L. Blanchard, and Peter J. Mumby. Vulnerability of coral reef fisheries to a loss of structural complexity. *Current Biology*, 24(9): 1000–1005, 2014. ISSN 09609822. doi: 10.1016/j.cub.2014.03.026.

[3] D. J. Coker, N. A J Graham, and M. S. Pratchett. Interactive effects of live coral and structural complexity on the recruitment of reef fishes. *Coral Reefs*, 31(4):919–927, 2012. ISSN 07224028. doi: 10.1007/s00338-012-0920-1.

[4] Adriana Vergés, Mathew A. Vanderklift, Christopher Doropoulos, and Glenn A. Hyndes. Spatial patterns in herbivory on a coral reef are influenced by structural complexity but not by algal traits. *PLoS ONE*, 6(2), 2011. ISSN 19326203. doi: 10.1371/journal.pone.0017115.

[5] David O Obura. Resilience and climate change: Lessons from coral reefs and bleaching in the Western Indian Ocean. *Estuarine, Coastal and Shelf Science*, 63(3):353–372, 2005. doi: 10.1016/j.ecss.2004.11.010.

[6] C. A. Radford, J. A. Stanley, S. D. Simpson, and A. G. Jeffs. Juvenile coral reef fish use sound to locate habitats. *Coral Reefs*, 30(2):295–305, 2011. ISSN 07224028. doi: 10.1007/s00338-010-0710-6.

[7] J. L. Johansen, D. R. Bellwood, and C. J. Fulton. Coral reef fishes exploit flow refuges in high-flow habitats. *Marine Ecology Progress Series*, 360:219–226, 2008. ISSN 01718630. doi: 10.3354/meps07482.

[8] B Gratwicke and Mr Speight. Effects of Habitat Complexity on Caribbean Marine Fish Assemblages. *Marine Ecology Progress Series*, 292:301–310, 2005. ISSN 0171-8630. doi: 10.3354/meps292301.

[9] Shaun K. Wilson, Nicholas A J Graham, Morgan S. Pratchett, Geoffrey P. Jones, and Nicholas V C Polunin. Multiple disturbances and the global degradation of coral reefs: Are reef fishes at risk or resilient? *Global Change Biology*, 12(11):2220–2234, 2006. ISSN 13541013. doi: 10.1111/j.1365-2486.2006.01252.x.

[10] Margaret F. J. Wilson, Brian O'Connell, Colin Brown, Janine C. Guinan, and Anthony J. Grehan. Multiscale Terrain Analysis of Multibeam Bathymetry Data for Habitat Mapping on the Continental Slope. *Marine Geodesy*, 30 (1-2):3–35, 2007. ISSN 0149-0419. doi: 10.1080/01490410701295962.

[11] J. Tews, U. Brose, V. Grimm, K. Tielbörger, M. C. Wichmann, M. Schwager, and F. Jeltsch. Animal species diversity driven by habitat heterogene-

ity/diversity: the importance of keystone structures. *Journal of Biogeography*, 31(1):79–92, 2004. ISSN 03050270. doi: 10.1046/j.0305-0270.2003.00994.x.

[12] N. A. J. Graham and K. L. Nash. The Importance of Structural Complexity in Coral Reef Ecosystems. *Coral Reefs*, 32:315–326, 2013. ISSN 07224028. doi: 10.1007/s00338-012-0984-y.

[13] E Luckhurst and K Luckhurst. Analysis of the Influence of Substrate Variables on Coral Reef Fish Communities. *Marine Biology*, 323(49):317–323, 1978.

[14] Curt D. Storlazzi, Peter Dartnell, Gerald A. Hatcher, and Ann E. Gibbs. End of the chain? Rugosity and fine-scale bathymetry from existing underwater digital imagery using structure-from-motion (SfM) technology. *Coral Reefs*, 2016. ISSN 0722-4028. doi: 10.1007/s00338-016-1462-8.

[15] B. M. Costa, T. A. Battista, and S. J. Pittman. Comparative evaluation of airborne LiDAR and ship-based multibeam SoNAR bathymetry and intensity for mapping coral reef ecosystems. *Remote Sensing of Environment*, 113(5): 1082–1100, 2009. ISSN 00344257. doi: 10.1016/j.rse.2009.01.015.

[16] Elisa Casella, Antoine Collin, Daniel Harris, Sebastian Ferse, Sonia Bejarano, Valeriano Parravicini, James L. Hench, and Alessio Rovere. Mapping coral reefs using consumer-grade drones and structure from motion photogrammetry techniques. *Coral Reefs*, 36(1), 2016. ISSN 07224028. doi: 10.1007/s00338-016-1522-0.

[17] Jhr Burns, D Delparte, Rd Gates, and M Takabayashi. Integrating Structure-from-Motion Photogrammetry with Geospatial Software as a Novel Technique for Quantifying 3D Ecological Characteristics of Coral Reefs. *PeerJ*, 3 (e1077), 2015. ISSN 2167-8359. doi: 10.7717/peerj.1077.

[18] Shaun K. Wilson, Russ C. Babcock, Rebecca Fisher, Thomas H. Holmes,

James A.Y. Moore, and Damian P. Thomson. Relative and combined effects of habitat and fishing on reef fish communities across a limited fishing gradient at Ningaloo. *Marine Environmental Research*, 81:1–11, 2012. ISSN 01411136. doi: 10.1016/j.marenvres.2012.08.002.

[19] Brian K. Walker, Lance K. B. Jordan, and Richard E. Spieler. Relationship of Reef Fish Assemblages and Topographic Complexity on Southeastern Florida Coral Reef Habitats. *Journal of Coastal Research*, 10053:39–48, 2009. ISSN 0749-0208. doi: 10.2112/SI53-005.1.

[20] Simon J. Pittman and Kerry A. Brown. Multi-Scale Approach for Predicting Fish Species Distributions across Coral Reef Seascapes. *PLoS ONE*, 6(5): e20583, 2011. ISSN 1932-6203. doi: 10.1371/journal.pone.0020583.

[21] Sonia Bejarano, Peter J. Mumby, and Ian Sotheran. Predicting structural complexity of reefs and fish abundance using acoustic remote sensing (RoxAnn). *Marine Biology*, 158(3):489–504, 2011. ISSN 00253162. doi: 10.1007/s00227-010-1575-5.

[22] Esteban A. Agudo-Adriani, Jose Cappelletto, Francoise Cavada-Blanco, and Aldo Croquer. Colony geometry and structural complexity of the endangered species Acropora cervicornis partly explains the structure of their associated fish assemblage. *PeerJ*, 4(e1861), 2016. ISSN 2167-8359. doi: 10.7717/peerj.1861.

[23] M. González-Rivero, A. R. Harborne, A. Herrera-Reveles, Y.-M. Bozec, A. Rogers, A. Friedman, A. Ganase, and O. Hoegh-Guldberg. Linking fishes to multiple metrics of coral reef structural complexity using three-dimensional technology. *Scientific Reports*, 7(1):13965, 2017. ISSN 2045-2322. doi: 10.1038/s41598-017-14272-5.

[24] Brian Gratwicke and Martin R. Speight. The Relationship Between Fish Species Richness, Abundance and Habitat Complexity in a Range of Shallow

Tropical Marine Habitats. *Journal of Fish Biology*, 66(3):650–667, 2005. ISSN 00221112. doi: 10.1111/j.1095-8649.2005.00629.x.

[25] Alastair R. Harborne, Peter J. Mumby, and Renata Ferrari. The effectiveness of different meso-scale rugosity metrics for predicting intra-habitat variation in coral-reef fish assemblages. *Environmental Biology of Fishes*, 94(2):431–442, 2012. ISSN 03781909. doi: 10.1007/s10641-011-9956-2.

[26] Christopher H R Goatley and David R Bellwood. The Roles of Dimensionality, Canopies and Complexity in Ecosystem Monitoring. *PLoS ONE*, 6(11), 2011. ISSN 1932-6203. doi: 10.1371/journal.pone.0027307.

[27] Jesús Aguirre-Gutiérrez, Luísa G. Carvalheiro, Chiara Polce, E. Emiel van Loon, Niels Raes, Menno Reemer, and Jacobus C. Biesmeijer. Fit-for-Purpose: Species Distribution Model Performance Depends on Evaluation Criteria - Dutch Hoverflies as a Case Study. *PLoS ONE*, 8(5), 2013. ISSN 19326203. doi: 10.1371/journal.pone.0063708.

[28] Kirsty L. Nash, Nicholas A.J. Graham, Shaun K. Wilson, and David R. Bellwood. Cross-scale Habitat Structure Drives Fish Body Size Distributions on Coral Reefs. *Ecosystems*, 16(3):478–490, 2013. ISSN 14329840. doi: 10.1007/s10021-012-9625-0.

[29] Simon J. Pittman, Bryan M. Costa, and Tim A. Battista. Using Lidar Bathymetry and Boosted Regression Trees to Predict the Diversity and Abundance of Fish and Corals. *Journal of Coastal Research*, 10053:27–38, 2009. ISSN 0749-0208. doi: 10.2112/SI53-004.1.

[30] Anders Knudby, Ellsworth LeDrew, and Alexander Brenning. Predictive mapping of reef fish species richness, diversity and biomass in Zanzibar using IKONOS imagery and machine-learning techniques. *Remote Sensing of Environment*, 114(6):1230–1241, 2010. ISSN 00344257. doi: 10.1016/j.rse.2010.01.007.

[31] Bryan Costa, J. Christopher Taylor, Laura Kracker, Tim Battista, and Simon Pittman. Mapping reef fish and the seascape: Using acoustics and spatial modeling to guide coastal management. *PLoS ONE*, 9(1), 2014. ISSN 19326203. doi: 10.1371/journal.pone.0085555.

[32] A. Mahmood, M. Bennamoun, S. An, F. Sohel, F. Boussaid, R. Hovey, G. Kendrick, and R. B. Fisher. Automatic annotation of coral reefs using deep learning. *OCEANS 2016 MTS/IEEE Monterey, OCE 2016*, 2016. doi: 10.1109/OCEANS.2016.7761105.

[33] Jonas Osterloff, Ingunn Nilssen, Johanna Järnegren, Pål Buhl-Mortensen, and Tim W. Nattkemper. Polyp activity estimation and monitoring for cold water corals with a deep learning approach. In *International Conference on Pattern Recognition 2nd Workshop on Computer Vision for Analysis of Underwater Imagery*, 2016. ISBN 9781509058709. doi: 10.1109/CVAUI.2016.14.

[34] G. C. Young, S. Dey, A. D. Rogers, and D. Exton. Cost and time-effective method for multi-scale measures of rugosity, fractal dimension, and vector dispersion from coral reef 3D models. *Plos One*, 12(4):e0175341, 2017. ISSN 1932-6203. doi: 10.1371/journal.pone.0175341.

[35] Vasileios Belagiannis, Christian Rupprecht, Gustavo Carneiro, and Nassir Navab. Robust optimization for deep regression. *Proceedings of the IEEE International Conference on Computer Vision*, 2015 Inter:2830–2838, 2015. ISSN 15505499. doi: 10.1109/ICCV.2015.324.

[36] Chiyuan Zhang, Samy Bengio, Moritz Hardt, Benjamin Recht, and Oriol Vinyals. Understanding deep learning requires rethinking generalization. *arXiv preprint arXiv:1611.03530*, 2017. ISSN 10414347. doi: 10.1109/TKDE.2015.2507132.

[37] Alex Krizhevsky, Ilya Sutskever, and Geoffrey E Hinton. ImageNet Clas-

sification with Deep Convolutional Neural Networks. *Advances In Neural Information Processing Systems*, 2012. ISSN 10495258. doi: http://dx.doi.org/10.1016/j.protcy.2014.09.007.

[38] Ian Goodfellow, Yoshua Bengio, and Aaron Courville. *Deep Learning*. MIT Press, Cambridge, MA, 2016. ISBN 978-0262035613.

[39] Karen Simonyan and Andrew Zisserman. Very Deep Convolutional Networks for Large-Scale Image Recognition. In *3rd International Conference on Learning Representations*, 2015. ISBN 0950-5849. doi: 10.1016/j.infsof.2008.09.005.

[40] Diederik P. Kingma and Jimmy Ba. Adam: A Method for Stochastic Optimization. In *3rd International Conference on Learning Representations (ICLR2015)*, 2015. ISBN 9781450300728. doi: http://doi.acm.org.ezproxy.lib.ucf.edu/10.1145/1830483.1830503.

[41] Gregory Chanan Adam Paszke, Sam Gross, Soumith Chintala. PyTorch, 2017.

[42] Steven P Newman, Erik H Meesters, Charlie S Dryden, Stacey M Williams, Cristina Sanchez, Peter J Mumby, and Nicholas V C Polunin. Reef Flattening Effects on Total Richness and Species Responses in the Caribbean. *Journal of Animal Ecology*, 84(6):1678–1689, 2015. doi: 10.1111/1365-2656.12429.

[43] Vincent Raoult, Peter A. David, Sally F. Dupont, Ciaran P. Mathewson, Samuel J. O'Neill, Nicholas N. Powell, and Jane E. Williamson. GoPros as an underwater photogrammetry tool for citizen science. *PeerJ*, 4:e1960, 2016. ISSN 2167-8359. doi: 10.7717/peerj.1960.

[44] Feiran Huang, Xiaoming Zhang, Zhoujun Li, Tao Mei, Yueying He, and Zhonghua Zhao. Learning Social Image Embedding with Deep Multimodal Attention Networks. In *Thematic Workshops, October 23–27, 2017, Moun-*

384 *tain View, CA, USA*, 2017. ISBN 9781450354165. doi: 10.1145/3126686.
385 3126720.

386 [45] Trevor Hastie, Robert Tibshirani, and Jerome Friedman. *The Elements of*
387 *Statistical Learning: Data Mining, Inference, and Prediction*. Springer, New
388 York City, second edition, 2009.

389 [46] M. Bryson, M. Johnson-Roberson, O. Pizarro, and S. B. Williams. Colour-
390 consistent structure-from-motion models using underwater imagery. In
391 *Robotics: Science and Systems VIII*, 2013.

392 [47] Gernot Riegler, Ali Osman Ulusoy, and Andreas Geiger. OctNet: Learning
393 Deep 3D Representations at High Resolutions. *arXiv preprint*, 2016. ISSN
394 1063-6919. doi: 10.1109/CVPR.2017.701.

395 [48] Yizhak Ben-Shabat, Michael Lindenbaum, and Anath Fischer. 3D Point
396 Cloud Classification and Segmentation using 3D Modified Fisher Vector Rep-
397 resentation for Convolutional Neural Networks. *arXiv preprint*, 2017.

We shape our buildings; thereafter they shape us.

— Winston Churchill

6 General Discussion

Contents

6.1 Key Findings & Implications 151
6.1.1 Method for 3D Modelling Coral Reefs 152
6.1.2 3D Models Tied to Ecological Data 152
6.1.3 Controlled Experiment 153
6.1.4 Machine Learning Trends 154
6.2 Broad Applications 155
6.2.1 Further Ecological Study 155
6.2.2 Reef Monitoring 155
6.2.3 Artificial Reef Design 157
6.2.4 Marine Archaeology 159
6.3 Limitations and Future Directions 161
6.3.1 Sizes and Resolutions of Underwater 3D Models 161
6.3.2 Overhangs, Underhangs, and Occluded Features 163
6.3.3 Quantification of Errors in Underwater 3D Models . . . 166
6.3.4 Controlling or Quantifying Slope 167
6.3.5 Colour Consistency 168
6.4 Concluding Remarks 169

6.1 Key Findings & Implications

This thesis has touched four lines of inquiry regarding the role of 3D structural complexity in a coral reef ecosystem. It designed a new technique for creating and analysing 3D models of underwater scenes (Chapter 2), showed how the 3D

models predicted fish populations in the Caribbean (Chapter 3), tested whether the structural complexity of 3D printed tiles affected epibenthic organism settlement after one year (Chapter 4), and, finally, applied methods from computer vision and machine learning to assess relationships between the 3D models and fish (Chapter 5). These four data chapters and their key findings are summarized in the following sections (6.1.1–6.1.4).

6.1.1 Method for 3D Modelling Coral Reefs

Chapter 2 presented a rigorously validated method for ecologists to non-invasively quantify coral reef 3D structural complexity with a variety of multi-scale metrics. The method is time and cost-effective; it requires only a single, uncalibrated consumer-grade camera and standard laptop. Resultant 3D models of 2 x 2 m patches of shallow reef were accurate to 1.48 cm in X-Y and 1.35 in Z (root mean square errors). The chapter also outlined the theory and rationale behind the multi-scale metrics of 3D structural complexity that are used in subsequent chapters, namely rugosity (R), fractal dimension (D), and vector dispersion ($1/k$). In terms of these metrics, the 3D models had accuracies of 86.8% (R), 99.6% (D at scales 30–60 cm), 93.6% (D at scales 1–5 cm), and 86.9 ($1/k$). 3D model-derived values of R were compared to *in-situ* chain-and-tape measurements of R, while 3D model-derived values of D and $1/k$ were compared to ground truths from 3D printed objects. All metrics varied less than 3% between independently rendered models. The chapter therefore quantified the precision and accuracy of the 3D modelling method.

All subsequent data chapters of this thesis (Chapters 3–5) used the method presented in Chapter 2 to create and analyse reef 3D models. Since summer 2017, researchers in Indonesia, Madagascar, Cuba, Honduras, Bonaire, and the Maldives have also used the method to create and analyse 3D models of coral reefs.

6.1.2 3D Models Tied to Ecological Data

Chapter 3 described an application of the method presented in Chapter 2. It was essentially a replication of Gratwicke and Speight (2005b), the seminal study that

showed how Habitat Assessment Score (HAS) could predict fish species richness and abundance in the Caribbean, except that we measured habitat complexity automatically from the 3D models, rather than from divers' recorded HAS. We conducted the fish surveys the same way as Gratwicke and Speight (2005b) over 2.0 x 2.0 m quadrats (whereas Gratwicke and Speight (2005b) used 2.5 x 2.5 m quadrats). For each quadrat, divers recorded the species of fish within the 2.0 x 2.0 x 2.0 m space over the quadrat. The 3D models automatically returned rugosity (from 1.75 m long virtual chains of link length 2 cm), fractal dimension (at fives scales 1–120 cm), and vector dispersion (at 1 cm scale). Of the seven 3D metrics, we wanted to establish the best predictor or best combination of predictors, much like how Gratwicke and Speight (2005b) combined several features into one easy-to-regress variable (HAS). R was the best predictor of fish variables, followed by $1/k$. D measured between 15–30 cm and 5–15 cm also correlated with fish variables, but D measured at other scales 1–120 cm did not. The 3D metrics had the same predictive power for fish abundance and Shannon diversity as chain-and-tape rugosity or HAS. Although their predictive powers are the same, we recommend researchers employ 3D modelling instead of chain-and-tape measurements or HAS because they can non-destructively produce a variety of 3D metrics at numerous spatial scales and keep a permanent record of reef structure over time.

6.1.3 Controlled Experiment

Chapter 4 described a controlled experiment that tested the role of structural complexity measured in terms of vector dispersion ($1/k$; Chapter 2) upon sessile epibenthic organism settlement after one year. Contrary to expectation, we found that $1/k$ affected only algae settlement, and not coral spat, sponge, polychaete, or bryozoan settlement. This finding went against the trend reported by Carleton and Sammarco (1987) in their 1986 study on the Great Barrier Reef, Australia. Chapter 4 highlighted nuances to structural complexity's role in early organism settlement that are not well captured by $1/k$. It also added quantitative evidence to the debate over whether an artificial reef (AR) should resemble a natural reef

or an artificial shape to effectively promote coral spat settlement: *e.g.,* should an AR be sculpted or 3D printed to match the undulations of a natural reef, or could it be made from breeze blocks or other existing concrete shapes and produce similar ecological outcomes? Older studies on ARs decisively concluded that the best way for an AR to cultivate a marine community mimicking a natural reef or to mitigate natural reef degradation is for the AR to possesses structural features similar to those of the natural surroundings (Perkol-Finkel et al., 2006), or for the AR to be as structurally similar as possible to natural reefs (Carr and Hixon, 1997). These qualitative descriptions of structural complexity are difficult to quantify, in part because quantitative metrics, such as the plethora reviewed in Chapter 1, are mathematics-based and therefore slightly abstracted from the underlying ecological theory. 3D metrics are now easier to compute and control, however, thanks to advances in 3D modelling technology and 3D printing in the last decade. The broad applications of this research in AR design are further discussed in section 6.2.3.

6.1.4 Machine Learning Trends

Chapter 5 forwent the 3D metrics used in previous chapters. Instead, the whole 3D model, or rather an image representation of the 3D model, was fed into a machine learning algorithm. The algorithm learned a pattern between the 85 3D models (represented as images) and fish abundance data from Chapter 3. The algorithm predicted how many fish would be on the reef represented by an input image consistently better than random. This is a promising result given the extremely limited data set. With hundreds to thousands of more data points, the prediction is expected to vastly improve. The improved algorithm could be used to compare proposed designs for an artificial reef. Additionally, given a large series of quadrats, it could predict which quadrats would have the highest fish abundance and thereby inform decisions about which representative areas should be conservation priorities.

6.2 Broad Applications

The research presented in this thesis has broad applications in marine ecology, reef monitoring (restoration and management), artificial reef design, and marine archaeology. The following sections (6.2.1–6.2.4) discuss how the research relates to broader themes.

6.2.1 Further Ecological Study

The photogrammetric 3D modelling methods presented in this thesis have enabled researchers to answer new questions about how marine organisms live with and rely on structural complexity. For example, one study is looking at how 3D complexity might be responsible for urchins (*Diadema antillarum*) recovering from disease in some parts of the Caribbean, but not others (M. Bodmer et al., *in prep.*). Another study is testing how 3D complexity might be a driver behind lionfish (*Pterois*) aggregations in the Caribbean (C. Hunt et al., *in prep.*). These lines of study would have been very difficult without the 3D modelling methods.

6.2.2 Reef Monitoring

3D models of coral reefs can improve or augment reef monitoring programs in a number of ways. Firstly, unlike some monitoring tools, the 3D models are non-destructive, relativity inexpensive, able to preserve structure over time, able to produce a range of metrics automatically (Chapter 2), and unbiased between observers (Raoult et al., 2017). Moreover, chapter 3 showed how the 3D models were as good predictors of fish metrics as the more traditional measures of chain-and-tape rugosity or the Habitat Assessment Score (HAS). Secondly, the 3D models can produce a range of measurements beyond structural complexity. They can be used, for example, to calculate the proportional surface area or volume of live coral cover (Fig. 6.1(a)), specific colonies (Fig. 6.1(b)), or disease. Because the software and tools are versatile and user-friendly, managers can customise them to their needs (Appendix C). Thirdly, the methods are time and cost effective; researchers can gain more data on a single 1 hour dive than from traditional survey techniques (*e.g.,*

chain-and-tape rugosity or visual surveys). This keeps costs down for researchers and/or allows more data to be collected with in a limited time frame.

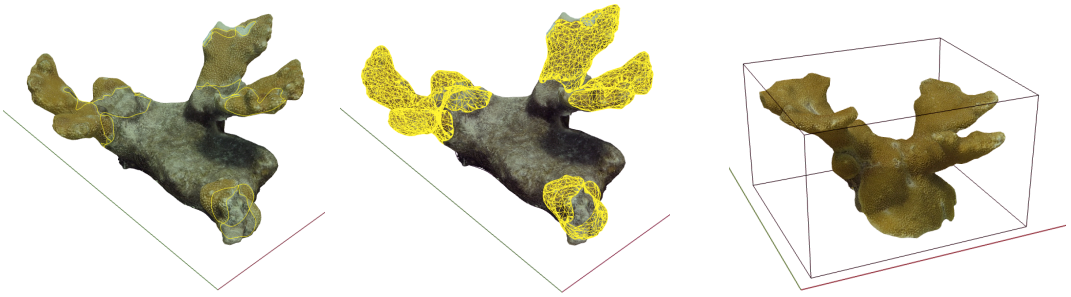

(a) (b)

Figure 6.1: Examples of reef monitoring applications. (a) Percentage of live coral tissue calculated by manually outlining areas and extracting the meshes with the build-in the command "SplitMeshWithCurve" in Rhinoceros 3D, the software used in Chapter 2. (b) The built-in command "BoundingBox" in Rhinoceros 3D automatically creates a rectilinear box around the selected object. Measures of maximum height, length and width can be extracted from the box. The 3D models in (a)–(b) were rendered from underwater footage of elkhorn coral from Bonaire National Marine Park following Chapter 2; they have millimetre precision and accuracy in terms of surface area and volume. Each coral's maximum dimensions are approximately 10 x 20 x 20 cm. Source: Julia Huisman with permission/Appendix C.

Additionally, the 3D models can be a way for people to engage with the reef even if they never dive. Conservation institutions can 3D print miniature versions of the 3D models of their reef to show to visitors. They can also show 3D models through virtual reality headsets. These means of engagement have the potential to affect the minds and decisions of managers, donors, and others who use the reef directly or indirectly.

Incorporating 3D modelling and analysis into monitoring programs could help, for example, (a) gauge the effectiveness of a marine protected area by showing visual and quantitative changes over time or with protection (*e.g.,* Burns et al. (2016)), (b) identify priority conservation regions by identifying regions of high or low complexity (*e.g.,* Agudo-Adriani et al. (2016)), or (c) track chronological growth of transplanted coral in response to independent variables (Appendix C).

6.2.3 Artificial Reef Design

An artificial reef (AR) is a submerged structure placed on the seabed deliberately to mimic some characteristics of a natural reef (Baine, 2001). Humans have created ARs for centuries, primarily to enhance fisheries yield and, more recently to help restore reefs, enhance recreational diving, prevent trawling, and/or avoid coastal erosion. They are becoming evermore important as we try to compensate for the worldwide degradation of reefs and their ecosystem services (Rogers et al., 2015; Agudo-Adriani et al., 2016).

All chapters of this thesis have possible implications for AR design in that they discuss reef structural complexity, a key feature of a healthy reef ecosystem (Chapter 1). If we understand how and why natural reefs are able to provide the ecosystem functions they do, then we can design better artificial reefs. In Chapter 3, we measured the structural complexity of randomly selected patches of reef around the Caribbean island of Utila. We found that in general the higher the 3D metrics, the higher the fish abundance and diversity. Correlations do not imply causations, however, and so Chapter 3 could answer the follow-on question that pertains to AR design: *If a surface hit the extremes of one or all of the structural complexity metrics of Chapter 3, would it necessarily have higher fish abundance and/or diversity?* This question must be answered through controlled experimentation. Several studies have run experiments along these lines (*e.g.,* Gratwicke and Speight (2005a)), although not using the structural complexity metrics of Chapter 3. We precisely controlled one of the metrics (*1/k*) in Chapter 4 by designing surfaces that could be 3D printed. Instead of fish we focused on a much smaller animal, juvenile corals or coral spat. Coral spat are thought to be affected by centimetre-scale surface complexity (Carleton and Sammarco, 1987; Edmunds et al., 2014; Whalan et al., 2015). While Chapter 4 did not find that coral spat settled differently upon surfaces with contrasting values of *1/k* at the 1 cm scale after one year, it did find that *1/k* at the 1 cm scale affected algae settlement after one year. This finding suggests that an AR wanting to minimise algae settlement should choose surfaces with lower *1/k*.

It also reiterates that availability of sheltered area increases coral spat settlement, a discovery made by Edmunds et al. (2014) among others.

Chapter 4 discussed applications of the research towards AR design, specifically regarding how to use structural complexity to optimise coral spat settlement after one year. We suggest future studies that further probe the cause-and-effect nature of structural complexity on coral reefs employ a similar structural complexity metric. That metric might not be $1/k$, but it should be one that satisfies our rationale for choosing to control $1/k$, namely:

(a) It is quantitative. Several studies use qualitative metrics that cannot be controlled in an experiment or compared across sites or times. Chapter 4 specifically addresses how several studies vaguely conclude that "natural" shapes best enable an AR to mimic an adjacent natural reef, but cannot precisely define "natural." Describing shapes quantitatively is more challenging because there is not a standard metric and mathematics can abstract metrics' ecological meanings (Chapter 1.3). There are nonetheless several multi-scale metrics available for describing shapes (Chapter 1.3).

(b) It has demonstrated ecological meaning to the organism of interest; *e.g.,* $1/k$ had been shown to correlate positively and tightly (more so than other metrics) with coral spat settlement after several months.

(c) It is measured on continuous scale (not just "high" or "low"), and therefore it is possible for artificial surfaces to reach the extremes.

The metrics presented in Chapter 1.3 and 2 offer a starting point for further studies using quantitative metrics of structural complexity. These will help standardize comparisons between AR studies and develop means of predicting and optimising AR effects.

6.2.4 Marine Archaeology

The technologies involved in 3D modelling underwater scenes are largely the same for applications in coral reef ecology or marine archaeology. That said, a marine archaeologist likely has different size, resolution, time, and budget requirements for their 3D modelling endeavours than a coral reef ecologist. For example, a marine archaeologist may be willing to spend hundreds of hours diving the site to capture high-quality footage and wait for optimal lighting and visibility conditions so that their 3D model of a shipwreck has near millimetre accuracy, enough to read engravings on plaques. The archaeology team may then be willing to spend hours artistically reconstructing portions of the 3D model shipwreck based on historical information. As the shipwreck would only be 3D modelled once, the team may choose to rent a week on a supercomputer to render the model. A marine ecologist, on the other hand, may wish to capture month-by-month changes in underwater structures, and is willing to trade up to centimetre resolution because most of the fish and other organisms of interest are well above the centimetre scale. The marine ecologist may wish to sample several, small portions of a reef spanning great distance underwater. At a remote location, they may not rely upon cloud-based supercomputing services and instead choose to distribute computing between volunteers' laptops. Meeting the functional requirements of these scenarios for the marine archaeologist and ecologist would require different customizations of the 3D modelling pipeline presented in Chapter 2, but the solutions could rely upon the same underlying technology (namely PhotoScan and/or Rhinoceros 3D).

Archaeologists could use their 3D models, derived via the method described in Chapter 2 or any other method, for applications beyond those presented and discussed in Chapters 3–5. Drap (2012) and Drap et al. (2015) discuss these and other applications in more detail, including:

(a) artistically reconstructing buried or fragmented artifacts as in Fig. 6.2 (Drap et al., 2015),

(b) arranging displaced cargo to help inform hull shape as in Fig. 6.3 (Beltrame et al., 2016)),

(c) showing submerged sites to researchers, museum guests, and donors through virtual-tours or 3D printed models (Scopigno et al., 2011),

(d) preserving site information without removing objects (Drap et al., 2015),

(e) printing fragments to fix artifacts (Arbace et al., 2013),

(f) measuring precisely dimensions, volumes, and surface areas of artifacts without removing them from the water or requiring excessive dive time (Drap et al., 2015),

(g) identifying shipwrecks as anomalous structures over large-area (*e.g.,* kilometer-wide swaths) of seabed (Ballard et al., 2002), or

(h) printing reconstructed artifacts (Scopigno et al., 2011).

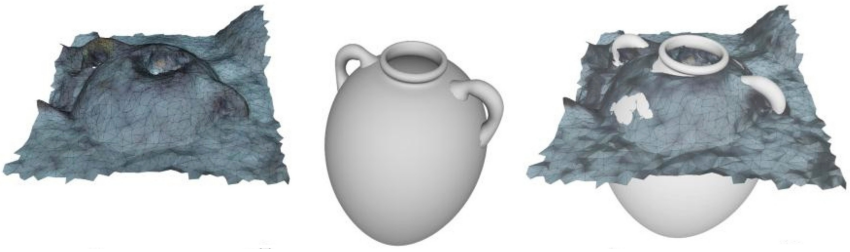

Figure 6.2: Example of photogrammetric 3D modelling used to reconstruct partially buried amphora on a shipwreck. The 3D model was rendered in Agisoft PhotoScan, similar to the method in Chapters 2–3 except that the cameras were mounted on a submarine and artificial lights illuminated the scene, which was 110 m deep. Source: Drap et al. (2015) available through Creative Commons Attribution License (CC BY 4.0).

Synergy between marine ecology and archaeology researchers in regards to underwater 3D modelling technology and practices could yield fruitful discoveries. It is also possible to consider a shipwreck as an artificial reef and compare it to neighbouring artificial reefs, as did Perkol-Finkel et al. (2006). 3D models in such a study could assess how the shipwreck/artificial reef shape affected marine community structures.

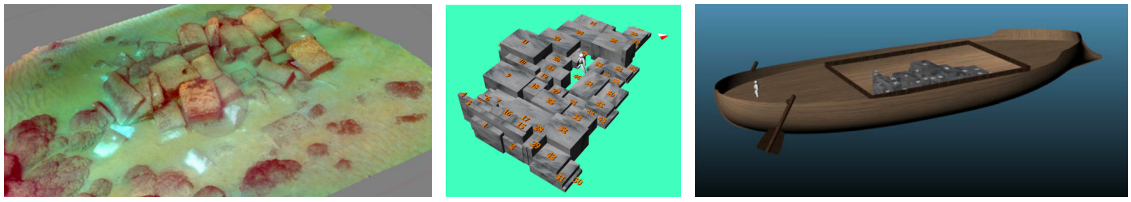

(a) (b) (c)

Figure 6.3: Examples of photogrammetric 3D modelling used to reconstruct cargo arrangment and hull shape from a shipwreck. (a) 3D model of shipwreck remains (marble cargo) rendered with Agisoft PhotoScan under ambient light at a site 6.5–7.0 m deep, very similar to the conditions in Chapters 2–3. From this 3D model, archaeologists can estimate dimensions and weights of the cargo. (b) The 3D modelled cargo manually re-arranged as it may have been inside the original ship hull, a cumbersome task without the 3D model. (c) Tentative reconstruction of the ship hull based on the 3D configuration of marble cargo. Source: Beltrame et al. (2016) with permission.

6.3 Limitations and Future Directions

3D modelling has proven to be a useful tool in coral reef ecology for structural complexity analysis (Chapters 1–5 & 6.2.1). It is also a useful tool for reef monitoring (6.2.2), restoration (6.2.3), and marine archaeology (6.2.4). That said, there are several limitations to the method that warrant further discussion. These limitations and their possible remedies are discussed below, along with future research directions.

6.3.1 Sizes and Resolutions of Underwater 3D Models

The 3D models created and analysed for this thesis were 2 x 2 m. While this is a relativity small size on the scale of reefs (which can be kilometres by kilometres), it means that each quadrat can be rendered and analysed discreetly on a standard laptop (Chapter 2). Many quadrats can be modelled on a dive site, so in total a sizeable amount of reef can be sampled (*e.g.,* 340 m^2 for Chapter 3). The "lawnmower" filming pattern presented in Chapter 2 does not scale well to larger reef areas, however (Pizarro et al., 2017).

To 3D model larger areas underwater (up to ≈113 m^2), Pizarro et al. (2017) suggest a very similar method to Chapter 2, except that divers film in a spiral pattern by winding a taught string around a central post. Pizarro et al. (2017) showed how this spiral swimming patten could produce 3D models with 12 m

diameter. Such models could straightforwardly be input into the analysis programs for *R, 1/k,* and *D* presented in Chapter 3 by changing the grid of points from a square to circular; no other modifications to the code or protocol would be needed. Another approach for creating models on a similar scale is for divers to lay down a "topographical net" underwater as described by Beltrame and Costa (2017) for 3D modelling marine archaeological sites. In Agisoft PhotoScan, a user can manually align the points on the net. Alternatively, if coded targets are present (Fig. 6.4), PhotoScan can automatically identify the points (Agisoft LLC, 2017, p. 51). In order to work reliably underwater, the targets must have a matte finish and be firmly secured so they that they do not move during filming (Yamafune et al., 2017). Our research team from the University of Oxford placed laminated targets underwater on quadrat corners in the Chagos Archipelago, but they did not render well because the laminations were too shiny and moved too much with the currents (limitations discussed in Chapter 2 and 6.3).

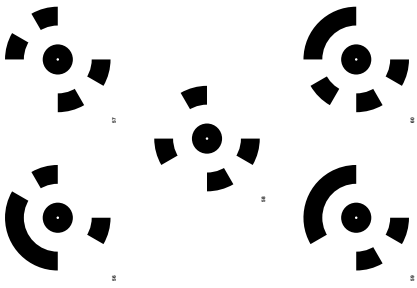

Figure 6.4: Example of five coded targets. If present in the imagery used for photogrammetry, PhotoScan can automatically identify the center of the target. Source: Agisoft PhotoScan.

To 3D model even larger areas underwater (hundreds of m^2 to km^2) with photogrammetry, the imagery should be co-registered with other position information, so the method becomes more technologically complex than that presented in Chapter 2. Sonar, LiDAR, or satellite data, perhaps augmented with photogrammetry, are likely better suited to the task of 3D modelling reefs at this scale (Chapter 1.4). Several papers propose methodologies that combine photogrammetry with

navigation and altitude information from underwater vehicles or diver-held stereo-vision cameras (*e.g.,* Pizarro et al. (2009); Johnson-Roberson et al. (2010); González-Rivero et al. (2017)). These all require a means of acquiring the camera's geo-referenced pose estimates underwater (*e.g.,* through Simultaneous Localisation and Mapping (SLAM)), which requires extensive computing power.

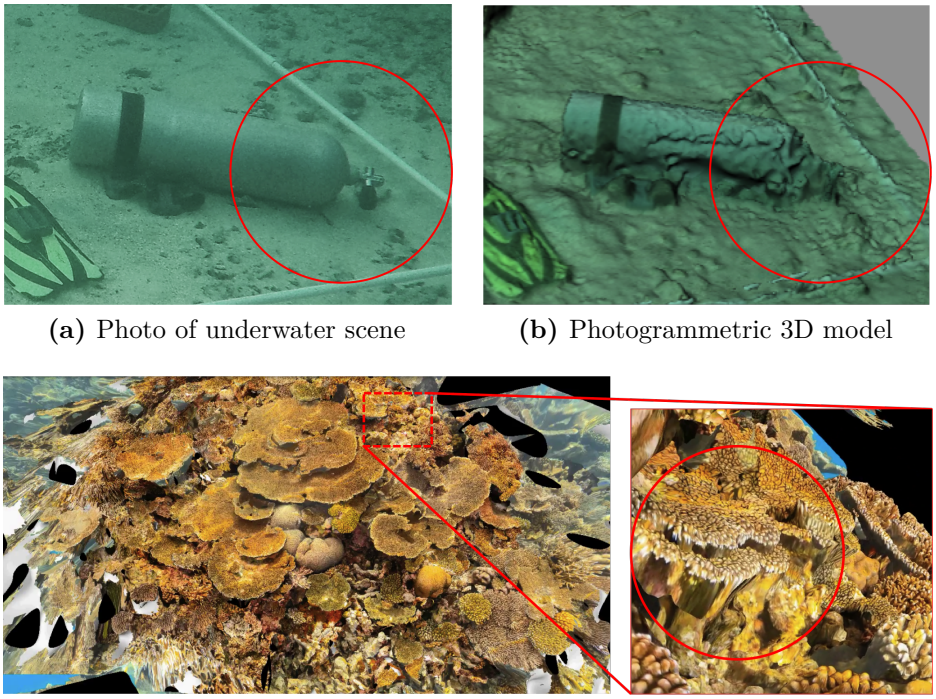

(a) Photo of underwater scene **(b)** Photogrammetric 3D model

(c) Photogrammetric 3D model

Figure 6.5: Examples of the limitations in capturing 3D structure underneath canopy structures. (a) SCUBA tank 3D modelled underwater (Chapter 2). (b) The neck of the tank appears connected to the seabed. Note that the tank did not render particularly well because it is reflective. Matte features rendered more realistically (*e.g.,* the the black band on the tank and the fin in the lower-left). (c) Photogrammetric 3D model of Hawaiian coral reef. Zoomed portion shows the ill-defined underneath of the tabular coral. Source (a)–(b): Author G. Young. Source (c): The Hydrous with permission.

6.3.2 Overhangs, Underhangs, and Occluded Features

Terrain reconstructions from downward-looking cameras (bird's eye view) do not generally capture the structure of occluded features, such as the underside of a tabular coral or canopy structure (Fig. 6.5; Friedman et al. (2012)). Moving the camera around the structure so that it captures more angles can help render

otherwise occluded features (Fig. 6.6; Appendix C and Friedman et al. (2012)). In practice this does not consistently work well underwater, however, unless the water is ultra-clear (personal observation). This is likely because the side-view images include an extended view of the water column and the moving particulate matter that it contains, which interfere with the photogrammetry algorithm (Chapter 2). Placing a mono-coloured background that blocked the extended view of the water column might help remedy the problem, although this has yet to be been tested. It is possible to mask the water column out of photos, but this is a manually intensive process (Agisoft LLC, 2017, p. 60–64). Future iterations of the PhotoScan or other photogrammetry software may be better able to automatically mask underwater images.

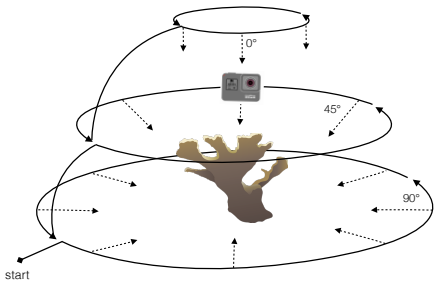

Figure 6.6: In-water filming method for the elkhorn coral *Acropora palmata* with GoPro camera. Source: Julia Huisman with permission/Appendix C.

For similar reasons, complex branching structures do not render well from photogrammetry, even in air (Fig. 6.7). This problem cannot be solved by masking images, however, and is more likely a fundamental limitation of photogrammetry (personal observation). Branches cast shadows on each other even in diffuse light and occlude features as the camera moves, which interferes with the photogrammetry algorithm (Chapter 2). The effect is that individual branches are ill-defined in the 3D model, and instead the dense branches meld together in a cauliflower-like shape (Fig. 6.7). In practice, for example, Elkhorn corals (*Acropora palmata*; Fig. 6.8(a)) will model well, but Staghorn coral (*Acropora cervicornis*; Fig. 6.8(b)) will not (Appendix C). The photo overlay can be misleading on models with dense branches because photo texture may show the branches photorealistically, but the underlying

3D mesh will not contain defined branches (Fig. 6.7(a)–(b)). If a study needs 3D representations of dense branching structures, light scanning (*e.g.,* as in Reichert et al. (2017)) is a more appropriate method than photogrammetry (Teza et al., 2016).

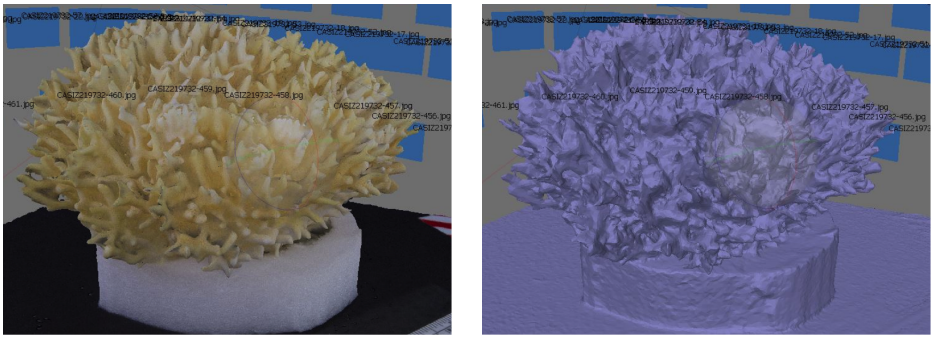

(a) 3D model with photo texture **(b)** 3D model without photo texture

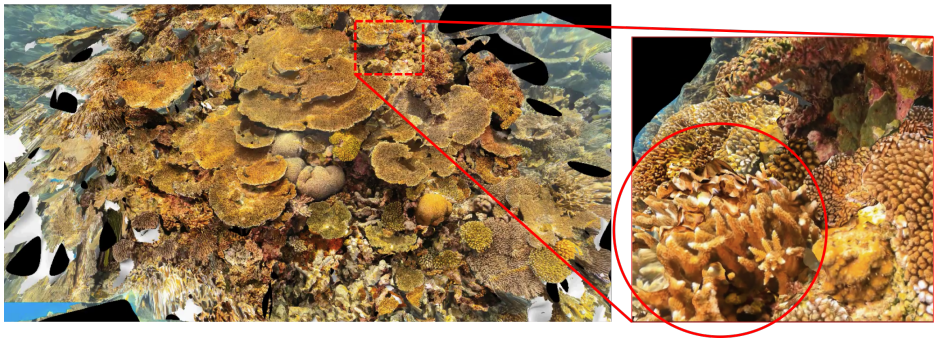

(c) Photogrammetric 3D model

Figure 6.7: Examples of how photogrammetry cannot well capture complex 3D branching structures (the "cauliflower effect"). (a) Photogrammetric 3D model of branching coral with photo-texture overlay. (b) 3D model without the photo-texture overlay, showing how the underlying 3D shape does not capture spatial of definition individual coral branches. (c) Photogrammetric 3D model of Hawaiian coral reef. Zoomed portion shows how coral branches are ill-defined individually. Sources (a)–(c): The Hydrous with permission.

These occluded features can have significant ecological importance by increasing surface area and providing shelter or refuge to organisms of different sizes (Halford et al., 2004; Goatley and Bellwood, 2011). Additionally, the occluded features could be important in algorithms that aim to automatically identify corals by their 3D structure. Further research is needed to engineer solutions to this problem and/or know how to correct for errors. The method presented in Chapter 2 avoided errors resulting from canopy effects because all analysis metrics were computed from a grid of points draped onto the uppermost points of the 3D model (replicating

a profile gauge), so canopy structures never factored into measurements. If our survey was to focus on parts of the 3D model under canopy structures, then the measurement errors should not only be quantified in terms of X, Y, and Z, but also in terms of Z-under canopy and Z-over canopy. It would be expected that accuracy of Z-under canopy would be less than Z-over canopy.

(a) *Acropora palmata* **(b)** *Acropora cervicornis*

Figure 6.8: Corals shapes that illustrate the borderline cases in photogrammetry's ability to 3D model branching structures. Elkhorn corals (*Acropora palmata*) will model well, but Staghorn coral (*Acropora cervicornis*) will not; individual branches will appear joined together (Appendix C). Source (a): Florida Fish and Wildlife Conservation Commission/Creative Commons licence (CC BY-NC-ND 2.0). Source (b): Albert Kok at Dutch Wikipedia/public domain.

6.3.3 Quantification of Errors in Underwater 3D Models

In Chapter 3 we knew that the errors of the 3D models were the same as those in Chapter 2 because the method, study site, and depth were exactly the same. If any part of the method, study site, or depth (and therefore lighting conditions) had changed, however, then we should have determined the spatial resolution of the 3D models by comparing them to ground truths (as in Chapter 2). Changes in environmental conditions (lighting and water quality) can bias model quality. Bryson et al. (2017) found that changes in environmental conditions caused up to 7.5% variation in model surface rugosity. Casella et al. (2016) noted that conditions of calm water, low winds, and minimal sun glint were ideal for using photogrammetry to 3D model a shallow coral reef from consumer-grade aerial drone footage. Measurement errors also tend to increase with structural complexity (Bryson et al., 2017), so these effects should be quantified for the range

of complexities a study is expected to encounter. For example, Figueira et al. (2015) found that the coefficient of variation between measurements of surface rugosity jumped from 1% to 10% between massive corals (low complexity) and bottlebrush corals (high complexity).

There should be a streamlined approach for routinely determining the precision and accuracy of measurements from underwater photogrammetric 3D models. For example, this could be a 3D version of a printer test sheet for underwater models. The "test shape" should include canopy structures, low complexity structures (*e.g.,* massive coral-like), and high complexity structures (*e.g.,* mimicking bottlebrush coral-like) to account for the effects observed by Friedman et al. (2012); Figueira et al. (2015); Bryson et al. (2017).

6.3.4 Controlling or Quantifying Slope

The slope of a reef significantly affects marine communities, as it controls how regions face the light and how sediment and other particulate matter roll or settle on the surface (Wilson et al., 2007a). The slope also affects measurements of all of the 3D metrics, including *R, D,* and *1/k* (Chapter 2). It should therefore be accounted for in the 3D model of a reef. In Chapter 3 we did not need to adjust the slopes of our 3D models because our dive sites were fairly flat, and we placed quadrats such that they were approximately parallel to the ocean surface. We were therefore justified in placing three corners of a quadrat flat on the X-Y-plane. That said, for future studies wishing to incorporate slope, there are two options:

1. When post-processing the photogrammetric 3D model in Rhinoceros 3D, instead of placing three corners of a quadrat on flat on the X-Y-plane, place the corners at the angles they were underwater. Divers could record these angles underwater by recording the depths of three corners or by estimating quadrat angle on a protractor with a float towards the surface serving as the vertical reference. For Chapter 2, we tried 3D modelling a quadrat with a float tied in the corner indicating vertical. The float did not consistently render

well in the 3D model, however, because it moved with the current and the photogrammetry can only render static objects (Chapter 2).

2. Use metrics of 3D structural complexity that are decoupled from slope. Friedman et al. (2012), for example, describe a means of calculating a variant of rugosity based on projections onto the plane of best fit (rather than flat-plane area).

Mapping steep slopes creates additional problems with photogrammetry because lighting can change dramatically over the scale of a few meters (personal observation). Other underwater 3D mapping techniques, besides photogrammetry, also often cannot adequately replicate the 3D structure of vertical surfaces because they are restricted to down-looking sensors (Robert et al., 2017). As a result, ecologists have missed valuable information on vertical surfaces, which can harbour high biodiversity and provide natural protection from bottom-trawling activities (Robert et al., 2017). Robert et al. (2017) successfully created 3D models of vertical walls by combining sideways and forward-looking multibeam echosounder data (mentioned in Chapter 1) with videos from underwater vehicles. To my knowledge, there is no method for 3D mapping steep vertical surfaces underwater with diver-held cameras or in situations where echosounders and underwater vehicles are not an option (because of budget, depth, location constraints, *etc.*). It may be possible by applying a similar method as in Chapter 2, but with artificial, diffuse lighting to correct for natural lighting variations along the depth gradient. At present, this is another limitation of underwater photogrammetry that warrants an engineered solution and at the very least should be accounted for when analysing sites with steep verticals underwater.

6.3.5 Colour Consistency

Colour in the 3D models may be another possible means of assessing reef health. Visual inspection of several 3D models revealed that quadrats varied greatly in color, mostly in blues and greens, unrelated to what they contained (personal observation). The water column imposes several effects on images that are negligible in air, such

as colour-dependent attenuation and lighting patterns (Bryson et al., 2013). If color is to be used in measurements on a 3D model, a ground-truth color scale should be included in each 3D model for referencing measurements. Alternatively, colour could be automatically corrected by an algorithm (*e.g.,* Bryson et al. (2013); Apollonio et al. (2014); Gaiani et al. (2017)). If colour was standardized, the information for each point could be included in a machine learning approach (*e.g.,* with modifications to the algorithm presented in Chapter 5).

6.4 Concluding Remarks

Imagine placing a luxury apartment building in a vast empty field. People will not necessarily move there. They may reside in nearby housing blocks, even if lesser quality, because they are tied to family and community traditions there and rely upon nearby grocery stores, salons, and other urban conveniences. However, over time people may move into the new apartment building, and in doing so they will establish an ecosystem similar to that in the older neighbourhood.

A reef with high structural complexity is like a luxury apartment building for reef organisms. Even so, structural complexity cannot explain all or even most variation in fish populations or other ecological variables. There are a multitude of other ecological and random effects at play, including latitude, temperature, interspecies interactions, stability of the environment, and nutrient flow. That said, structural complexity is a reasonable tool for predicting fish populations and other ecological variables. It is an especially powerful tool considering how relativity straightforward it is to measure compared to other environmental factors. Additionally, structural complexity is important to study because it is the only ecosystem feature most artificial reefs contribute to an ecosystem, unless organisms are also actively transplanted onto the artificial reef. An understanding of how structural complexity shapes reef communities not only contributes to our scientific knowledge about marine ecosystems, but also can inform designs for reef restoration and monitoring programmes.

The photogrammetric methods presented in this thesis for creating and analysing 3D models of underwater scenes have broad applications for ecology research, reef monitoring, artificial reef design, and marine archaeology. The 3D models are a uniquely non-destructive means of recording reef structure in such a way that the models can be analysed and compared against each other over time with a vast array of multi-scale metrics. The models can also be 3D printed. The work presented in this thesis has improved and rigorously validated a tool for ecologists to cost and time-effectively 3D model coral reefs. It has showed how the 3D models can predict trends in fish abundance and diversity, and how they can be 3D printed to test for effects upon organism settlement in a controlled experiment. Additionally, we showed how a machine learning algorithm can learn patterns that tie the 3D models to ecological data. Together the research helps build a framework for interpreting and analysing 3D models of underwater scenes and their associated ecological data.

References

Agisoft LLC (2017). Agisoft PhotoScan User Manual: Professional Edition, Version 1.3.

Agudo-Adriani, E. A., Cappelletto, J., Cavada-Blanco, F., and Croquer, A. (2016). Colony geometry and structural complexity of the endangered species Acropora cervicornis partly explains the structure of their associated fish assemblage. *PeerJ*, 4(e1861).

Allen, L., Scott, J., Brand, A., Hlava, M., and Altman, M. (2014). Publishing: Credit where credit is due. *Nature*, 508(7496):312–313.

Alvarez-Filip, L., Dulvy, N. K., Gill, J. a., Cote, I. M., and Watkinson, a. R. (2009). Flattening of Caribbean Coral Reefs: Region-Wide Declines in Architectural Complexity. *Proceedings of the Royal Society B: Biological Sciences*, 276(1669):3019–3025.

Apollonio, F. I., Ballabeni, M., Gaiani, M., Architettura, D., Mater, A., and Università, S. (2014). Color enhanced pipelines for reality-based 3D modeling of on site medium sized archeological artifacts Fuentes de color mejoradas para el modelado tridimensional de artefactos arqueológicos de tamaño medio localizados in. *Virtual Archaeology Review*, 5(10):59–76.

Appeltans, W., Ahyong, S. T., Anderson, G., Angel, M. V., Artois, T., Bailly, N., . . . , and Costello, M. J. (2012). The Magnitude of Global Marine Species Diversity. *Current Biology*, 22(23):2189–2202.

Arbace, L., Sonnino, E., Callieri, M., Dellepiane, M., Fabbri, M., Iaccarino Idelson, A., and Scopigno, R. (2013). Innovative uses of 3D digital technologies to assist the restoration of a fragmented terracotta statue. *Journal of Cultural Heritage*, 14(4):332–345.

Baine, M. (2001). Artificial reefs: a review of their design, application, management and performance. *Ocean & Coastal Management*, 44(3-4):241–259.

Ballard, R. D., Stager, L. E., Master, D., Yoerger, D., Whitcomb, L. L., Singh, H., Piechota, D., Ballard, R. D., Stager, L. E., Master, D., Yoerger, D., Mindell, D., Whitcomb, L. L., Singh, H., and Piechota, D. (2002). Iron Age Shipwrecks in Deep Water off Ashkelon, Israel. *American Journal of Archaeology*, 106(2):151–168.

Beall, C., Lawrence, B. J., Ila, V., and Dellaert, F. (2010). 3D reconstruction of underwater structures. *IEEE/RSJ 2010 International Conference on Intelligent Robots and Systems, IROS 2010 - Conference Proceedings*, 0448111:4418–4423.

Beltrame, C. and Costa, E. (2017). 3D survey and modelling of shipwrecks in different underwater environments. *Journal of Cultural Heritage*, pages 3–9.

Beltrame, C., Lazzarini, L., and Parizzi, S. (2016). The Roman Ship 'punta Scifo d' and its Marble Cargo (Crotone, Italy). *Oxford Journal of Archaeology*, 35(3):295–326.

Beukers, J. S. and Jones, G. P. (1997). Habitat Complexity Modifies the Impact of Piscivores on a Coral Reef Fish Population. *Oecologia*, 114(1):50–59.

Bozec, Y.-M., O'Farrell, S., Bruggemann, J. H., Luckhurst, B. E., and Mumby, P. J. (2016). Tradeoffs between fisheries harvest and the resilience of coral reefs. *Proceedings of the National Academy of Sciences*, 113(16):4536–4541.

Brand, A., Allen, L., Altman, M., Hlava, M., and Scott, J. (2015). Beyond authorship: Attribution, contribution, collaboration, and credit. *Learned Publishing*, 28(2):151–155.

Bruno, J. F., Stachowicz, J. J., and Bertness, M. D. (2003). Inclusion of facilitation into ecological theory. *Trends in Ecology and Evolution*, 18(3):119–125.

Bryson, M., Ferrari, R., Figueira, W., Pizarro, O., Madin, J., Williams, S., and Byrne, M. (2017). Characterization of measurement errors using structure-from-motion and photogrammetry to measure marine habitat structural complexity. *Ecology and Evolution*, 7(15):5669–5681.

Bryson, M., Johnson-Roberson, M., Pizarro, O., and Williams, S. B. (2013). Colour-consistent structure-from-motion models using underwater imagery. In *Robotics: Science and Systems VIII*.

Burke, L., Reytar, K., and Mark Spalding, A. P. (2011). *Reefs at Risk Revisited*. World Resources Institute (WRI).

Burns, J., Delparte, D., Gates, R., and Takabayashi, M. (2015). Integrating Structure-from-Motion Photogrammetry with Geospatial Software as a Novel Technique for Quantifying 3D Ecological Characteristics of Coral Reefs. *PeerJ*, 3(e1077).

Burns, J., Delparte, D., Kapono, L., Belt, M., Gates, R., and Takabayashi, M. (2016). Assessing the impact of acute disturbances on the structure and composition of a coral community using innovative 3D reconstruction techniques. *Methods in Oceanography*, 15-16:49–59.

Bythell, J., Pan, P., and Lee, J. (2001). Three-dimensional morphometric measurements of reef corals using underwater photogrammetry techniques. *Coral Reefs*, 20(3):193–199.

Campos, R., Garcia, R., Alliez, P., and Yvinec, M. (2015). A Surface Reconstruction Method for In-Detail Underwater 3D Optical Mapping. *International Journal of Robotics Research*, 34(1):64–89.

Campos, R., Garcia, R., and Nicosevici, T. (2011). Surface reconstruction methods for the recovery of 3D models from underwater interest areas. *OCEANS 2011 IEEE - Spain*.

Carleton, J. H. and Sammarco, P. W. (1987). Effects of Substratum Irregularity on Success of Coral Settlement: Quantification by Comparative Geomorphological Techniques. *Bulletin of Marine Science*, 40(1):85–98.

Carpenter, K. E., Abrar, M., Aeby, G., Aronson, R. B., Banks, S., Bruckner, A., Chiriboga, A., Cortés, J., Delbeek, J. C., Devantier, L., Edgar, G. J., Edwards, A. J., Fenner, D., Guzmán, H. M., Hoeksema, B. W., Hodgson, G., Johan, O., Licuanan, W. Y., Livingstone, S. R., Lovell, E. R., Moore, J. A., Obura, D. O., Ochavillo, D., Polidoro, B. A., Precht, W. F., Quibilan, M. C., Reboton, C., Richards, Z. T., Rogers, A. D., Sanciangco, J., Sheppard, A., Sheppard, C., Smith, J., Stuart, S., Turak, E., Veron, J. E. N., Wallace, C., Weil, E., and Wood, E. (2008). One-Third of Reef-Building Corals Face Elevated Extinction Risk from Climate Change and Local Impacts. *Science*, 321(5888):560–563.

Carr, M. and Hixon, M. (1997). Artificial Reefs: The Importance of Comparisons with Natural Reefs. *Fisheries*, 22(4):28–33.

Casella, E., Collin, A., Harris, D., Ferse, S., Bejarano, S., Parravicini, V., Hench, J. L., and Rovere, A. (2016). Mapping coral reefs using consumer-grade drones and structure from motion photogrammetry techniques. *Coral Reefs*, 36(1).

Costa, B. M., Battista, T. A., and Pittman, S. J. (2009). Comparative evaluation of airborne LiDAR and ship-based multibeam SoNAR bathymetry and intensity for mapping coral reef ecosystems. *Remote Sensing of Environment*, 113(5):1082–1100.

Costanza, R., de Groot, R., Sutton, P., van der Ploeg, S., Anderson, S. J., Kubiszewski, I., Farber, S., and Turner, R. K. (2014). Changes in the global value of ecosystem services. *Global Environmental Change*, 26(1):152–158.

Darling, E. S., Graham, N. A., Januchowski-Hartley, F. A., Nash, K. L., Pratchett, M. S., and Wilson, S. K. (2017). Relationships between structural complexity, coral traits, and reef fish assemblages. *Coral Reefs*, 36(2):561–575.

Dartnell, P. and Gardner, J. (2004). Predicting seafloor facies from multibeam bathymetry and backscatter data. *Photogrammetric Engineering & Remote Sensing*, 70(9):1081–1091.

Drap, P. (2012). Underwater Photogrammetry for Archaeology. In *Special Applications of Photogrammetry*, pages 111–136. InTech.

Drap, P., Merad, D., Hijazi, B., Gaoua, L., Nawaf, M. M., Saccone, M., Chemisky, B., Seinturier, J., Sourisseau, J. C., Gambin, T., and Castro, F. (2015). Underwater photogrammetry and object modeling: A case study of xlendiwreck in malta. *Sensors (Switzerland)*, 15(12):30351–30384.

Dustan, P., Doherty, O., and Pardede, S. (2013). Digital Reef Rugosity Estimates Coral Reef Habitat Complexity. *PLoS ONE*, 8(2).

Edmunds, P. J., Nozawa, Y., and Villanueva, R. D. (2014). Refuges modulate coral recruitment in the Caribbean and the Pacific. *Journal of Experimental Marine Biology and Ecology*, 454:78–84.

Figueira, W., Ferrari, R., Weatherby, E., Porter, A., Hawes, S., and Byrne, M. (2015). Accuracy and Precision of Habitat Structural Complexity Metrics Derived from Underwater Photogrammetry. *Remote Sensing*, 7(12):16883–16900.

Fisher, R., Leary, R. A. O., Brainard, R. E., Caley, M. J., Fisher, R., Leary, R. A. O., Low-choy, S., Mengersen, K., Knowlton, N., and Brainard, R. E. (2014). Report Species Richness on Coral Reefs and the Pursuit of Convergent Global Estimates Species Richness on Coral Reefs and the Pursuit of Convergent Global Estimates. *Current Biology*, 25(4):500–505.

Friedlander, A. M. and Parrish, J. D. (1998). Habitat Characteristics Affecting Fish Assemblages on a Hawaiian Coral Reef. *Journal of Experimental Marine Biology and Ecology*, 224(1).

Friedman, A., Pizarro, O., Williams, S. B., and Johnson-Roberson, M. (2012). Multi-Scale Measures of Rugosity, Slope and Aspect from Benthic Stereo Image Reconstructions. *PLoS ONE*, 7(12).

Gaiani, M., Apollonio, F. I., Ballabeni, A., and Remondino, F. (2017). Securing color fidelity in 3D architectural heritage scenarios. *Sensors*, 17(11).

Goatley, C. H. R. and Bellwood, D. R. (2011). The Roles of Dimensionality, Canopies and Complexity in Ecosystem Monitoring. *PLoS ONE*, 6(11).

González-Rivero, M., Harborne, A. R., Herrera-Reveles, A., Bozec, Y.-M., Rogers, A., Friedman, A., Ganase, A., and Hoegh-Guldberg, O. (2017). Linking fishes to multiple metrics of coral reef structural complexity using three-dimensional technology. *Scientific Reports*, 7(1):13965.

Graham, N. A. J. (2014). Habitat complexity: Coral structural loss leads to fisheries declines. *Current Biology*, 24(9):R359–R361.

Graham, N. A. J. and Nash, K. L. (2013). The Importance of Structural Complexity in Coral Reef Ecosystems. *Coral Reefs*, 32:315–326.

Gratwicke, B. and Speight, M. (2005a). Effects of Habitat Complexity on Caribbean Marine Fish Assemblages. *Marine Ecology Progress Series*, 292:301–310.

Gratwicke, B. and Speight, M. R. (2005b). The Relationship Between Fish Species Richness, Abundance and Habitat Complexity in a Range of Shallow Tropical Marine Habitats. *Journal of Fish Biology*, 66(3):650–667.

Halford, A., Cheal, A. J., Ryan, D., and Williams, D. M. (2004). Resilience to large-scale disturbance in coral and fish assemblages on the great barrier reef. *Ecology*, 85(7):1892–1905.

Hearn, C., Atkinson, M., and Falter, J. (2001). A physical derivation of nutrient-uptake rates in coral reefs: Effects of roughness and waves. *Coral Reefs*, 20(4):347–356.

Heron, S. F., Eakin, C. M., Douvere, F., Anderson, K. D., Day, J. C., Geiger, E., Hoegh-Guldberg, O., van Hooidonk, R., Hughes, T., Marshall, P. A., and Obura, D. (2017). Impacts of Climate Change on World Heritage Coral Reefs A First Global Scientific Assessment. Technical report, UNESCO World Heritage Centre, Paris.

Hiatt, R. W., Strasburg, D. W., Monographs, S. E., and Jan, N. (1960). Ecological Relationships of the Fish Fauna on Coral Reefs of the Marshall Islands. *Ecological Monographs*, 30(1):65–127.

Hills, J. M. and Thomason, J. C. (1998). On the effect of tile size and surface texture on recruitment pattern and density of the barnacle, Semibalanus balanoides. *Biofouling*, 13(1):31–50.

Hinderstein, L. M., Marr, J. C. A., Martinez, F. A., Dowgiallo, M. J., Puglise, K. A., Pyle, R. L., Zawada, D. G., and Appeldoorn, R. (2010). Theme section on "Mesophotic Coral Ecosystems: Characterization, Ecology, and Management". *Coral Reefs*, 29:247–251.

Hobson, R. D. (1972). Surface Roughness in Topography: Quantitative Approach. In Chorley, R. J., editor, *Spatial Analysis in Geomorphology*, pages 221 – 245. Methue & Co.

Hoegh-Guldberg, O., Thezar, M., Boulos, M., Guerraoui, M., Harris, A., Graham, A., Llewellyn, G., Singer, S., Ath, W. D., Hirsch, D., and Soede, L. P. (2015). Reviving the Ocean Economy: the case for action - 2015. Technical report, WWF International, Gland, Switzerland.

Hoey, A. S., Wilson, S. K., Pratchett, M. S., Hoey, A. S., and Wilson, S. K. (2014). Reef degradation and the loss of critical ecosystem goods and services provided by coral reef fishes. *Current Opinion in Environmental Sustainability*, 7:37–43.

Hopley, D., editor (2011). *Encyclopedia of Modern Coral Reefs: Structure, Form and Process*. Springer, Dordrecht, The Netherlands.

Hopley, D., Smithers, S., and Parnell, K. (2007). *The geomorphology of the Great Barrier Reef: development, diversity and change*. Cambridge University Press.

Hu, H., Ferrari, R., Mckinnon, D., Roff, G. a., Smith, R., Mumby, P. J., and Upcroft, B. (2012). Measuring reef complexity and rugosity from monocular video bathymetric reconstruction. In *Proceedings of the 12th International Coral Reef Symposium*, volume 12.

Huvenne, V. a. I., Blondel, P., and Henriet, J. P. (2002). Textural analyses of sidescan sonar imagery from two mound provinces in the Porcupine Seabight. *Marine Geology*, 189(3-4):323–341.

Idjadi, J. A. and Edmunds, P. J. (2006). Scleractinian corals as facilitators for other invertebrates on a Caribbean reef. *Marine Ecology Progress Series*, 319:117–127.

Johansen, J. L., Bellwood, D. R., and Fulton, C. J. (2008). Coral reef fishes exploit flow refuges in high-flow habitats. *Marine Ecology Progress Series*, 360:219–226.

Johnson-Roberson, M., Pizarro, O., Williams, S. B., and Mahon, I. (2010). Generation and Visualization of Large-Scale Three-Dimensional Reconstructions from Underwater Robotic Surveys. *Journal of Field Robotics*, 21(1).

Jones, C. G., Lawron, J. H., and Shachak, M. (1997). Positive and negative effects of organisms as physical ecosystem engineers. *Ecology*, 78(7):1946–1957.

Knudby, A. and LeDrew, E. (2007). Measuring Structural Complexity on Coral Reefs. *Proceedings of the American Acadamy of Underwater Sciences 26th Symposium*, pages 181–188.

Kraus, K. (2007). *Photogrammetry: Geometry from Images and Laser Scans, Volume 1*. Walter de Gruyter GmbH & Co., Berlin, Germany, second edition.

Kunz, C. and Singh, H. (2013). Map building fusing acoustic and visual information using autonomous underwater vehicles. *Journal of field robotics*, 30(5):763–783.

Leatherdale, J. D. and Turner, D. J. (1983). Underwater Photogrammetry in the North Sea. *The Photogrammetric Record*, 11(62):151–167.

Leon, J., Roelfsema, C. M., Saunders, M. I., and Phinn, S. R. (2015). Measuring Coral Reef Terrain Roughness using 'Structure-from-Motion' Close-Range Photogrammetry. *Geomorphology*, 242:21–28.

Luckhurst, E. and Luckhurst, K. (1978). Analysis of the Influence of Substrate Variables on Coral Reef Fish Communities. *Marine Biology*, 323(49):317–323.

Mahon, I., Pizarro, O., Johnson-Roberson, M., Friedman, A., Williams, S. B., and Henderson, J. C. (2011). Reconstructing pavlopetri: Mapping the world's oldest submerged town using stereo-vision. *Proceedings - IEEE International Conference on Robotics and Automation*, pages 2315–2321.

Mandelbrot, B. B. (1982). *The Fractal Geometry of Nature*. W.H. Freeman, New York.

Mark, D. (1984). Fractal Dimension of a Coral Reef at Ecological Scales: A Discussion. *Marine Ecology Progress Series*, 14:293–294.

Martin-Garin, B., Lathuilière, B., Verrecchia, E. P., and Geister, J. (2007). Use of Fractal Dimensions to Quantify Coral Shape. *Coral Reefs*, 26(3):541–550.

McClanahan, T. R., Graham, N. A., and Darling, E. S. (2014). Coral reefs in a crystal ball: Predicting the future from the vulnerability of corals and reef fishes to multiple stressors. *Current Opinion in Environmental Sustainability*, 7:59–64.

McCormick, M. I. (1994). Comparison of Field Methods for Measuring Surface Topography and their Associations with a Tropical Reef Fish Assemblage. *Marine Ecology Progress Series*, 112:87–96.

McCoy, E. D. and Bell, S. S. (1991). Habitat structure: the evolution and diversification of a complex topic. In Bell, S. S., McCoy, E. D., and Mushinsky, H. R., editors, *Habitat Structure: the physical arrangement of objects in space*. Chapman and Hall.

McElhinny, C., Gibbons, P., Brack, C., and Bauhus, J. (2005). Forest and Woodland Stand Structural Complexity: Its Definition and Measurement. *Forest Ecology and Management*, 218(1-3):1–24.

Merks, R., Hoekstra, A., Kaandorp, J., and Sloot, P. (2003). A Problem Solving Environment for Modelling Stony Coral Morphogenesis. *Computational Science - ICCS 2003*, 2657:639–648.

Moberg, F. and Folke, C. (1999). Ecological Goods and Services of Coral Reef Ecosystems. *Ecol Econ*, 29(2):215–233.

Moore, J. G. and Normark, W. R. (1994). Giant Hawaiian Landslides. *Annual Review of Earth and Planetary Sciences*, 22:119–144.

Mora, C., Tittensor, D. P., Adl, S., Simpson, A. G. B., and Worm, B. (2011). How many species are there on earth and in the ocean? *PLoS Biology*, 9(8).

Mumby, P., Flower, J., Chollett, I., Box, S., and Bozec, Y. (2014). *Towards reef resilience and sustainable livelihoods: A handbook for Caribbean Coral Reef Managers*. University of Exeter, Exeter, Devon, UK.

Mumby, P. J. and Steneck, R. S. (2008). Coral reef management and conservation in light of rapidly evolving ecological paradigms. *Trends in Ecology and Evolution*, 23(10):555–563.

Myers, N. (1962). Characterization of Surface Roughness. *Wear*, 5(3):182–189.

Newman, S. P., Meesters, E. H., Dryden, C. S., Williams, S. M., Sanchez, C., Mumby, P. J., and Polunin, N. V. C. (2015). Reef Flattening Effects on Total Richness and Species Responses in the Caribbean. *Journal of Animal Ecology*, 84(6):1678–1689.

Obura, D. O. (2005). Resilience and climate change: Lessons from coral reefs and bleaching in the Western Indian Ocean. *Estuarine, Coastal and Shelf Science*, 63(3):353–372.

Perkol-Finkel, S., Shashar, N., and Benayahu, Y. (2006). Can artificial reefs mimic natural reef communities? The roles of structural features and age. *Marine Environmental Research*, 61(2):121–135.

Pittman, S. J. and Brown, K. A. (2011). Multi-Scale Approach for Predicting Fish Species Distributions across Coral Reef Seascapes. *PLoS ONE*, 6(5):e20583.

Pittman, S. J., Costa, B. M., and Battista, T. A. (2009). Using Lidar Bathymetry and Boosted Regression Trees to Predict the Diversity and Abundance of Fish and Corals. *Journal of Coastal Research*, 10053:27–38.

Pizarro, O., Eustice, R. M., and Singh, H. (2009). Large area 3D reconstructions from underwater surveys. *IEEE Journal of Oceanic Engineering*, 34(2):150–169.

Pizarro, O., Friedman, A., Bryson, M., Williams, S. B., and Madin, J. (2017). A simple, fast, and repeatable survey method for underwater visual 3D benthic mapping and monitoring. *Ecology and Evolution*, 7(6):1770–1782.

Plaisance, L., Caley, M. J., Brainard, R. E., and Knowlton, N. (2011). The Diversity of Coral Reefs: What are We Missing? *PLoS ONE*, 6(10).

Pollio, J. (1968). Applications of underwater photogrammetry. Technical report, Naval Oceanographic Office National Space Technology Laboratory (NSTL).

Pratson, L. and Edwards, M. (1996). Introduction to advances in seafloor mapping using sidescan sonar and multibeam bathymetry data. *Marine Geophysical Research*, 35(14-15):1448–1462.

Purkis, S. J., Graham, N. A. J., and Riegl, B. M. (2008). Predictability of reef fish diversity and abundance using remote sensing data in Diego Garcia (Chagos Archipelago). *Coral Reefs*, 27(1):167–178.

Purkis, S. J., Riegl, B. M., and Andrefouet, S. (2005). Remote Sensing of Geomorphology and Facies Patterns on a Modern Carbonate Ramp (Arabian Gulf, Dubai, U.A.E.). *Journal of Sedimentary Research*, 75(5):861–876.

Raoult, V., Reid-Anderson, S., Ferri, A., and Williamson, J. (2017). How Reliable Is Structure from Motion (SfM) over Time and between Observers? A Case Study Using Coral Reef Bommies. *Remote Sensing*, 9(7):740.

Reichert, J., Backes, A. R., Schubert, P., and Wilke, T. (2017). The power of 3D fractal dimensions for comparative shape and structural complexity analyses of irregularly shaped organisms. *Methods in Ecology and Evolution*, 32.

Richardson, L. E., Graham, N. A., Pratchett, M. S., and Hoey, A. S. (2017). Structural complexity mediates functional structure of reef fish assemblages among coral habitats. *Environmental Biology of Fishes*, 100(3):193–207.

Risk, M. J. (1972). Fish Diversity on a Coral Reef in The Virgin Islands. *Atoll Research Bulletin*, 153.

Ritson-Williams, R., Arnold, S., Fogarty, N., Steneck, R. S., Vermeij, M., and Paul, V. J. (2009). New perspectives on ecological mechanisms affecting coral recruitment on reefs. *Smithsonian Contributions to the Marine Sciences*, pages 437–457.

Robert, K., Huvenne, V. A. I., Georgiopoulou, A., Jones, D. O. B., Marsh, L., D. O. Carter, G., and Chaumillon, L. (2017). New approaches to high-resolution mapping of marine vertical structures. *Scientific Reports*, 7(1):9005.

Rogers, A., Blanchard, J. L., and Mumby, P. J. (2014). Vulnerability of coral reef fisheries to a loss of structural complexity. *Current Biology*, 24(9):1000–1005.

Rogers, A., Harborne, A. R., Brown, C. J., Bozec, Y.-M., Castro, C., Chollett, I., Hock, K., Knowland, C. A., Marshell, A., Ortiz, J. C., Razak, T., Roff, G., Samper-Villarreal, J., Saunders, M. I., Wolff, N. H., and Mumby, P. J. (2015). Anticipative management for coral reef ecosystem services in the 21st century. *Global Change Biology*, 21(2):504–514.

Scopigno, R., Callieri, M., Cignoni, P., Corsini, M., Dellepiane, M., Ponchio, F., and Ranzuglia, G. (2011). 3D models for cultural heritage: Beyond plain visualization. *Computer*, 44(7):48–55.

Sebens, K. P. (1991). Habitat structure and community dynamics in marine benthic systems. In Bell, S. S., McCoy, E. D., and Mushinsky, H. R., editors, *Habitat Structure: the physical arrangement of objects in space*. Chapman and Hall.

Siddiqui, S. A., Salman, A., Malik, M. I., Shafait, F., Mian, A., Shortis, M. R., and Harvey, E. S. (2017). Automatic fish species classification in underwater videos: exploiting pre-trained deep neural network models to compensate for limited labelled data. *ICES Journal of Marine Science*.

TEEB (2010). *The Economics of Ecosystems and Biodiversity: Mainstreaming the Economics of Nature: A synthesis of the approach, conclusions and recommendations of TEEB*. The Economics of Ecosystems and Biodiversity (TEEB).

Teza, G., Pesci, A., and Ninfo, A. (2016). Morphological Analysis for Architectural Applications: Comparison between Laser Scanning and Structure-from-Motion Photogrammetry. *Journal of Surveying Engineering*, 142(2014):1–10.

Thomas, T. (1981). Characterization of Surface Roughness. *Precision Engineering*, 3(2):97–104.

Walker, B. K., Jordan, L. K. B., and Spieler, R. E. (2009). Relationship of Reef Fish Assemblages and Topographic Complexity on Southeastern Florida Coral Reef Habitats. *Journal of Coastal Research*, 10053:39–48.

Wedding, L. M., Friedlander, A. M., McGranaghan, M., Yost, R. S., and Monaco, M. E. (2008). Using Bathymetric Lidar to Define Nearshore Benthic Habitat Complexity: Implications for Management of Reef Fish Assemblages in Hawaii. *Remote Sensing of Environment*, 112(11):4159–4165.

Whalan, S., Abdul Wahab, M. A., Sprungala, S., Poole, A. J., and De Nys, R. (2015). Larval settlement: The role of surface topography for sessile coral reef invertebrates. *PLoS ONE*, 10(2):1–17.

Williams, R., Wright, A. J., Ashe, E., Blight, L. K., Bruintjes, R., Canessa, R., Clark, C. W., Cullis-Suzuki, S., Dakin, D. T., Erbe, C., Hammond, P. S., Merchant, N. D., O'Hara, P. D., Purser, J., Radford, A. N., Simpson, S. D., Thomas, L., and Wale, M. A. (2015). Impacts of anthropogenic noise on marine life: Publication patterns, new discoveries, and future directions in research and management. *Ocean and Coastal Management*, 115:17–24.

Wilson, M. F. J., O'Connell, B., Brown, C., Guinan, J. C., and Grehan, A. J. (2007a). Multiscale Terrain Analysis of Multibeam Bathymetry Data for Habitat Mapping on the Continental Slope. *Marine Geodesy*, 30(1-2):3–35.

Wilson, S., Graham, N. A. J., and Polunin, N. V. C. (2007b). Appraisal of Visual Assessments of Habitat Complexity and Benthic Composition on Coral Reefs. *Marine Biology*, 151:1069–1076.

Yamafune, K., Torres, R., and Castro, F. (2017). Multi-Image Photogrammetry to Record and Reconstruct Underwater Shipwreck Sites. *Journal of Archaeological Method and Theory*, 24(3):703–725.

Yanovski, R., Nelson, P. A., and Abelson, A. (2017). Structural Complexity in Coral Reefs: Examination of a Novel Evaluation Tool on Different Spatial Scales. *Frontiers in Ecology and Evolution*, 5(27).

Zawada, D. G., Piniak, G. A., and Hearn, C. J. (2010). Topographic complexity and roughness of a tropical benthic seascape. *Geophysical Research Letters*, 37(14).

Appendices

A

Description of Data: 3D Models and Fish Data from Bonaire, Summer 2017 (Summer Following Chapter 3)

Publication: Denise Swanborn, Julia Huisman, Grace C. Young, Alex D. Rogers. "Three-dimensional coral reef models predict fish diversity in Bonaire, Caribbean." *In prep.*

Summary: This study repeated Chapter 3 on the Caribbean island of Bonaire with 90 quadrats. One difference was that it only assessed 3D models in terms of rugosity (R); this was done not only to simplify analysis, but also because R can be as powerful a predictor as Habitat Assessment Scores or combinations of R, D, and $1/k$ (Chapter 3). All correlations between R and fish variables were significant and moderately strong, with Pearson's correlation coefficients of 0.66 (95% confidence interval (CI): 0.52-0.76), 0.56 (CI: 0.40-0.69), and 0.52 (CI: 0.35-0.66) respectively with species richness, Simpson index, and Shannon index. Additionally, the study found that location on the reef profile (either terrace, drop off, or slope) explained 23% of the variability in R ($P < 0.0001$), with the reef drop off having the highest R. The correlations were stronger than those in data from the Caribbean island of Utila (Chapter 3), possibly because Bonaire's reefs are healthier. Bonaire is known to have some of the healthiest Caribbean reefs in part because they have been protected in the National Marine Park since 1979 (Newman et al., 2015; Bozec et al., 2016). Alternatively, the differences in correlations strengths could be evidence of a plateau effect; *e.g.,* fish diversity and abundance may increase with structural complexity, but only up to a threshold (Hoey et al., 2014).

The research was conducted with permission from the National Park Authority STINAPA (Stichting Nationale Parken) through Coral Restoration Foundation, Bonaire.

B

Description of Data: 3D Models and Fish Data from Honduras, Summer 2017 (Summer Following Chapter 3)

Publication: Duncan O'Brien, Grace C. Young, Dan Exton. "The relationship between three-dimensional complexity and coral reef fish abundance from video surveys, Caribbean Bay Island." *In prep.*

Summary: This study repeated Chapter 3 at the same study site (south-east coast of Utila, Honduras) with 48 quadrats exactly one year later. The only methodological difference was that fish were recorded from 10-minute video surveys instead of 10-minute diver surveys. In many cases videos surveys are preferable to diver surveys because (a) they enable more data to be collected during limited dive time, (b) experts who need not be present on the dive can identify fish from the videos, and (c) emerging technologies may be able to automatically identify fish from video using cutting-edge applications of machine-learning (Siddiqui et al., 2017). Curiously, however, this study found a *negative* significant relationship between $D_{5-15\ cm}$ and species richness (Spearman's rank correlation coefficient $\rho = -0.41$; P-adjusted < 0.05). No other 3D metrics correlated with either fish abundance, richness, or Shannon diversity. One explanation for this anomaly with the literature could be that as complexity increased more fish were obstructed from the view of camera conducting the video survey. Additionally, the data may also have not been sufficiently distinct in terms of the independent variables (R, D, and $1/k$) to generalize trends. These effects warrant further investigation as to how video surveys affected the data.

The research was conducted under a research permit from the Instituto de Conservación Forestal through Operation Wallacea.

C

3D Reconstruction as a Monitoring Strategy for Restoration of *Acropora palmata* on Coral Reefs in Bonaire

Publication: Julia Huisman, Denise Swanborn, Grace C. Young, Alex D. Rogers. "Three-dimensional reconstruction as a monitoring strategy for coral reef restoration of *Acropora palmate*." *In prep.*

Summary: With thousands of *Acropora* corals out-planted on Caribbean reefs annually, reef restoration practitioners need tools to help monitor and optimise their approaches. This study adapted the methods presented in Chapter 2 to model individual elkhorn corals on Bonaire and demonstrated how the 3D models could provide reliable measurements for restoration. 3D models provided measurements of coral volume, surface area, dimensions (height x width x length), and proportion of live cover or mortality. User-end differences in manually editing and analysing the 3D models - even by analysts with minimal prior training and guidance ($\sim$2 hours total) - did not significantly affect measurement reliability (quantified by Krippendorff's α). Direct sunlight was found to have a slight but significant adverse effect on model reconstruction, with measurement mean coefficient of variance rising from 2.06 to 3.67% with direct sunlight (Two-paired sample T-test, t(6)=7.59, P <0.001). This is likely because the sun can cause caustics and dramatic changes in light in the water, which interfere with the photogrammetry algorithm (Chapter 6.3.3).

The research was conducted with permission from the National Park Authority STINAPA (Stichting Nationale Parken) through Coral Restoration Foundation, Bonaire.